The University Of Sheffield.

Faculty of Engineering

Department of Civil and Structural Engineering

A SIMPLIFIED STEEL BEAM-TO-COLUMN CONNECTION MODELLING APPROACH

AND

INFLUENCE OF CONNECTION DUCTILITY ON FRAME BEHAVIOUR IN FIRE

By

Ruoxi Shi

A thesis submitted in partial fulfilment of the requirements for the degree of Doctor of Philosophy

September 2016

Acknowledgements

I would like to express my sincere gratitude to my supervisors, Dr. Shan-Shan Huang and Professor Buick Davison, for their continuous guidance, support and encouragement throughout my research project. I am truly enlightened and inspired by them. It was my luck to be under their supervision, and I will always cherish this experience.

I am very proud to be a member of the Structural Fire Engineering Research Group. Thanks for the brilliant memories we have created together with my research group members. Special thanks also go to my colleagues in Room D120, from whom I have learned so much from, both professional knowledge from different fields and fun of life.

Finally my deepest appreciation must go to my parents, Qilin and Guangying, and my husband, Han. I wouldn't be able to complete my research project without their unconditional support, both emotionally and financially. Your confidence in me was my greatest motivation and I will be a daughter and a wife you will be proud of for life.

Declaration

I declare that this thesis is the result of my own work except where specific reference has been made to the work of others. No portion of it has been submitted for another degree, qualification, diploma to any other university or institution.

Ruoxi Shi

September 2016

Abstract

Steel beam-to-column connections are vulnerable structural elements when a fire strikes a building, as observed in fire incidents and full-scale fire tests. Existing techniques allow researchers to model the behaviour of different types of connections in fire but are difficult to use when conducting simulations on full-scale frames with multiple connections due to time and computation requirements. Therefore a need for a simplified connection modelling approach that can significantly reduce the computational time required without compromising on the accuracy of the simulation results so that large-scale simulations of structures with multiple connections in fire can be performed.

A simplified spring connection modelling approach for steel flush endplate beam-to-column connections in fire has been developed in this research project so that the realistic behaviour of connections can be incorporated into full-scale frame analyses at elevated temperature. The proposed modelling approach divides the connection into two or three (depending on the connection size) T-stubs and employs *ABAQUS* as a pre-processor to generate the force-displacement characteristics for each T-stub by detailed finite element modelling. These characteristics are then input into specialised software (*VULCAN*) to simulate the behaviour of structure in fire including realistic representation of the steel beam-to-column connections. As a result of

its simplicity and reliability, the proposed approach permits full-scale frame analysis in fire to be conducted efficiently.

The proposed simplified spring connection modelling approach has been used to investigate the influence of connection ductility (both axial and rotational) on frame behaviour in fire. 2D steel and 3D composite frames across a range of spans were modelled to aid the understanding of the differences in frame response in fire when the beam-to-column connections have different axial and rotational ductility assumptions. The research study highlights that adopting the conventional rigid or pinned connection assumptions does not permit the axial forces acting on the connections to be predicted accurately, since the *axial* ductility of the connection is completely neglected when the *rotational* ductility is either fully restrained or free. By including realistic *axial* and *rotational* ductility of the beam-to-column connections, the frame response in fire can be predicted more accurately, which is advantageous in performance-based structural fire engineering design.

Contents

List of figures

List of tables

1

Introduction

Page | 2

Page Intentionally Left Blank

1.1   Background

Fire has served humans since earliest history to provide necessities such as warmth, light and a means of cooking, and is one the most common forms of energy release. Although fire is useful for human beings, it can also become one of the greatest dangers to both life and property. Disastrous accidents related to building fires all around the world remind designers and researchers of the importance of correctly understanding the frame behaviour in fire so that the losses of life and property can be reduced.

Structural Fire Engineering focuses on analysing the behaviour of structures in fire conditions in order to design structural members with sufficient fire resistance. Unlike ambient temperature design, in which the loading conditions are generally assumed to be relatively simple combinations of permanent and variable actions and material response is well defined, designing structures for fire loading can be difficult due to the complexity of possible load combinations, material and geometrical non-linearities as a result of temperature, together with excessive deflections. Extra complexity also arises from the restraint to thermal expansion and contraction induced by the cooler adjacent structures to the heated frame elements. Conventionally, a prescriptive fire protection approach is usually adopted which aims to control the temperature of certain structural members by applying various passive fire protection schemes such as intumescent coating or

boarding. For example, the temperatures of steel members are generally kept below 550°C within the statutory fire resistance period of the building when the ISO 834 standard fire is applied (ISO, 1999).

It must be recognised that the prescriptive fire protection approach has been tested and proven satisfactory in many real building fires, but with the invention of new building materials and construction technologies, the prescriptive approach has limitations. The need of a more advanced design philosophy led to the development of performance-based approaches, which consider the fire requirements of the building based on its performance in fire, hence the name.

Structural fire engineering standards and guidance, such as BS EN 1991-1-2 (CEN, 2002) and BS EN 1993-1-2 (CEN, 2005b), are based on the performance-based design approach. To aid the understanding of frame behaviour in fire so that the performance-based design approach can be accurately implemented, six full-scale fire tests were conducted on an 8-storey composite frame at Cardington by Building Research Establishment in the 1990s (Newman, et al., 2006). The results from the Cardington tests highlighted the importance of assessing the behaviour of the entire structure rather than individual structural members, because the restraints induced by the adjacent cooler structures should be taken into consideration. If designers intend to include the interactions between structural members or vary certain design conditions in performance-based fire design, it is obviously impractical

to perform full-scale fire tests because of the excessive costs and potential prolonged design period. Hence, numerical modelling becomes the top choice for designers to conduct performance-based fire design. Numerical modelling can provide adequately accurate structural behaviour simulations at elevated temperatures at much lower costs.

The behaviour of steel beam-to-column connections under fire conditions has been of interest to many researchers over decades. Large-scale fire tests and the collapse of WTC7 suggest that connections are the most vulnerable structural elements (Gann, 2008). Since the connections form the links between structural members, their failure in fire can lead to collapse of connected beams, buckling of the columns and eventually initiate the progressive collapse of the whole structure. Therefore, modelling of the connections correctly and efficiently is a vital component to produce accurate frame behaviour prediction in structural fire engineering design. Various modelling approaches have been proposed throughout the process of understanding the behaviour of connections in fire, which can be classed into the three main categories: (a) Curve-fitting methods, (b) finite element simulations and (c) component-based connection models. The first approach, the curve-fitting methods, is based on existing test data to predict moment-rotation characteristics and is straightforward to conduct. However, as the process is highly dependent on the availability of test data, this approach is only applicable for connections that have very close

geometrical and mechanical properties to connections that have been tested and for which published data is available. The second approach, the finite element simulation method, can produce accurate predictions of frame behaviour in fire with correctly selected input parameters, but can be very computationally and time costly, especially for complex or large-scale structures. The last approach, the component-based connection models, simulates the connections as assemblies of springs which can represent accurately connection behaviour under fire conditions. This approach also bears the same deficiency as the second approach, which is not computational and time efficient when frames with multiple connections are modelled.

3D modelling and analysis of frame behaviour in fire has always been limited due to shortage of reliable analytical tools, techniques and methodologies (Sun, 2012). Many limitations are rooted in the complexity of correctly modelling the behaviour of connections in fire. For instance, researchers are interested to understand how different types of connections can influence the behaviour of the whole frame, but it cannot be achieved easily with the currently available connection modelling approaches. There is a need for a simplified connection model that can significantly reduce the amount of computational time required without compromising on the accuracy of the simulation results.

1.2   Scope of research

The primary aim of this research project is to develop a simplified spring model for steel beam-to-column connections under elevated temperature suitable for use in global frame analysis. The proposed simplified spring connection model divides connections into two or three T-stubs depending on the size of the connections and adopts the finite element package *ABAQUS* as a pre-processor to determine the spring force-displacement characteristics for these T-stubs to be used as input into the high temperature finite element software *VULCAN* to perform frame analyses. Compared with the existing 2-node Ordinary Spring Element Method (introduced in Section 3.1) and the Component Based Method, the proposed simplified connection modelling approach is more time and computationally efficient but still includes both axial and rotational ductility of the connections, especially for multi-bay frame simulations where a significant numbers of connections exist. With the proposed simplified spring connection model, investigations of the importance of incorporating connection axial and rotational ductility in frame analysis under elevated temperature can be conducted.

In order to achieve the above aims, the objectives of this research project are:

- To demonstrate the advantages of Component Based Method approach in connection modelling compared with an Ordinary

Spring Element connection model. This is achieved by conducting simulations on 2D steel individual frames with the connections modelled as either linearly connected axial and rotational spring (2-node Ordinary Spring Element model) or assemblies of springs representing active components of the connection.

- To construct reliable *ABAQUS* models of connection behaviour in fire for when test data is not available. The constructed *ABAQUS* model is validated against existing experimental results to prove its reliability.

- To study the effect of bolt stress-strain characteristics on *ABAQUS* modelling results by simulating the same connection model with various bolt stress-strain strain curves from both BS EN 1993-1-2 (CEN, 2005b) and test data (Hu, 2009b; Bull, 2014).

- To develop and validate a simplified spring connection model for steel and composite beam-to-column flush endplate connection, which is validated against *ABAQUS* simulation results.

- To perform parametric studies to investigate the influence of axial and rotational ductility of the connections on frame performance in fire. 2D steel and 3D composite internal bay models are adopted for these investigations comparing the frame performances when the gridline secondary beams are connected to the columns rigidly, pinned or by using the proposed simplified spring connection model.

1.3   Thesis outline

This thesis consists of six chapters each containing a brief introduction and concluding with a summary of the staged achievements. The contents of each chapter are briefly stated below.

Chapter 2 – Literature review

This chapter presents relevant structural fire engineering background information and previous research work related to steel beam-to-column connections in fire. Various research approaches for connections in fire are discussed and compared in this chapter, with their advantages and deficiencies highlighted. *VULCAN*, the finite element analysis software for modelling 3D composite steel-framed structures in fire, is introduced in this chapter.

Chapter 3 – Simulation of Steel Beam-to-Column Flush Endplate Connections under Elevated Temperature using *VULCAN* and *ABAQUS*

Two studies are conducted in this chapter. The first study focuses on presenting the differences between using the Ordinary Spring Element Method and the Component Based Method for connections in fire modelling in *VULCAN*. The second study investigates a suitable and reliable modelling technique in *ABAQUS* for steel flush endplate connection simulation. In addition, the effect of bolt material properties on the connection simulation is presented.

Chapter 4 – Development of a Simplified Spring Connection Model

In this chapter, a simplified spring model for steel beam-to-column connection is proposed. The simplified connection model is developed in *ABAQUS*, validated against detailed FE models and test data. In the latter section of this chapter, the implementation of the proposed connection model into the research version of *VULCAN* is presented and validated against the same model in *ABAQUS* at both ambient and elevated temperature.

Chapter 5 – Performance of 2D steel and 3D composite frames in fire

In this chapter, investigations are conducted with *VULCAN* to demonstrate the importance of incorporating connection axial and rotational ductility in frame analysis. Both 2D steel and 3D composite internal sub-frames in fire are modelled with a range of beam spans. The effect of load ratio on connection ductility demand in 3D composite frames is studied.

Chapter 6 – Conclusions and recommendations

This chapter summarises the main findings and concludes the research work conducted. Recommendations for future work are also presented.

2
Literature Review

Page Intentionally Left Blank

2.1   Chapter introduction

This chapter reviews the fundamental knowledge of structural fire engineering related to this research project, including how temperature increases can be represented by fire curves and the way material properties degrade with elevated temperature. The various types of steel beam-to-column connections and their classifications are introduced, followed by a description of their performance under fire conditions. Three principal methods for modelling the behaviour of steel beam-to-column connections at high temperatures are reviewed and compared. The finite element modelling software *VULCAN* is also introduced in this chapter.

2.2   Steel structures under fire conditions

2.2.1   Fire curves in structural fire engineering

To enable an accurate prediction of structural performance at elevated temperature it is vital to understand fire development. For fires, three key elements are required: fuel, heat and oxidising agent (usually oxygen), which together are known as the "fire triangle". Two types of fire curves are used most commonly in structural fire engineering research: the natural compartment fire (also known as a "parametric fire" in BS EN 1991-1-2 (CEN, 2002)) and the ISO 834 standard fire (ISO, 1999). Both are shown in Figure 2-1.
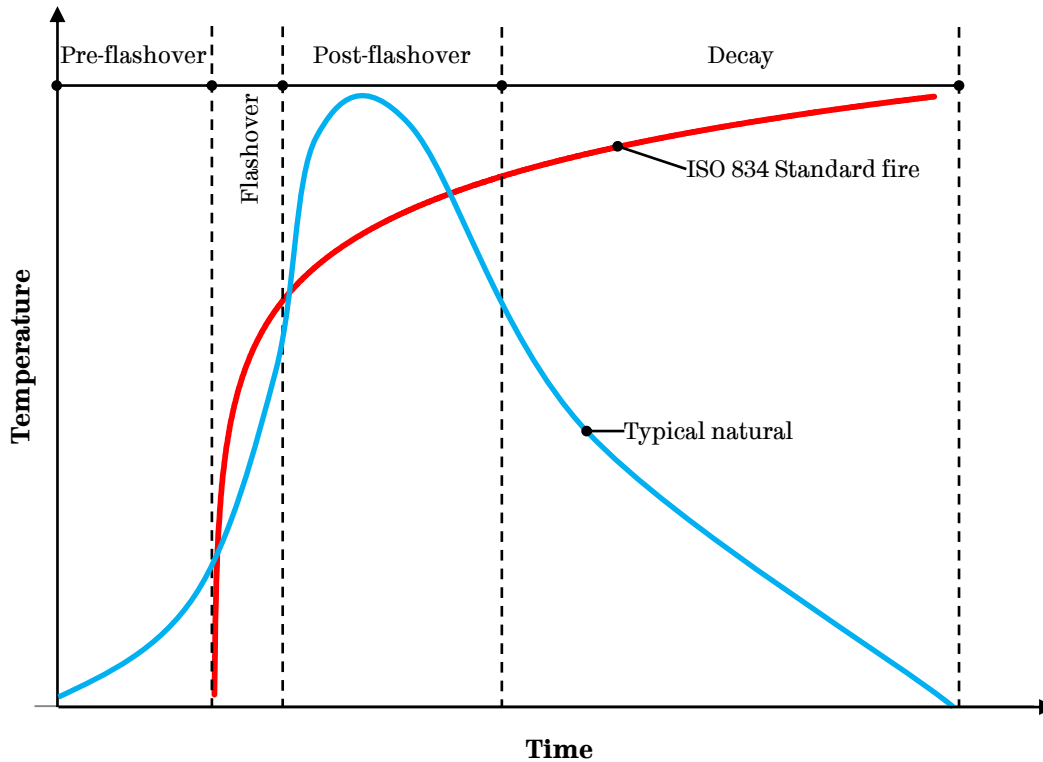
Figure 2-1 ISO 834 standard fire curve and typical natural fire development (phases apply to natural fire only)

The development of a natural compartment fire consists of four phases: pre-flashover, flashover, post-flashover and decay. During the pre-flashover stage, the fire is ignited locally in the compartment and grows slowly due to the limited supply of either or both of the combustive material or the oxygen. The average temperature increment in the compartment is small during this stage. Many fire cases do not continue to the next stage because of the lack of combustible material or oxygen supply. Flashover is the next stage when the fire spreads throughout the compartment due to the surrounding temperature reaching the flash point of the combustible material. This phase is relatively short compared to the other phases but the average temperature of the compartment increases rapidly during flashover.

Post-flashover is the next phase during which the fire becomes fully developed and reaches its peak temperature. Depending on the amount of the combustible materials and the oxygen, the peak temperatures can vary and exceeding 1000°C is possible. With the continuous consumption of the combustible materials and the oxygen, the fire burns at a steady rate and releases a substantial amount of heat. During this phase, the strength and stability of the structural elements are significantly affected due to fire exposure, which may lead to breaching of structural integrity, possible loss of strength of structural elements and progressive collapse. The final stage of a natural fire is decay and, eventually, extinction. The rate of temperature increase slows down and the overall temperature starts to decrease when the rate of heat generation is lower than the rate of heat discharge. Eventually the fire ceases when either the combustible material or the oxygen are consumed completely, which depends on whether the fire is fuel-controlled or ventilation-controlled. The overall temperature decreases back to ambient temperature and this phase can be very long depending on the surrounding environment (Purkiss, 2007).

BS EN 1991-1-2 (CEN, 2002) provides a natural (parametric) compartment fire temperature-time relationship for the heating phase. This curve includes the impacts of the compartment size, the ventilation condition, the available combustible material, the fire load and the material of surrounding surfaces. For the heating stage, the gas temperature of the parametric fire, Θ_g, is given by

$$\Theta_g = 20 + 1325(1 - 0.324e^{-0.2t^*} - 0.204e^{-1.7t^*} - 0.472e^{-19t^*}) \quad (2.1)$$

where t^* is the product of time t and the time factor function Γ

$$t^* = t \cdot \Gamma \tag{2.2}$$

with

$$\Gamma = \frac{(O/b)^2}{(0.04/1160)^2} \tag{2.3}$$

where $b = \sqrt{\rho c \lambda}$ is the thermal absorptivity for the total enclosure considering the density ρ, the specific heat c and the thermal conductivity λ of the boundary of the enclosure. The opening factor

$$O = \frac{A_v \sqrt{h_{eq}}}{A_t} \tag{2.4}$$

which depends on the total area of the vertical opening on all walls A_v, the weighted average of window heights on all walls h_{eq} and the total area (walls, ceilings and floor, including openings) of the enclosure A_t. When the time factor function $\Gamma = 1$, the parametric fire curve given in Equation (2.1) is considered to be equivalent to the standard temperature-time curve (Equation (2.9)). For the cooling stage, the gas temperature-time curves are defined as below:

$$\Theta_g = \Theta_{max} - 625(t^* - t^*_{max} \cdot x) \qquad \text{for } t^*_{max} \le 0.5 \tag{2.5}$$

$$\Theta_g = \Theta_{max} - 250(3 - t^*_{max})(t^* - t^*_{max} \cdot x) \quad \text{for } 0.5 < t^*_{max} < 2 \tag{2.6}$$

$$\Theta_g = \Theta_{max} - 250(t^* - t^*_{max} \cdot x) \qquad \text{for } t^*_{max} \ge 2 \tag{2.7}$$

where

Θ_{max} is the maximum temperature in °C

t^* is defined in Equation (2.2)

$$t^*_{max} = \frac{0.2 \times 10^{-3} \cdot q_{t,d}}{O} \cdot \Gamma \qquad (2.8)$$

$q_{t,d}$ is the design fire load density related to the total surface area A_t

Γ is defined in Equation (2.3)

O is defined in Equation (2.3)

$x = 1.0$ for $t_{max} > t_{lim}$ or $x = \frac{t_{lim} \cdot \Gamma}{t^*_{max}}$ for $t_{max} = t_{lim}$

t_{lim} is the time for maximum gas temperature in case of fuel controlled fire

The values of t_{lim} in BS EN 1991-1-2 (CEN, 2002) are 25min, 20min and 15min for slow, medium and fast fire growth rates respectively.

It has been seen from the above equations that the natural (parametric) fire is a dependent on many factors, which makes it complicated to adopt in tests or simulations. Instead, the standard temperature-time fire curve presented in ISO 834 (ISO, 1999) and in BS 476: Part 20 (BSI, 1987) is used globally as a standardised fire curve for tests and simulations, which is described by the formula:

$$T = 345 log_{10}(8t + 1) + 20 \qquad (2.9)$$

where T is the gas temperature in °C and t is the time elapsed in minutes. Even though the temperatures generated standard fire curve cannot reflect the temperatures in real structural fire, it is still believed

reliable since there is only one variable and easy to control, and can provide structural behaviour under certain temperature.

2.2.2   Material degradation of steel at high temperature

Elevated temperature results in material degradation in common structural materials. For example, concrete loses its stiffness and strength under fire conditions, initiating at around 300°C caused by the thermal expansion rates difference in aggregates and cement matrix. However, because of concrete's very low thermal conductivity, the interior heats up much slower than the fire temperature, leading to a much slower rate of material degradation. Steel under elevated temperature starts to lose strength from around 300°C as well, then its strength decreases significantly from around 400°C up to around 800°C with a steady rate, after which its strength continues to reduce at a lower rate until its melting point at about 1500°C (Bailey, 1995). The residual strength at 800°C is only around 11% of its ambient temperature strength and 6% at 900°C (Burgess, 2002). In order to understand the behaviour of the steel and composite structures at high temperature, the temperature-dependent mechanical and thermal properties of steel need to be appreciated. The mechanical properties include strength, stiffness and ductility and the thermal properties include thermal expansion, specific heat and thermal conductivity.

In BS EN 1993-1-2 (CEN, 2005b), the degradation of steel strength and stiffness are described with reduction factors, as shown in Figure 2-2.

These reduction factors enable the generation of the residual strength and elastic stiffness which will then be adopted to produce the stress-strain relationship for carbon steel at a specific temperature. The general stress-strain relationship is presented in Figure 2-3. The stresses are calculated for each range of strain respectively up to 0.2 strain and are presented in Table 2-1.
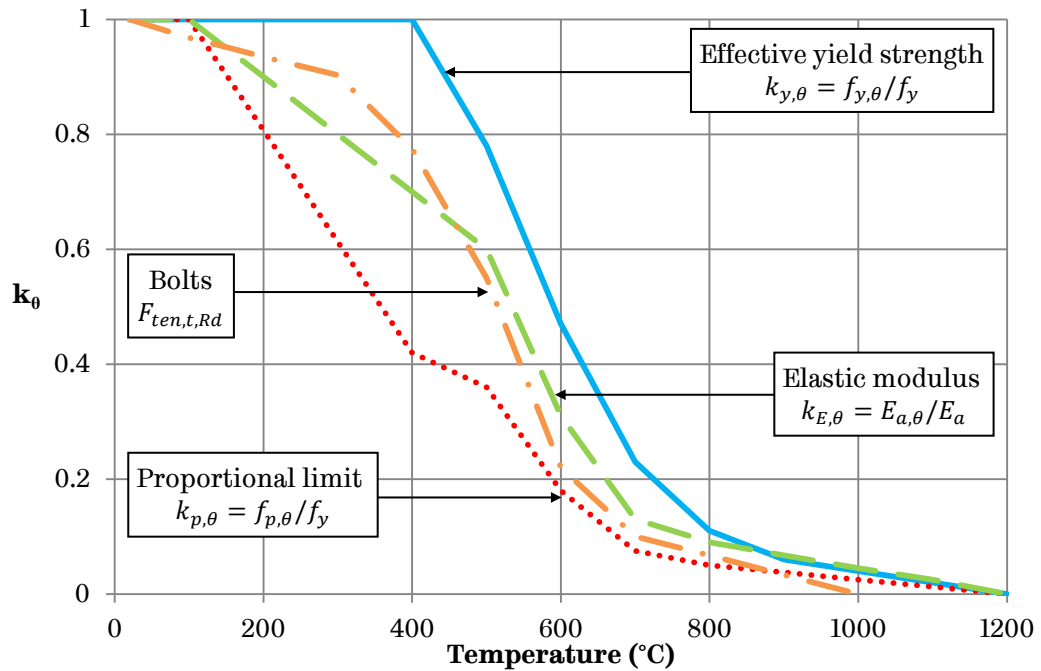
Figure 2-2 Strength reduction factors for structural steel and bolts at elevated temperature (CEN, 2005b)

Table 2-1 Stress-strain relationship for carbon steel at elevated temperature (CEN, 2005b)

Strain range	Stress σ
$\varepsilon \leq \varepsilon_{p,\theta}$	$\varepsilon E_{a,\theta}$
$\varepsilon_{p,\theta} < \varepsilon < \varepsilon_{y,\theta}$	$f_{p,\theta} - c + (b/a)\left[a^2 - \left(\varepsilon_{y,\theta} - \varepsilon\right)^2\right]^{0.5}$
$\varepsilon_{y,\theta} < \varepsilon < \varepsilon_{t,\theta}$	$f_{y,\theta}$
$\varepsilon_{t,\theta} < \varepsilon < \varepsilon_{u,\theta}$	$f_{y,\theta}\left[1 - \left(\varepsilon - \varepsilon_{t,\theta}\right)/(\varepsilon_{u,\theta - }\varepsilon_{t,\theta})\right]$
$\varepsilon = \varepsilon_{u,\theta}$	0

$f_{y,\theta}$	Effective yield strength
$f_{p,\theta}$	Proportional limit
$E_{a,\theta}$	Slope of the linear elastic range
$\varepsilon_{p,\theta} = f_{p,\theta}/E_{a,\theta}$	Strain at the proportional limit
$\varepsilon_{y,\theta} = 0.02$	Yield strain
$\varepsilon_{t,\theta} = 0.15$	Limiting strain for yield strength
$\varepsilon_{u,\theta} = 0.20$	Ultimate strain
θ_a	Steel temperature
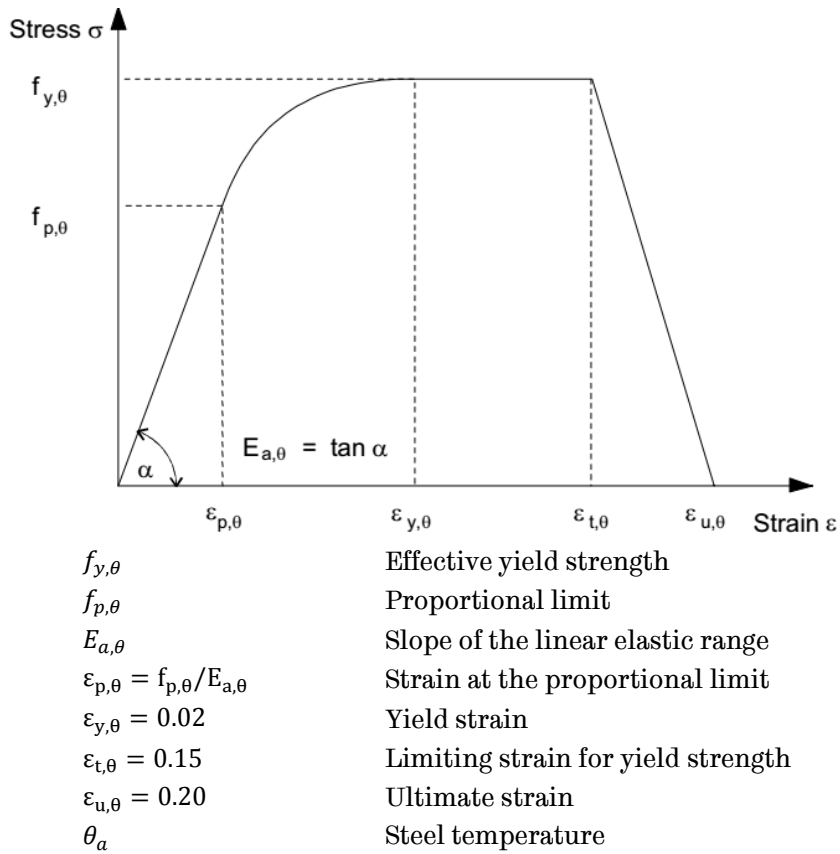
Figure 2-3 Stress-strain relationship for carbon steel at elevated temperature (CEN, 2005b)

a, b and c in the above formulae are parameter functions which are defined as:

$$a^2 = \left(\varepsilon_{y,\theta-}\varepsilon_{p,\theta}\right)\left(\varepsilon_{y,\theta-}\varepsilon_{p,\theta} + c/E_{a,\theta}\right)$$

$$b^2 = c\left(\varepsilon_{y,\theta-}\varepsilon_{p,\theta}\right)E_{a,\theta} + c^2$$

$$c^2 = \frac{\left(f_{y,\theta}-f_{p,\theta}\right)^2}{\left(\varepsilon_{y,\theta-}\varepsilon_{p,\theta}\right)E_{a,\theta}-2\left(f_{y,\theta}-f_{p,\theta}\right)}$$

A different set of reduction factors, $k_{b,\theta}$, shown in Figure 2-2, is provided in BS EN 1993-1-2 (CEN, 2005b) for the design tensile resistance of a single bolt under high temperature, $F_{ten,t,Rd}$, which is determined as:

$$F_{ten,t,Rd} = F_{t,Rd} k_{b,\theta} \frac{\gamma_{M2}}{\gamma_{M,fi}}$$

Conventionally, two test methods are adopted to determine the stress-strain relationships at high temperature: (a) steady-state test and (b) transient test. The steady-state test is conducted on specimens that are heated up to a specific temperature and then the stress-strain curve is generated for this pre-determined temperature. The transient test starts with loading the specimen to a specified load, followed by raising the temperature. The latter is the more realistic presentation of the actual stress-strain characteristics of structural members under elevated temperature, which is also the test method used in BS EN 1993-1-2 (CEN, 2005b).

The thermal expansion is defined in BS EN 1993-1-2 (CEN, 2005b) by a curve for three temperature ranges as shown in Figure 2-4. The plateau from 750°C to 860°C is caused by a phase-change in the steel crystal structure. When the steel absorbs energy and adopts a denser internal structure, the change in the expansion characteristics takes place (Lawson & Newman, 1996).

The specific heat of steel is the amount of heat stored in a unit mass of steel for 1°C temperature rise, in Joules. BS EN 1993-1-2 (CEN, 2005b) presents the specific heat of carbon steel as a function of temperature and is shown in Figure 2-5. A spike can be observed at around 750°C indicating a sudden increase in the specific heat of the material, which is also caused by the phase change mentioned in the last section.

$$l \quad \text{Length at 20°C}$$
$$\Delta l \quad \text{Temperature-induced expansion}$$
$$\theta_a \quad \text{Steel temperature}$$
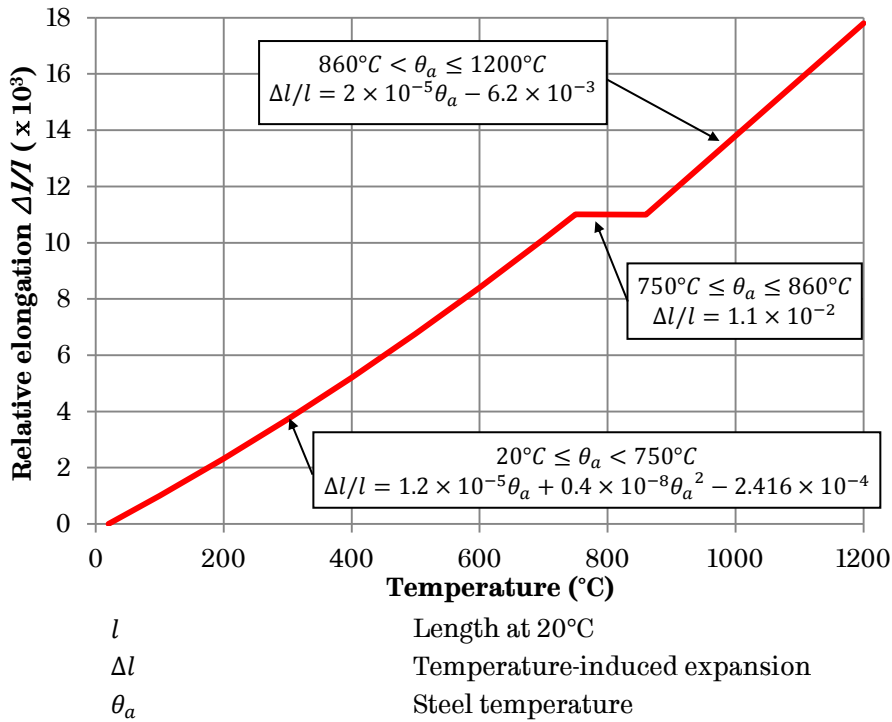
Figure 2-4 Relative thermal elongation of carbon steel (CEN, 2005b)

$$c_a \quad \text{Specific heat of steel in J/kgK}$$
$$\theta_a \quad \text{Steel temperature}$$
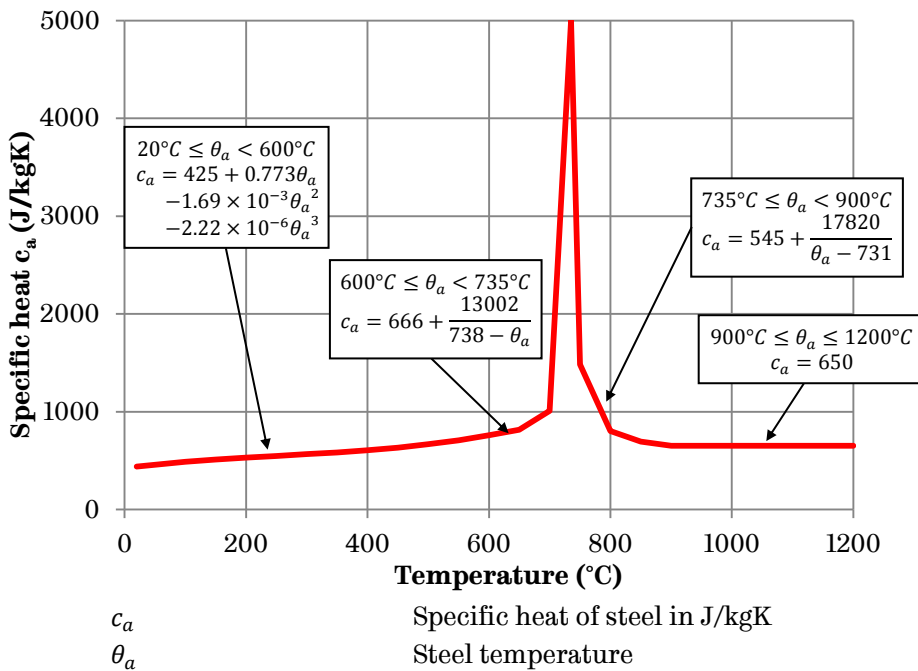
Figure 2-5 Specific heat of carbon steel as a function of the temperature (CEN, 2005b)

The thermal conductivity is the rate of heat energy transferred which passes through a unit cross-sectional area of material per unit temperature gradient, in Watts per meter Kelvin. According to BS EN

1993-1-2 and BS EN 1994-1-2 (CEN, 2005b, 2005d), the thermal conductivity at ambient temperature for steel is 54W/mK, which is much greater than that of concrete at 1.6W/mK. This means steel conducts heat much faster than concrete and heats up much more uniformely. The thermal conductivity of steel is a bi-linear function of temperature which is illustrated in Figure 2-6.

$$20°C \leq \theta_a < 800°C$$
$$\lambda_a = 54 - 3.33 \times 10^{-2}\theta_a$$

$$800°C \leq \theta_a \leq 1200°C$$
$$\lambda_a = 27.3$$

λ_a	Thermal conductivity of steel in W/mK
θ_a	Steel temperature
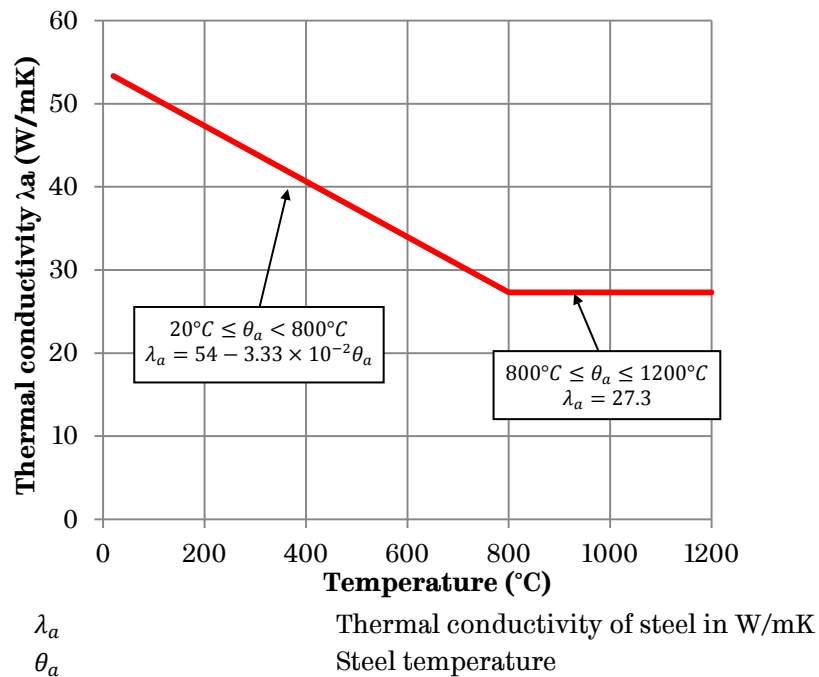
Figure 2-6 Thermal conductivity of carbon steel as a function of the temperature (CEN, 2005b)

2.3   Steel beam-to-column connections

2.3.1   Steel beam-to-column connections and classifications

Connections in steel and composite structures act as links between key structural elements. From large-scale fire tests and the collapse of WTC7, it has been suggested that connections are the weakest link

between structural elements (Yu, et al., 2007). Connections are traditionally designed and studied in terms of their moment-rotation behaviour solely under ambient temperature. At elevated temperature, however, it has been established through full-scale building fire tests that axial tying capacity of connections is distinctly important in keeping structural integrity (Burgess & Davison, 2012). As connections are attached to structural elements, under high temperature relatively large axial forces develop in the beams from (a) thermal expansion and later (b) axial displacement caused by vertical deflection.

Steel connections can be classified into three main categories – rigid, semi-rigid and pinned, according to their moment-rotation characteristics (CEN, 2005c). The connection's rotational stiffness is determined by the initial gradient of the moment-rotation curve. Conventionally, to simplify the analysis and design process connections are modelled as either extremely rigid (fully restrained, equivalent to a welded connection or a heavy, stiffened endplate) or extremely flexible (able to rotate freely, equivalent to a pinned connection). However, these two types do not represent the actual connection behaviour and what are used in practice are semi-rigid connections which have moment-rotation characteristics between the two extremes. Extremely flexible connections would show some degrees of rotational stiffness and extremely rigid connections would display some degrees of flexibility (Astaneh, 1989). Therefore, it is necessary to investigate the behaviour of semi-rigid connections, which
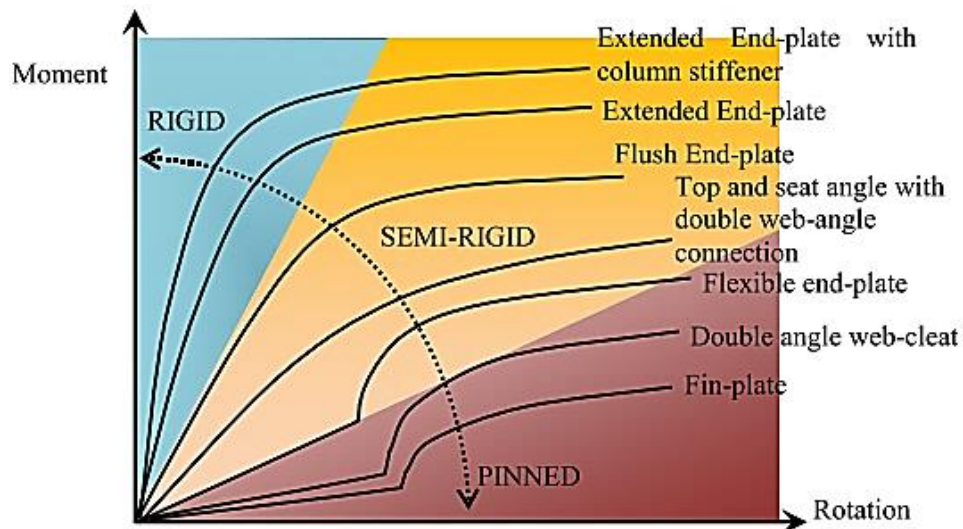
Figure 2-7 Conventional beam-to-column connections with stiffness classification (Taib, 2012)

are connections that have certain degrees of both axial and rotational stiffness. Models of these connections in frames can produce results that are closer to reality. Figure 2-7 shows the moment-rotation relationship of some conventional types of beam-to-column connections, ranging from rotationally rigid to pinned. In BS EN 1993-1-8 (CEN, 2005c), the boundaries of the connection classifications are defined as:

Rigid $\quad\quad S_{j,int} \geq \frac{k_b EI_{beam}}{L_{beam}}$

Pinned $\quad\quad S_{j,int} \leq \frac{0.5 EI_{beam}}{L_{beam}}$

where $k_b = 8$ for braced frames or $k_b = 25$ for other frames, I_{beam} is the second moment of area of a beam and L_{beam} is the span of a beam.

2.3.2 Connection performance under fire conditions

In current design practice, connections are treated as less vulnerable than the structural elements that they link together because (a) the

connections have the same level of protection as the linked members and (b) the temperature of the connections increase more slowly than the other structural members due to their relative mass and low exposed surface area. However, information from full-scale fire tests at the Building Research Establishment's Large Building Test Facility at Cardington (Newman, et al., 2006) as well as the World Trade Centre building collapses (FEMA, 2002a, 2002b; Shyam-Sunder, 2005; Gann, 2008) suggested otherwise. Due to the heating and cooling phases experienced by the whole frame during a fire, the connections are subjected to significant internal force redistributions, which make them more of a concern than expected (Burgess, 2008).

At ambient temperature, the moment-rotation behaviour is often used to describe the behaviour of the connection, including the connection's rotational stiffness, rotational ductility and moment capacity. But at elevated temperature, the robustness of the connection needs to be taken into the design consideration to ensure that the connections can provide structural integrity even as large rotational and translational deformations occur. When the frame heats up, the thermal expansion of the beam is restrained by the surrounding structure, causing compressive forces to be generated at the connections. While the temperature continues to increase, the compression is gradually lessened as the degradation of material strength and stiffness causes the beam to sag into large deflection. Eventually, at very high temperature when the bending stiffness of a beam is almost all lost, the

beam hangs in catenary action between its two end connections, pulling the connections inwards, thus exerting a tensile force on the connections. If the frame goes into a cooling phase from any temperature, the thermal contraction caused as the material cools and stiffens generates high tensile forces very quickly and the connections might be pulled inwards even further. Therefore even if a connection survives during the heat of a fire, it might fracture during the cooling stage possibly leading to progressive collapse putting the lives of firefighters and rescue workers in danger (Burgess, et al., 2012).

Investigations of the behaviour of various types of steel beam-to-column connections under elevated temperature have been undertaken during the last three decades. The understanding of the steel/composite frame buildings and their components has been significantly improved, especially with the help of the experimental work conducted.

Lawson (1990) carried out eight tests on beam-to-column connections, including five on non-composite beams, two on composite beams and one on a shelf-angle floor beam, under standard fire conditions to generate their moment capacities. Three types of connection were investigated in this project: extended endplate, flush endplate and double-sided web cleat connections. The results of these tests were used to generate the high-temperature time-rotation characteristics of connections, and highlighted that, even under significantly larger rotations than those at ambient temperature, the connecting bolts and

welds did not fail. However, Lawson's tests did not illustrate the full moment-rotation-temperature characteristics of the connections under high temperature adequately, due to lack of data recorded.

Leston-Jones (1997a) conducted eleven tests on steel/composite flush endplate connections under both ambient and fire conditions, which revealed that with rising temperature, both the stiffnesses and moment capacities of connections reduced. He also highlighted that between 500°C to 600°C steel temperature, significant reductions in capacities of the connections were observed. Results from these tests allowed the flush endplate connection moment-rotation characteristics to be constructed across a range of temperatures for the first time, representing well the full rotational behaviour of flush endplate connections in fire conditions. Despite the success of Leston-Jones's work, only small section sizes and one type of connection were considered.

Al-Jabri (1999), following Leston-Jones's work, expanded the investigations into the influences of parameters (section size, endplate thickness and failure mechanism) on the behaviour of both flush endplate and partial-depth endplate connections with eleven transient experiments (specimens initially loaded to a certain level, then heated according to a certain curve until failure takes place). Based on the results of these tests, a family of high-temperature moment-rotation characteristics was produced for each connection type. In addition, two

series of experiments on composite partial-depth endplate connections were carried out at both ambient and high temperatures to compare with results from non-composite versions of the same connections. The results suggested that at small rotation composite action contributed significantly to the moment capacity of the connections.

Spyrou (2002) and Spyrou et al. (2004a, 2004b) steered away from the moment-rotation characteristics of connections and performed 45 tests on T-stub assemblies and 29 tests on column webs to investigate the behaviour of the tension and compression zones of steel connections in fire. Three T-stub assembly failure mechanisms were identified from the test observations. Spyrou's work provided a very good starting point for component-based investigation and modelling of connections, but both shear or axial loads were neglected in the column web tests.

Following Spyrou's work, Block (2006) further investigated the effect of axial compressive load ratios in column webs on the behaviour of the column-web compression component under fire conditions. A group of force-displacement curves of column webs at elevated temperature were summarised, which were then adopted as validation data in further numerical simulations.

Wang et al. (2007) conducted four transient tests on structural subframes with extended endplate connections under fire conditions, to study the influences of rib stiffeners and the depth of the endplate on the fire resistance capacity of this type of connection. The results

indicated that both of these factors have some impact on the critical temperature of the extended endplate connections.

To investigate the behaviour and robustness of conventional connections in fire, the University of Sheffield and the University of Manchester collaborated to conduct a research programme. The part of the project conducted by the Sheffield team investigated four types of connections: flush endplate, partial-depth endplate, fin-plate and web cleat connections. Hu et al. (2008) studied partial-depth endplate connections and performed twelve experiments at both ambient and elevated temperature, with various combinations of vertical shear, axial tension and moment. The two-stage rotational behaviour and the contact between the beam bottom flange and the column flange at large rotation were observed, and indicated that the rupture of the endplate near the toe of the weld was the cause of the failure of partial-depth endplate connections. Yu et al. performed experimental work on fin-plate, web-cleat and flush endplate connections (2009a, 2009b, 2011) in this project, all under steady-state heating conditions (specimens initially heated to a certain temperature, then loaded until failure takes place). Fourteen tests on fin-plate connections with various combinations of tying and shear forces at three different high temperatures were conducted, including studies on the influences of bolt grade on the connection's behaviour. Results from the above tests showed that bolt shear controlled the failure of fin-plate connections, which highlighted that by adopting stronger bolts the resistance of the

connections could be increased significantly. Yu et al. also performed another fourteen tests on web cleat connections at elevated temperatures, again with various tying and shear force combinations. Results from this group of tests showed that the failure mode of web cleat connections was not as highly affected by the load combination as by the temperature level. Two main failure modes were captured in these tests, which were the web cleat fracture near the heel and the shear failure of the bolts that connect the cleats to the beam web. A final set of fifteen tests on flush endplate connections were performed with various combinations of axial and shear forces and rotation. The results of this set of tests demonstrated that the steel temperature was the key deciding factor of the connection failure mode rather than the ratio between the tying and shear forces. At lower temperatures, the endplate is the vital component to determine the failure mode of the connection, while at higher temperatures the bolts are the critical components. This project provided a large quantity of valuable data for the understanding of connection behaviour in fire and the development and validation of numerical models of these connection types.

Daryan and Yahyai (2009) adopted two types of top-and-seat-angle, beam-to-column connections to study their fire behaviour and resistance. The types chosen included layout with two additional web angles. The parameters such as the angle thickness and the existence of the two additional web angles were considered. Results from these tests revealed that the connection's fire resistance could be improved by

increasing angle thickness but not so much by adding the two web angles.

Huang et al. (2013a, 2013b) carried out a range of experiments on three types of connections between steel beams and composite columns (both filled and partially-concrete-encased) with combinations of large tying forces and rotations under elevated temperatures. The same test setup and instruments which were used in Yu et al.'s tests discussed above were adopted. The results from these tests suggested that reverse-channel connections achieved much higher ductility compared to flush endplates without sacrificing ultimate strength. The failure mode of the reverse-channel connections was generally web fracture. However they were also capable of large deformations in different patterns, depending on numerous factors such as the test temperature, channel type and physical dimensions.

It needs to be highlighted that some of these tests with scale-down and isolated members do not accurately represent the true behaviour of connections in buildings under fire conditions, due to the absence of the adjacent structure, which may provide significant restraint at high temperature. The physical dimensions of the furnaces used in these tests also restricted the sizes of the connections studied, which is another reason why these test results cannot be fully reliable when used for long-span structures with larger connections.

Sub-frame and full-scale fire tests were also carried out by Liu et al. (2002) and at the Building Research Establishment Cardington Laboratories (Swinden Technology Centre, 1999; Simoes da Silva & Santiago, 2005). Even though these tests provide valuable data on structural behaviour under fire, including aspects of both whole frame and structural element responses, the financial and time costs of designing and operating large scale tests cannot be ignored. It is therefore not possible to undertake experimental investigations on all occasions. Hence simulations which can provide reliable representations of the connection behaviours under elevated temperatures are in demand.

2.3.3 Simulations on the connection behaviour in fire

To increase understanding of the behaviour of the connections under both ambient and elevated temperatures, researchers have been working on developing numerical models to provide reliable data. During the development process, the approaches adopted can be classified into three main groups: (a) curve-fitting methods (b) finite element simulations and (c) Component Based Method models.

2.3.3.1 Curve-fitting method

The curve-fitting method, sometimes referred to as empirical approach, is used when experimental data is available to generate mathematical expressions which can fit the moment-rotation curves of the connections. Parameters chosen for the equations are ideally related to

the physical dimensions of the connections and their materials. This method was adopted by El-Rimawi et al. (1997) on describing the moment-rotation-temperature relationships of connections and modified the metal stress-strain relationship equation, which is a continuation of Ramberg and Osgood's work (1943); Leston-Jones (1997a) and Al-Jabri (1999) then adopted the modified Ramberg-Osgood stress-stain equation and used on semi-rigid connections in fire experimental data. Although this approach is relatively simple to conduct when compared with the other two approaches it has severe limitations due to the fact that the foundation of the curve-fitting method is experimental data. The generated mathematical equations can only be used for connections which have similar geometrical, material, loading scenario, temperature combinations as those investigated in the experiments, meaning any change in the frame or the connections may void the reliability of the results from the curve-fitting equations. Due to the high financial and time cost associated with conducting tests on numerous combinations of the above parameters, it is simply impractical.

2.3.3.2   Finite element modelling method

The finite element modelling method (using commercial packages such as *ABAQUS* and *ANSYS*) was developed in parallel with the curve-fitting method and has been extensively adopted by researchers due to its advantages compared with the curve-fitting method. Connections are

modelled as assemblies of 3D, finite sized solid, shell, wire and contact elements, which include the geometrical and material non-linearities of each component into the simulations. The contact elements in the finite element modelling method enable researchers to mimic the complicated interactions between component parts of the connections. Finite element modelling is much cheaper to conduct compared with experiments, and once a robust model is built, parametric studies can often be done with ease. This approach was adopted by Liu (1996, 1999) to create connection models with shell elements as the flanges and the webs, and beam elements as the bolts, which were validated against Lawson's tests on extended endplate connections (Lawson, 1990); Spyrou (2002) adopted finite element modelling approach to investigate the connection behaviour under high temperature by modelling the elements as 3D T-stubs, which produced closer correlation to tests data than using 2D analysis; Al-Jabri et al. (2006) modelled steel flush endplate connections in fire to generate their moment-rotation characteristics; Sarraj et al. (2007a) simulated the behaviour of fin-plate connections at elevated temperatures; Dai et al. (2010) proposed finite element models for connections on restrained beams with solid elements in fire, for fin-plate, partial endplate, web cleats, flush and extended endplates; Selamet and Garlock (2014) investigated the behaviour of three types of shear connections (single-plate, single-angle and double-angle connections) under fire conditions and found that the type of shear connections used does not have great influences on the

connection behaviour, but does have significant impact during the cooling stage due to the catenary action; Augusto et al. (2016) presented a model of double extended endplate connection and validated using test data, based on which a force-deformation characteristics of the column web components have been generated; and Haremza et al. (2016) proposed a method to predict composite endplate connection behaviour under moment and force combined loading in fire. There is no doubt that the finite element modelling approach can provide accurate predictions of the behaviour of the connections and frames under elevated temperature, but the lengthy computational time means the size of the models are often restricted to localized small-scaled model.

2.3.3.3   Component Based Method

The Component Based Method was proposed by Tschemmernegg and Humer (1988). In the Component Based Method appraoch, the connections are modelled as assemblies of a group of non-linear springs, which each represents an active component of the connection either in tension, compression or shear. The characteristics of the springs can include physical configurations, behaviour under ambient and high temperatures and loading-unloading properties of their corresponding components. Figure 2-8 shows an example of a flush endplate connection represented in its components form. The Component Based

Method approach has been adapted for structural fire engineering design from BS EN 1993-1-8 (CEN, 2005c).

CW-C	Column web in compression
CF-B	Column flange in bending
B-T	Bolt in tension
EP-B	Endplate in bending
CW-S	Column web in shear
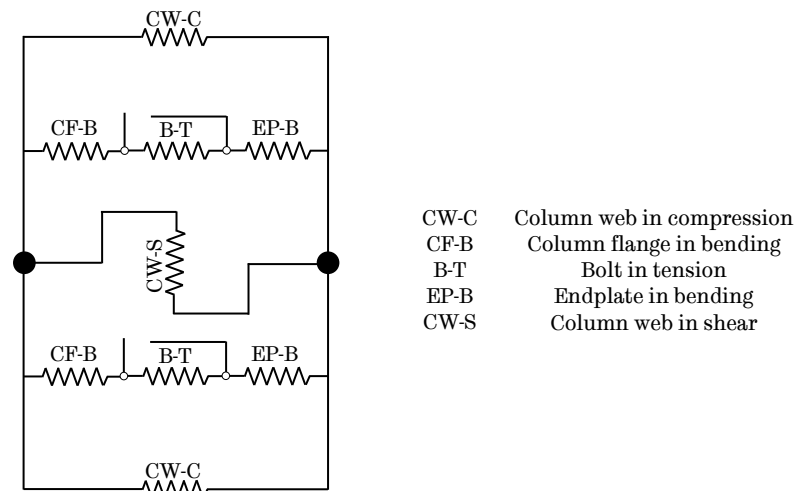
Component Based Method

Figure 2-8 Flush endplate connection in Component Based Method

The Component Based Method has been adopted and developed by many researchers. Leston-Jones (1997a) used Component Based Method on modelling his steel and composite connection tests; Al-Jabri (1999) modelled his tests on flexible endplate connection behaviour under elevated temperature with this method, but the moment-rotation characteristics were only modelled until the contact between the beam bottom flange and the column flange due to the shortage of test data; Simões da Silva et al. (2001) investigated and predicted the high temperature flush endplate connection behaviour using the Component Based Method appraoch; Spyrou (2002) established a model of flush endplate connection based on a large number of connection component tests which can be used to model tension and compression zones under both ambient and high temperature; Block et al. (2004,

2007) considered the connection in-plane behaviour in 3D frame analysis and the compression zone of the endplate connections; Hu et al. (2009a) developed a Component Based Method model for partial depth endplate connections for ambient and high temperatures and was able to simulate the moment-rotational behaviour of the connections before and after the beam bottom flange touched the column flange; Yu et al. (2009c) created a Component Based Method model for the web cleat connections under high temperature and validated against tests data; Ramli-Sulong et al. (2010) developed a high temperature Component Based Method connection model in the finite element software *ADAPTIC*; Dong et al. (2011, 2012, 2015) established a Component Based Method endplate connection model for simulations of steel frame behaviour in fire, including the connection ducitlity and failure so that progressive failure of the frame can be traced; Taib (2012) further developed the Component Based Method model for fin-plate connections so that it can predict their behaviours under fire; Gentili et al. (2014) proposed a mechanical model based on Component Based Method to simulate connections as assemblies of springs and rigid links, so that modelling of connections with different depth can be achieved by choosing the springs and rigid bars appropriately; and Sun et al. (2015) developed a static-dynamic solution process in *VULCAN* to enable the continuation of simulation when any parts of the connection fracture so that the progressive collapse can be monitored.

With the above information in mind, the Component Based connection model can be assembled in the following steps:

(1) Identification of the active components

According to Block (2006), those components that would affect the deformation or limit a connection's strength are called the active components. For example, bolts in tension can be called active components because they can contribute to the strength of the connection or be the limitation, depending on the relative strength of the bolts and other components.

(2) Assembly of the active components

With the general behaviour of each individual component known, a connection finite element model can then be built by representing each component with a translational spring. These springs are chained together linearly by rigid links; both the springs and the links do not have any physical length. After assembly, the component based model of the joint can be expressed as a collection of interlinked translational springs that are connected between the beam and the column.

(3) Specification of the component characteristics

After the spring assembly, their properties under fire can be assigned individually. Based on previous studies and experiments, the behaviour of each component can then be established using a simplified analytical model (Dong et al., 2012).

Normally the force-displacement characteristics are assigned to each spring.

Compared with the other modelling approaches, the Component Based Method models can produce accurate simulation results under fire conditions within a relatively shorter period of time. But again, due to the possible high numbers of springs each connection may contain, frame simulation with multiple connections is still very time-consuming to operate and not computationally efficient. There is a need for a simplified connection modelling approach that can enable the inclusion of a large number of connections in multi-bay frame analyses.

2.4 *VULCAN* – Finite element analysis package for structures in fire

VULCAN is a finite element software package developed specially for structures in fire at the University of Sheffield since the 1990s. It is used to simulate the behaviours of 2D or 3D steel and composite structures under elevated temperature. Originated from the finite element software *INSTAF* (2D steel frame behaviour analysis at ambinet temperature), Saab (1990) included the high temperature material stress-strain relationships, which was further developed by Najjar & Burgess (1996) to expand the usage of the programme to 3D steel frames. Bailey (1995) then included the analysis of the behaviour of semi-rigid

connections under fire conditions by implanting the spring elements. Huang et al. (1999a, 1999b, 2009) contributed greatly on the development of *VULCAN* so that simulations of 3D composite frame in fire can be conducted. A number of researchers implanted or improved component based connection elements in *VULCAN* for flush, extended and flexible endplate connections and web cleat connection, which have been reviewed in Section 2.3.3.3 (Spyrou, 2002; Block, 2006; Sarraj, 2007b; Hu, 2009b; Yu, et al., 2009c; Dong, et al., 2011; Taib, 2012). Sun (2012) also developed a hybrid static-dynamic solver for *VULCAN* and has been reviewed in Section 2.3.3.3. Tian (2014) proposed a penalty function method to analyse composite floor slabs under fire coditions to investigate the influences of tensile memberance action on the behaviour of the slabs. Quan et al. (2016) created a component based model of the beam web buckling zone which can show the beam-web shear buckling and the beam bottom flange buckling.

VULCAN was created based on the finite element modelling theory, which treats models as assemblies of beam/column, connection (spring), shear connector and layered floor slab elements. A fixed universal reference plane is assumed for various types of elements across any cross-section of the model, which is taken to be the mid-surface of the slab elements for composite structures or the centre of the beam cross-section for steel frames models without the slab. The beam elements, also used for columns, are modelled as 3-node line elements. In order to allow the user to apply temperature distribution or material property

variation, the beam/column element cross-sections can be divided into a number of segments according to user's preference. The 2-node spring elements are used in *VULCAN* to represent the connections and the user can define the springs to be fully rigid or pinned, or to be Ordinary Spring Elements (the translational and the rotational springs are connected linearly and work independently), or to be the Component Based connections. A combination of various spring types for one frame is achievable. The spring element has zero length, and its end nodes share the same boundary conditions as their connected beam or column elements. The slab elements will be introduced in Chapter 5 when composite frames are adopted for parametric studies. Both geometrical and material non-linearities can be included in *VULCAN* simulations.

Conventionally, frame simulations with connections modelled using the component based method are run in the static solver. The most concerned problem related to static solver is that once any spring in the connection model fails, the numerical problem may develop in the stiffness matrix and this may lead to numerical singularity and stop the analysis. However, one or more spring failures might not be equivalent to the failure of the entire connection. In order to conquer this problem to enable the continuity of the simulation, a dynamic solver was proposed by Sun (2012) and has been validated extensively. This hybrid static-dynamic solver allowed the behaviour of the structures in fire to be modelled starting with conventional static solver, switching to

dynamic solver whenever the instability is detected in the model, and then if equilibrium is acquired again, *VULCAN* switches back to the static solver. The end of this cyclic simulation terminates when the global failure of the frame is detected, which is indicated by the divergence of the kinetic energy over at large deflections over a number of time steps.

During the process of developing *VULCAN*, extensive experimental data and other resources have been employed to validate each improvement. *VULCAN* has also been used for a number of commercial projects to provide performance-based structural fire engineering solutions. Comparing with the detailed finite element modelling software *ABAQUS*, *VULCAN* is more time- and computationally- efficient in term of simulating the behaviour of both 2D steel and 3D composite frames under elevated temperature because it is a purpose-developed programme specialised in performing high temperature structural fire analysis. Hence *VULCAN* is chosen for this PhD research project and can provide reliable simulation results for the behaviour of steel/composite frames in fire.

2.5   Chapter conclusion

This chapter reviewed essential structural fire engineering knowledge including the use of fire curves to describe temperature development in a fire and the effects of high temperature on material mechanical

properties. As the main research objective of this project is to develop a simplified spring connection model in *VULCAN* and to investigate the effects of including connection axial and rotational ductility in frame analysis, the behaviour of steel beam-to-column connections at both ambient and elevated temperatures have been introduced together with relevant up-to-date research. The main modelling approaches for high-temperature connection performance were reviewed.

Steel beam-to-column connections play a vital role in keeping the whole frame intact and they influence greatly the fire resistance of the frame. Due to the shortcomings of the modelling methods reviewed in this chapter, a simpler yet reliable connection model needs to be created for multi-connection steel/composite 3D frame analysis. The desired connection model should closely resemble the behaviour of the connections under fire conditions and also be time and computationally efficient, which will be especially beneficial for 3D frame simulations when there multiple connections exist and/or the symmetry of the frame cannot be easily established.

3

Simulation of Steel Beam-to-Column Flush Endplate Connections under Elevated Temperature using *VULCAN* and *ABAQUS*

Page | 46

Page Intentionally Left Blank

3.1   Chapter introduction

The behaviour of steel beam-to-column connections can be modelled both under ambient and elevated temperatures using Finite Element Modelling (FEM) packages such as *VULCAN* and *ABAQUS*. There are currently two major modelling approaches in *VULCAN* for the above task: the Ordinary Spring Element Method and the Component Based Method. *ABAQUS* can be used for connection modelling when detailed connection configurations are provided, which makes it especially useful when test data is not available.

In this chapter, two main preliminary studies were conducted to investigate (a) the differences between the Ordinary Spring Element Method (OSE) and the Component Based Method (CBM) for connection modelling in *VULCAN*; and (b) suitable modelling techniques using *ABAQUS* for steel flush endplate connection modelling. Part (a) was conducted on a two-dimensional rugby goal-post frame which has flush endplate connections at both ends of the beam. The two connections were modelled as either assemblies of linked axial and rotational linear springs, which represent the axial and rotational characteristics of the connections independently (OSE), or as assemblies of multiple non-linear springs each of which corresponds to one active component of the connections in tension, compression, bending or shear (CBM). Three flush endplate connection configurations were adopted with the only difference being the bolt size, from M12, M20 to M36. The results

were then compared and the differences between the two modelling approaches were assessed. Part (b) consists of an *ABAQUS* finite element model of a flush endplate connection tested by Yu et al. (2008a). Test setup was presented in this part followed by details of the inputs for the *ABAQUS* simulation. A parametric study of the effect of the bolt stress-strain relationship on the connection behaviour was also carried out in this part. In these studies, the advantages and the disadvantages of the two FEM packages for steel beam-to-column connections were also explored. The results of this chapter highlighted the need for an innovative method for realistic sized flush endplate connections modelling when all of the existing methods failed to meet the requirement.

3.2   Modelling flush endplate connections in 2D frames using the Ordinary Spring Elements Method (OSE) and the Component Based Method (CBM) at elevated temperature

3.2.1   Model configurations

VULCAN can model semi-rigid steel beam-to-column connections using the Ordinary Spring Element Method (OSE) or the Component Based Method (CBM). In Section 3.2, a simple 2D rugby-goal post model was employed in order to investigate the differences between these two approaches in *VULCAN* with three bolt sizes (M12, M20 and M36).

The basic configurations of the 6m span rugby goal-post model adopted in this study are shown in Figure 3-1 with the details of the connection illustrated in Figure 3-2. The two beam-to-column connections are represented using two zero-length boxes at the ends of the beam. These two connections were modelled using the Component Based Method and Ordinary Spring Element Method and the details are shown in Figure 3-3. In the Ordinary Spring Element Method, the connection is simulated as one translational spring interlinking with one rotational spring to represent the axial and rotational behaviour of the connections respectively. For the Component Based Method, the overall connection's translational and rotational stiffnesses are based on the combination of the linear springs, which represent each individual element, as illustrated in Figure 3-3. In order to implement component based connection model into *VULCAN*, it is necessary to provide detailed connection geometrical information. For both models, UB305×165×54 and UC254×254×89 in steel grade S355 were chosen as beams and columns respectively. The bolts were all in property class 8.8 and their sizes were changed from M20, which is the recommended bolt size for the depth of the beam in the Green Book (UK Connections Group, 2015) to a smaller size of M12 and a larger size of M36 in both models. A gravity point load of 100kN was applied to the centre of the beam. As these were 2D models, out-of-plane deflection and rotation was not permitted. Both of the column bases were fixed, i.e. they were restrained in all directions axially and rotationally, while the column

tops were allowed to move vertically and rotate about the y-axis only. The fire curve adopted in this model was ISO 834 (1999) standard fire curve, with temperature patterns of 'top flange–web–bottom flange'
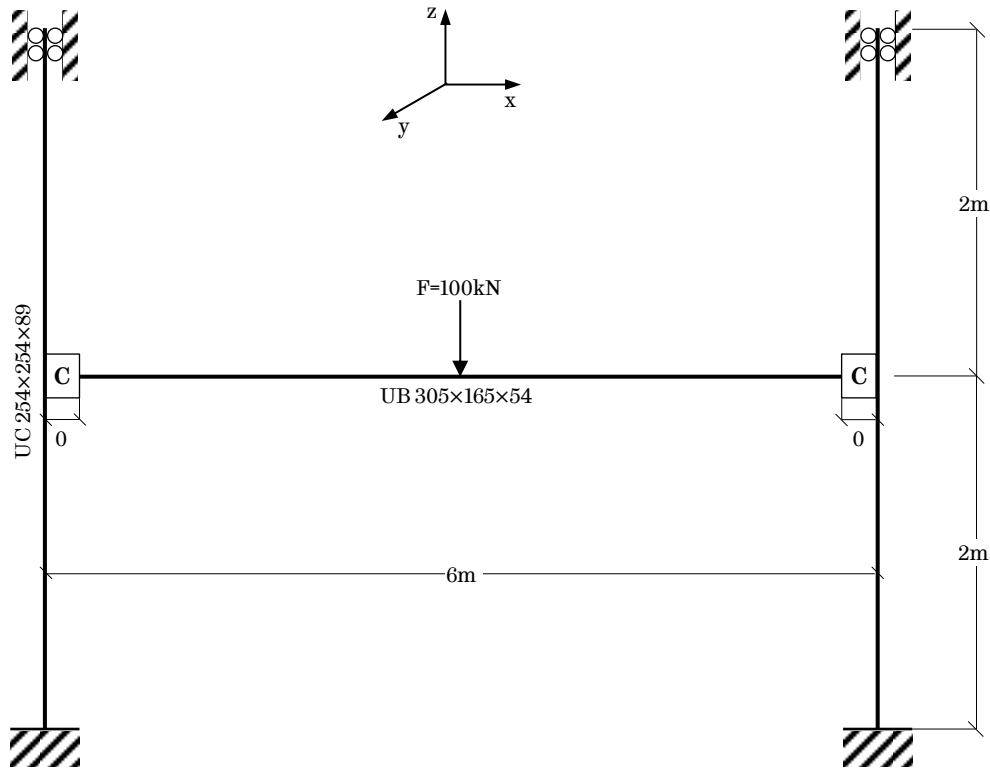
Figure 3-1 Two-dimensional rugby goal-post frame
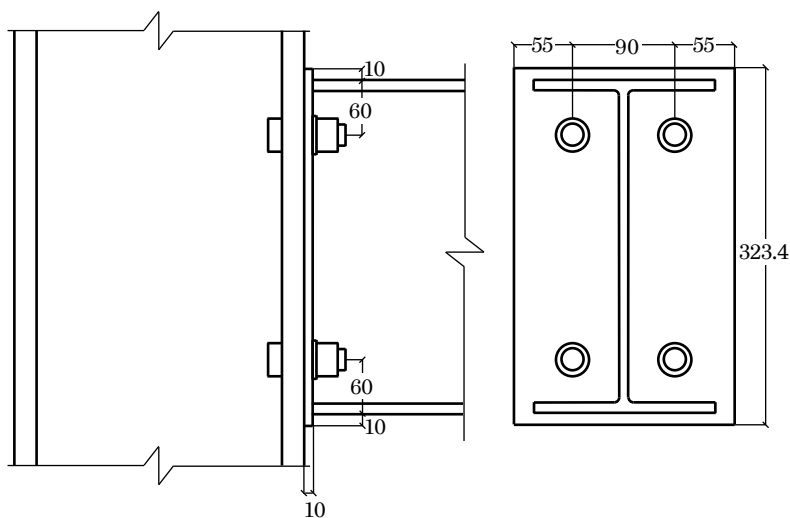
Figure 3-2 Flush endplate test specimen detailed configurations (unit: mm)
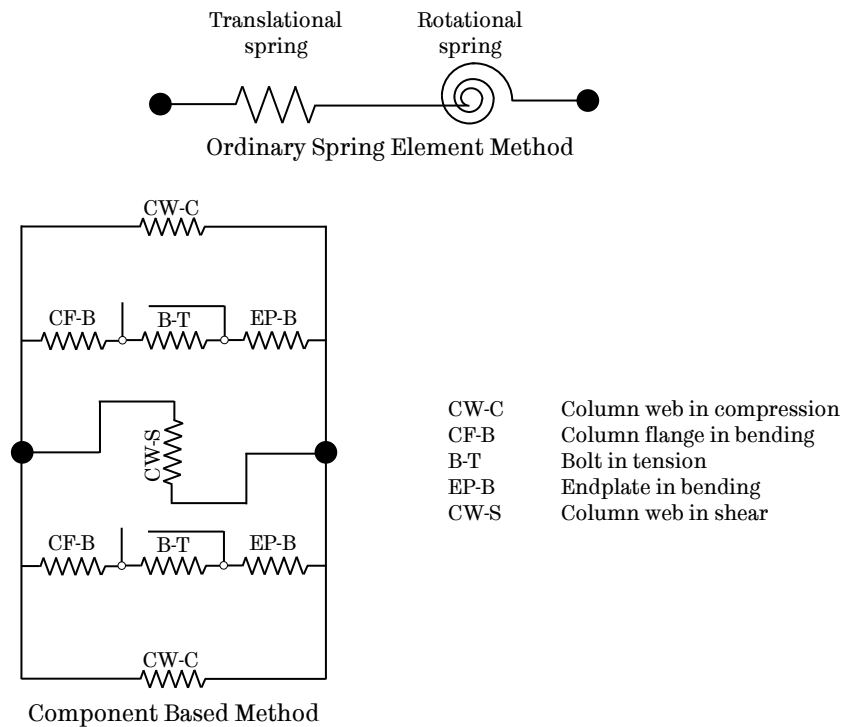
Figure 3-3 Connection modelling approaches in *VULCAN*

(reduction factors: 0.8–1.0–1.0) for the un-protected beam, 'uniform' distribution for the top columns (ambient temperature) and the bottom columns (reduction factor: 0.7). In order to conduct the study with different bolt sizes, a range of input parameters in *VULCAN* needed to be amended. For the Ordinary Spring Element Method used in the commercial version and research version of *VULCAN*, linear translational and rotational spring stiffnesses were calculated and input into the software to represent the connections. A sample calculation of the two stiffnesses based on the M20 bolt model is presented in Appendix. The equivalent translational and rotational stiffness of the three bolt sizes are summarised in Table 3-1. For the Component Based Method, various bolt sizes were considered by

changing a series of input data related to the bolts in the *VULCAN* research version, which are presented in Table 3-2 based on data in BS EN ISO 7091, BS EN ISO 4014, BS EN ISO 4032 and BS EN ISO 898-1 (BSI, 2000, 2011, 2012, 2013).

Table 3-1 Equivalent translational and rotational stiffness of various bolt sizes

Bolt size	Equivalent translational stiffness (N/mm)	Equivalent rotational stiffness (Nmm/rad)
M12	6.44×10^5	2.52×10^{10}
M20	1.19×10^6	4.22×10^{10}
M36	2.06×10^6	6.27×10^{10}

Table 3-2 Amended parameters for various bolt sizes (units: mm or mm^2)

Input parameter		Bolt size		
		M12	M20	M36
washerdia	washer outer diameter	24	37	66
washerthick	washer thickness	2.5	3	5
boltarea	bolt nominal stress area	84.3	245	817
boltthick	bolt head thickness	7.5	12.5	22.5
nutthick	nut thickness	108	18	31

3.2.2 Results comparisons and discussions

Investigation results are revealed in Figure 3-4, Figure 3-5 and Figure 3-6. For each model with a different bolt size, graphs of the mid-span deflection and the axial force at the connection are plotted against the beam bottom flange temperature based on results from the modelling approaches: Component Based Method (CBM), Ordinary Spring Element Method in *VULCAN*. The tensile strength of beam and connection are also presented for comparison.

It can be seen that by using the Ordinary Spring Element Method the results are less conservative in general i.e. either stopped at higher temperature or finished all given temperature steps. This is because this approach cannot detect whether any part of the connection has

fractured and also the translational and rotational springs inputted were linear; it is not possible to include non-linear behaviour of individual connection components using the OSE method.

The advantage of using the Component Based Method is that it can detect any failed connection component and exclude its contribution to the stiffness of the connection, hence the results from the three models using the Component Based Method stopped when both of the bolt rows were fractured. By relating to what would have happened in reality, at this stage there would no longer be any physical connection between the endplate and the column flange, therefore the simulation stopped due to this discontinuity. By observing the connection axial force plots, it can be seen that both modelling approaches are capable of modelling the tension on the connection during initial loading at ambient temperature which was caused by the beam trying to pull the connections inwards. In reality, when heating starts material degradation causes increasing tension in the connections. At the same time, due to the thermal expansion the beam-ends push the connections outwards, which compensate some of the tension caused by material degradation. As temperature rises further, the thermal expansion becomes dominant and the whole connection would go into compression. Eventually the beam would lose so much of its strength and stiffness that it would hang like a cable between the connections (beam catenary behaviour), negating the compression on the connections. But it can be seen clearly from the connection axial force

(a)

(b)
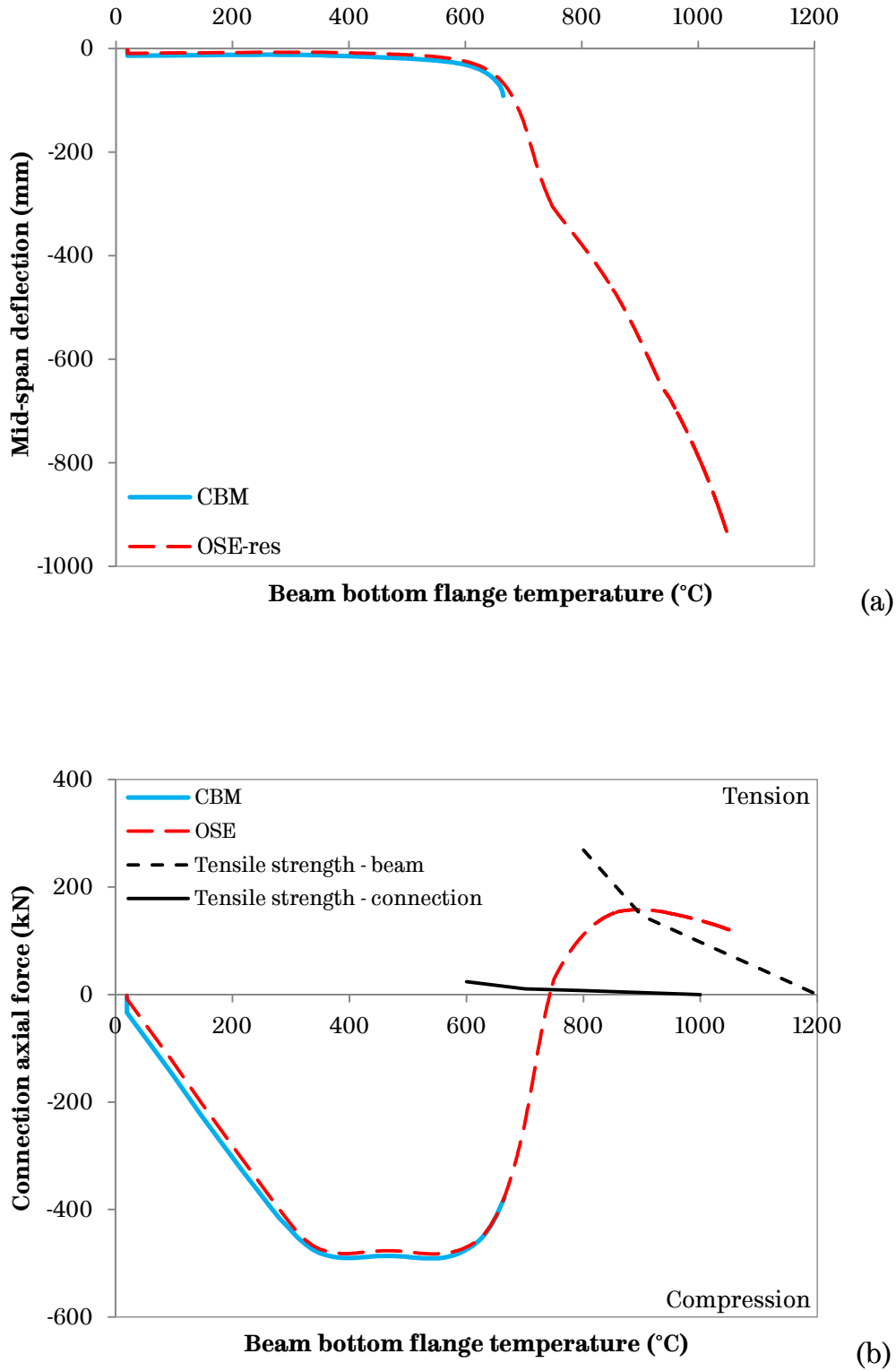
Figure 3-4 Result comparisons of frame with M12 bolts

(a) Mid-span deflection comparisons
(b) Connection axial force comparisons

(a)

(b)
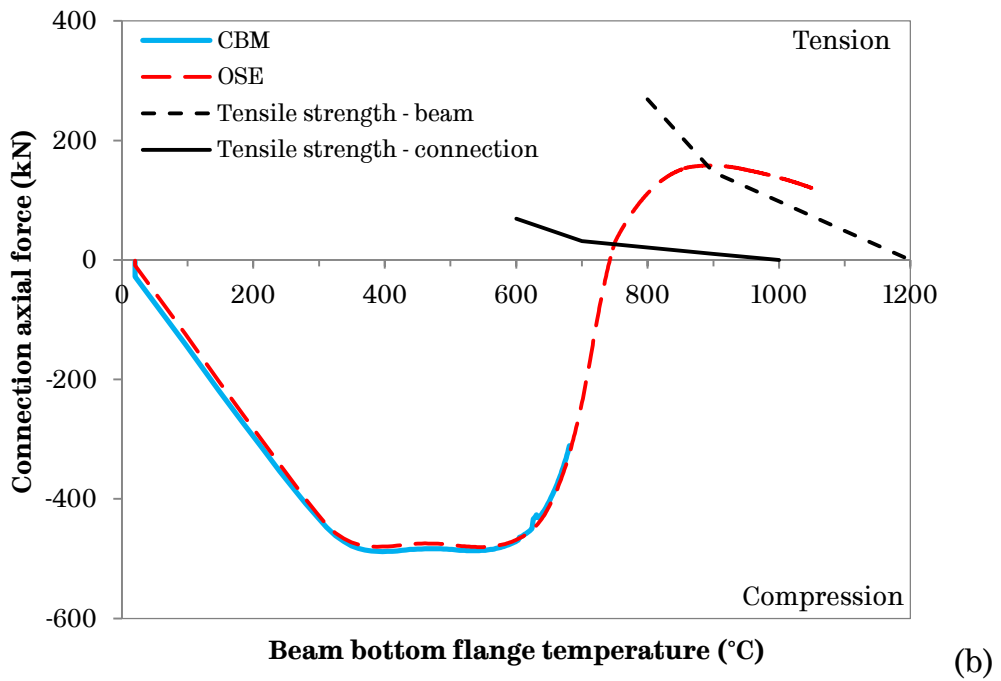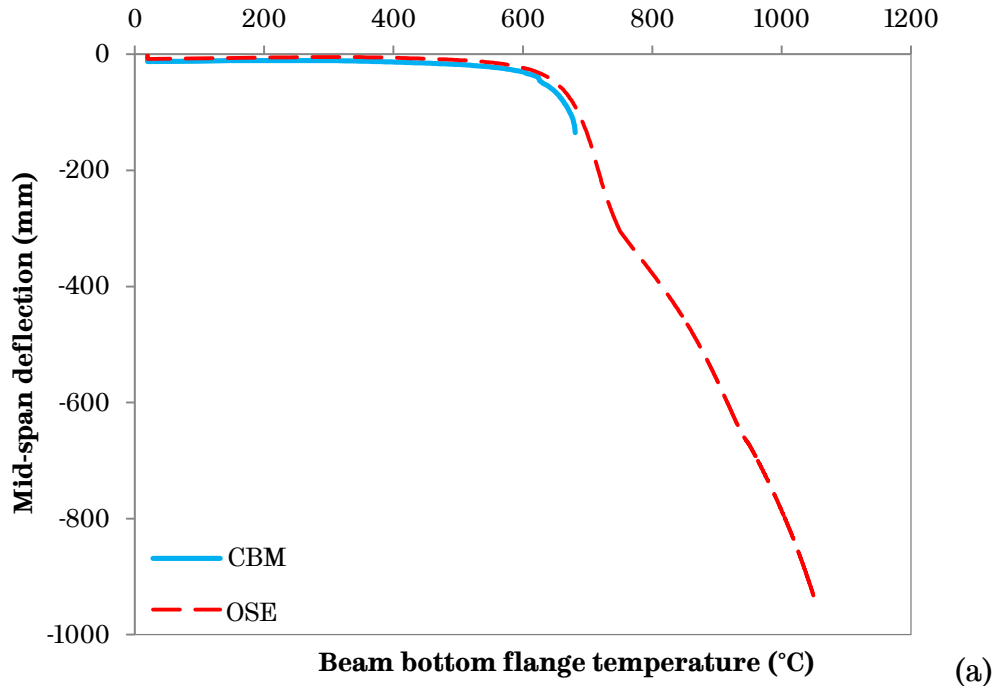
Figure 3-5 Result comparisons of frame with M20 bolts

(a) Mid-span deflection comparisons
(b) Connection axial force comparisons

(a)

(b)
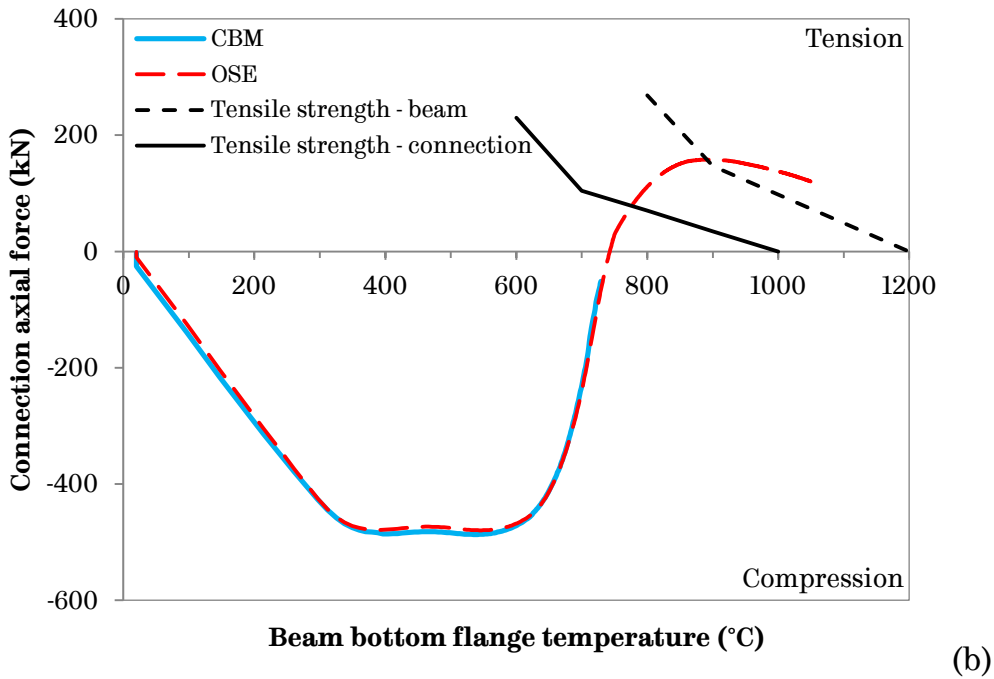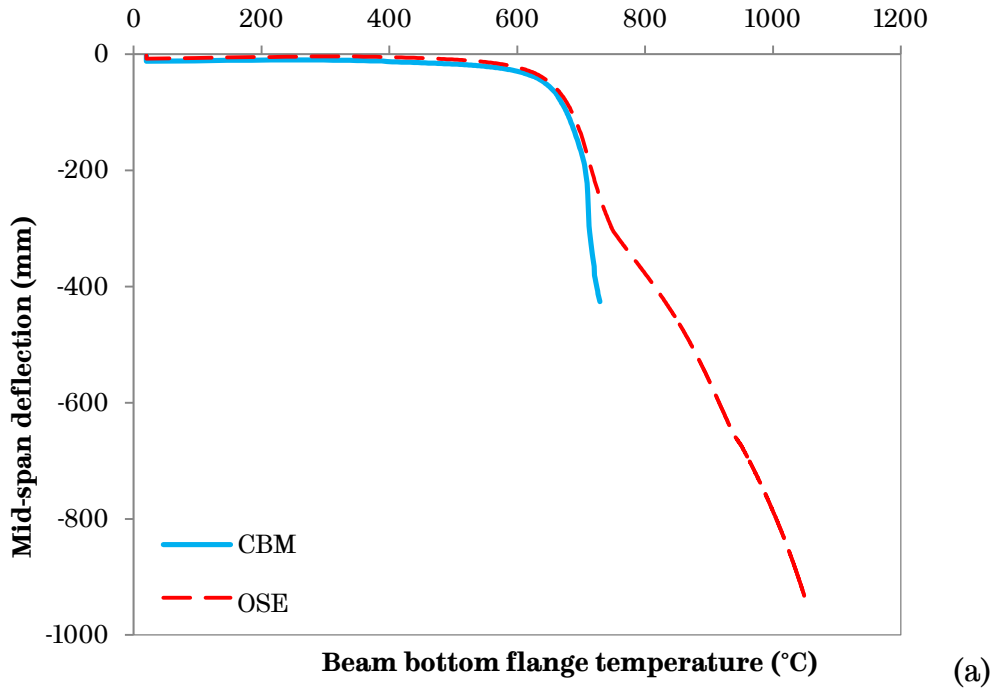
Figure 3-6 Result comparisons of frame with M36 bolts

(a) Mid-span deflection comparisons
(b) Connection axial force comparisons

plots that models using Ordinary Spring Element Method predicted the connections were capable of resisting the maximum compressions on them and the simulations stopped due to large beam deformation, while models using the Component Based Method indicated that the connections failed before reaching tension region resulting a 'run-away' failure of the frame. It is again shown that results from the Component Based Method are more conservative and this method captures the behaviour of the connections more closely to the reality by including material and geometrical non-linearity and failure of connection components.

Despite the advantages of the Component Based Method in modelling steel beam-to-column connections compared to the Ordinary Spring Element Method, the restriction of the current connection models in *VULCAN* needs to be highlighted. For flush endplate connections, the maximum number of bolt rows that *VULCAN* can simulate is five. According to the Green Book capacity table (UK Connections Group, 1995), the maximum beam depth of S355 or S275 steel for flush endplate with five bolt rows or less is UB610 series. This issue can be solved by develop and expand the current version *VULCAN*, which will required good understanding of the existing *VULCAN* code. On top of the above issue, the computational time when using the Component Based Method was high considering the limited size of the frame adopted in this study. This is due to the complex interactions among the individual springs and the non-linearity of each spring. The popularity

of long-span structures necessitates the use of deeper beams and larger connections than the current *VULCAN* research code is able to handle. Thus an innovative modelling approach needs to be developed.

3.3 Finite element modelling of flush endplate connections at elevated temperature

3.3.1 Test setup

A flush endplate connection test conducted by Yu (2008a) was modelled using finite element package *ABAQUS* to verify that this package can provide reliable simulation results for validation. This test was part of a collaborative research project by the University of Sheffield and the University of Manchester during 2005–2008 to investigate the tying capacity and ductility of steel beam-to-column connections at elevated temperatures (Yu, et al., 2008a). Four conventional types of connections in total were tested, including flush endplates, flexible endplates, fin plates and web cleats. For each test configuration, various combinations of temperatures and loading angles were. With different loading angles, a range of combinations of tying and shear forces can be achieved (Yu et al., 2008a, 2008b, 2009a, 2009b, 2009c and 2011; Hu et al., 2009; Dai et al., 2009a, 2009b, 2010a and 2010b).

Yu's tests were conducted at the University of Sheffield under high constant temperature. This was achieved by placing the test specimens in a electric furnace to heat up and the temperature was kept

unchanged thoughout the whole test process. A general test setup is presented in Figure 3-7. The steel beam-to-column connection was held in the centre of the furnace by a UC 203×203×86 support beam on the column flange, together with two Macalloy bars (Grade 1030) linking the top of the column to the reaction frame. The test specimens were loaded through a specially designed articulated loading device which consisted of three Macalloy bars (26.5mm diameter): the furnace bar, the link bar and the jack bar. These three bars were all pin-connected to a central node. The furnace bar was pin-connected to the beam end loading piece and formed an angle between the furnace bar and the centreline of the beam, α, which determines the combination of the shear and tying force applied to the connection. A desired load angle α was difficult to achieved due to the equipment arrangement, therefore the actual initial loading angle was recorded and compared with the final loading angle, to generate the total rotation during the tests. In order for the furnace bar to move freely with large rotation, the whole test specimen was rotated anti-clockwise by 25°. The link bar was pin-connected to the reaction frame to support the loading device. The jack bar was pin-connected to the top of the load jack. During the tests, the displacement controlled load jack moved downwards to produce inclined tensile force, which then transferred through the furnace bar to the connection. The specially designed loading device enabled large rotation to be achieved during the tests. In total 17 tests were conducted on flush endplate connections with UB305×165×40 in steel

grade S355 as the beam while UC254×254×89 in steel grade S355 as the column. The bolts were all M20 class 8.8 structural bolts. Four parameters were studied during these tests, inlcuding the temerature (20°C, 450°C, 550°C and 650°C), the load angle α (35°, 45° and 55°), the endplate thickness (8mm, 10mm and 15mm) and the number of bolt rows (2 and 3 bolt rows) (Yu, et al., 2008a).
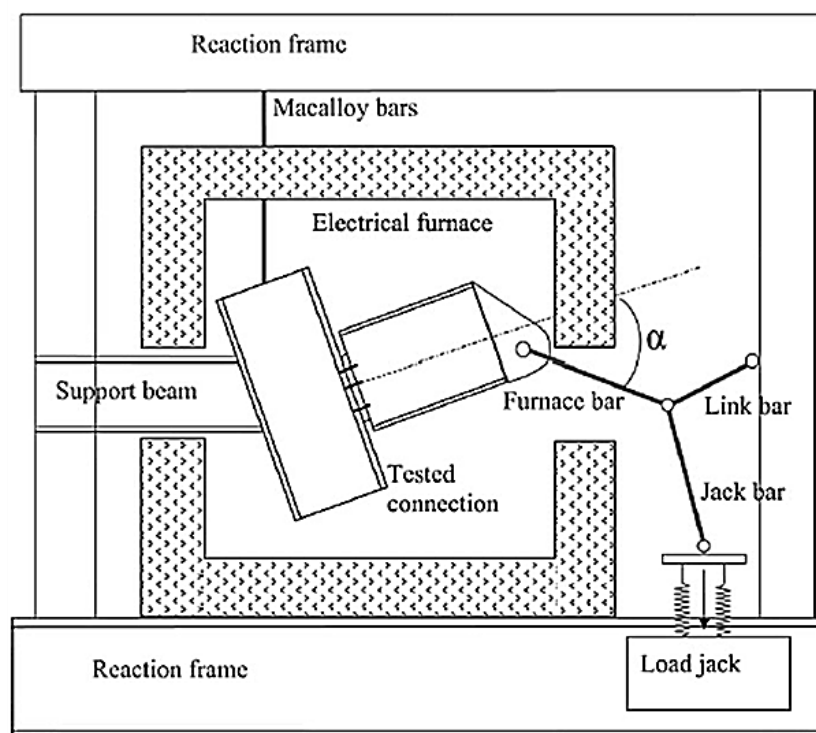
Figure 3-7 Test setup by Yu et al. (2009a)

3.3.2   Model configurations

3.3.2.1   Geometry

For this study, the test conducted at 550°C, 35° load angle on a three bolt rowed connection with 8mm thick endplate was chosen. The detailed test specimen configurations are shown in Figure 3-8. To resemble the actual test specimens, the model was tiltled above the

horizontal axis by 25°. The angle of the furnace bar can be adjusted to provide desired initial loading angle, α. Due to the symmetry of the connection about its vertical axis, only half of connection and the loading block were simulated. The symmetry was achieved by using appropriate boundary conditions on the symmetrical surfaces of each part of the model. The model consisted of: a beam stub, a column flange, a full length flush endplate, three bolt assemblies, a rigid plate, a loading block and three wire elements representing the furnace bar, the link bar and the jack bar (Figure 3-9). In this model, only the column flange was modelled rather than the entire column section. This is because when compared to the beam section, the column section was very stiff thus its deformation can be neglected. The bolt assemblies were modelled as one integrated element as thread stripping was neglected, which included a bolt head, a bolt shank, a washer and a nut each. The threads were not included in this simulation to save computational time, hence the diameter of the unthreaded shank needed to be calculated. According to ISO 898-1 (BSI, 2013) and BS 3643-1 (BSI, 1981), the nominal stress area for bolts, $A_{s,nom}$, are calculated from an average of the basic pitch diameter (d_2) and the minor diameter (d_3, $d_3 = d_1 - \frac{H}{6}$, d_1 is the basic minor diameter and H is the height of the fundamental triangle) of the bolt external thread as labelled in Figure 3-10. Thus it was reasonable to use $A_{s,nom}$ to calculate the diameters of unthreaded shanks in the model which were equivalent to the threaded ones. For M24 bolts $A_{s,nom}$ is 353mm^2 and $d_b = \sqrt{(4A_{s,nom}))/\pi} \approx 21.2$mm.
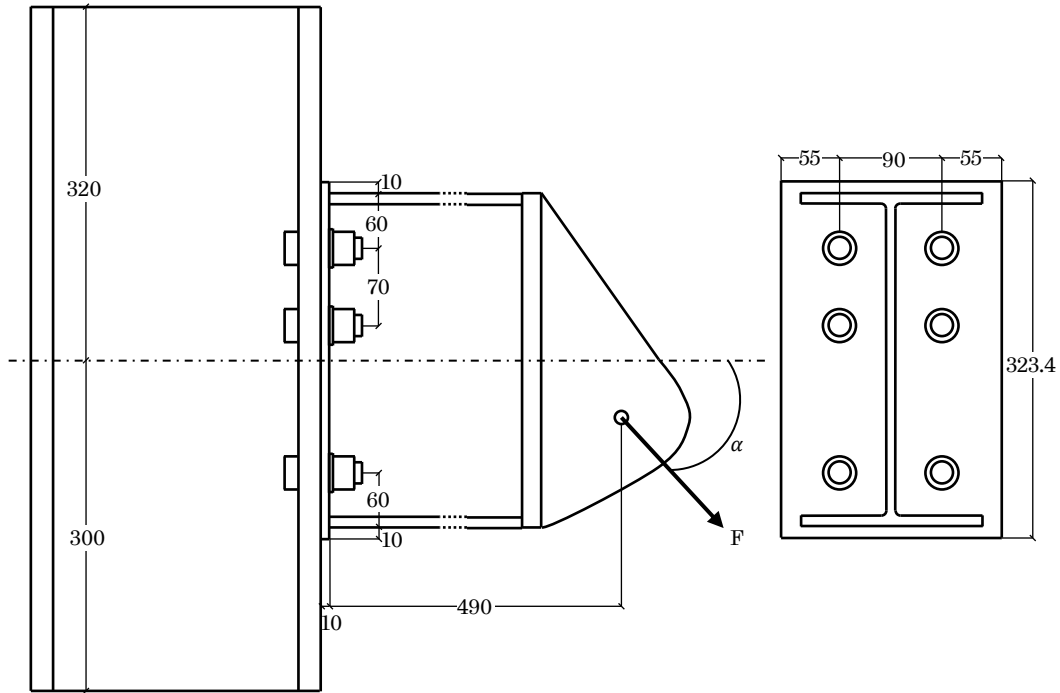
Figure 3-8 Flush endplate test specimen detailed configurations
(units: mm)
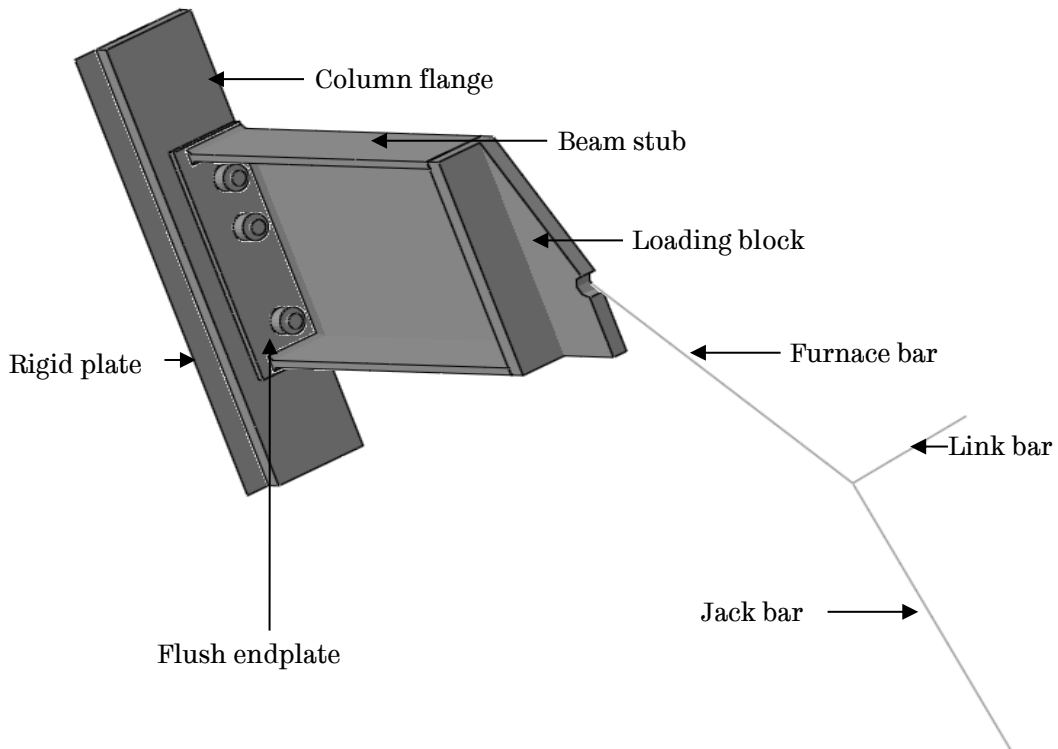
Figure 3-9 3D flush endplate connection detailed model in *ABAQUS*

The bolt holes were assumed to be 2mm greater than the diameter of the bolt shanks. All parts were modelled as solid elements apart from the rigid plate, which was modelled using discrete rigid shell element.
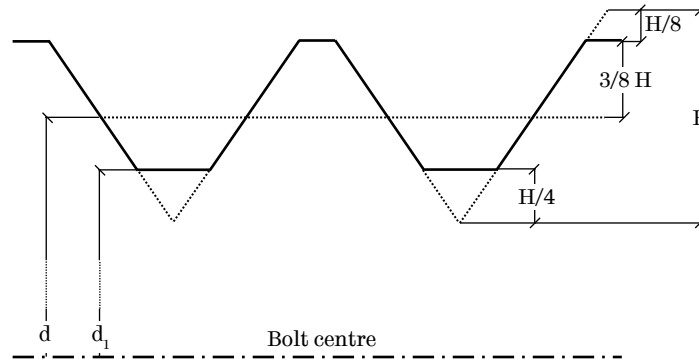
$$A_{s,nom} = \frac{\pi}{4}\left(\frac{d_2+d_3}{2}\right)^2 \quad d_3 = d_1 - \frac{H}{6}$$

Figure 3-10 Basic thread geometry for the modelled bolt diameter calculation

3.3.2.2 Material properties

Density and Poisson's ratio were assumed to be independent of temperature with values of 7850kg/m^3 and 0.3 respectively.

To model the high constant temperature at 550°C used in the tests, the temperature field function in *ABAQUS* has been adopted. High constant temperature affects material properties in simulations and only 500°C and 600°C material properties were available; the temperature field enabled *ABAQUS* to read in the available data and extrapolate desired material properties for 550°C. This is not the best method as material properties do not change linearly with elevated temperatures, especially under such high temperature, but with limited source of material properties it is legitimate to do so. Temperature field was

applied to parts which were temperature affected, such as the endplate, the column and the beam, but because bolts data at 550°C was available, a temperature field was not applied to them.

According to the method introduced above, material properties at 500°C and 600°C for the steel sections and the bolts are required. The material coupon tests were only conducted at ambient temperature and the key results are shown in Table 3-3. In order to generate material properties at 550°C, a suitable approximation model was required. The material model proposed in BS EN 1993-1-2 (CEN, 2005b) is not intended to be used for steady-state conditions, therefore, test results by Renner (2005) were adopted. Renner's material model was created based on the test results on structural steel at high constant temperatures, which provided reduction factors for Young's Modulus (E_T), plastic stress (σ_{pl}) and plastic strain (ε_{pl}) up to 700°C at 100°C intervals. The plastic stress was given in the format of a ratio between the plastic stress (σ_{pl}) and the yield stress at ambient temperature (f_y), which are partially presented for 20°C, 500°C and 600°C in Table 3-4. Steel material properties listed in Table 3-3 can then be used to derive desired data and these are summarised in Figure 3-11.

The Grade 8.8 M20 bolt material properties at 550°C are available from Bull (2014). Bull conducted a series of bolt uniaxial tensile tests on machined down property class 8.8 M20 bolts to obtain stress-strain behaviour under various loading rates at elevated temperature. From

Table 3-3 Steel material properties at ambient temperature (Yu, et al., 2009b)

Part	Young's modulus E (kN/mm^2)	Yield stress f_y (kN)	Ultimate stress f_u (kN)
Beam/Endplate	134.62	350	455
Column	176.35	355	502

Table 3-4 Renner's material model at 20 °C, 500°C and 600 °C (Renner, 2005)

20°C		500°C, $E_T = 0.437E$		600°C, $E_T = 0.278E$	
ε_{pl}	σ_{pl}	ε_{pl}	σ_{pl}/f_y	ε_{pl}	σ_{pl}/f_y
0	f_y	0.0000	0.361	0.0000	0.230
0.0116	$f_u + 0.5(f_u - f_y)$	0.0025	0.501	0.0009	0.268
0.0286	$f_u + 0.75(f_u - f_y)$	0.0068	0.562	0.0114	0.310
0.0786	f_u	0.0156	0.618	0.0284	0.331
0.1986	f_u	0.0270	0.652	0.0551	0.336
		0.0467	0.668	0.1072	0.337
		0.0843	0.678	0.1804	0.335
		0.1238	0.677	0.2420	0.333
		0.1643	0.675	0.2729	0.332
		0.1856	0.675	0.3040	0.328
		0.2196	0.671	0.3348	0.313
		0.2503	0.667	0.3597	0.299
		0.2690	0.649	0.3903	0.285
		0.2778	0.627	0.4274	0.255
		0.2899	0.582	0.4519	0.231
		0.2994	0.532	0.4937	0.121
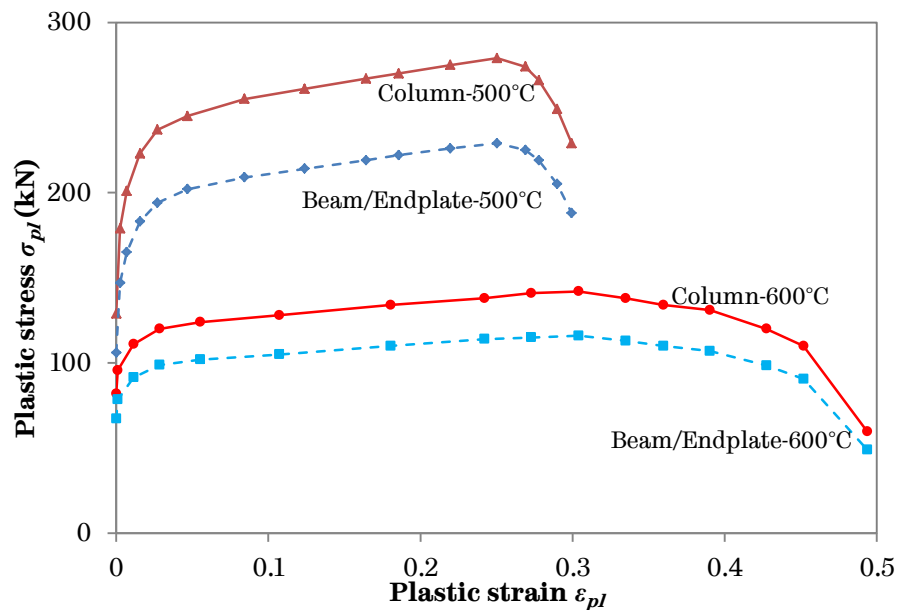
Figure 3-11 Steel plastic stress - plastic strain at 500 °C and 600 °C generated from Renner's material model

Bull's test results, the test which was loaded at a strain-rate of 0.002/min was chosen. (Detailed studies on the reason why this set of

results were chosen will be presented in the Section 3.3.4, together with a study on the Grade 8.8 bolt material properties.) The stress-strain relationship provided needed to be transformed into true stress-strain, which *ABAQUS* needs. Before necking, this can be achieved using the following formulae

$$\sigma_T = \sigma_E(1 + \varepsilon_E) \tag{3.1}$$

$$\varepsilon_T = \ln(1 + \varepsilon_E) \tag{3.2}$$

where subscripts '*T*' indicates true stress/strain and '*E*' indicates engineering stress/strain. However, after the necking point these formulae are not suitable due to the reduction in specimen's cross-sectional area. Unfortunately, the reduction was not recorded in Bull's tests, thus a 'corrected' true stress-strain curve needed to be created. Based on the material mechanics, this part of the curve can be approximated by

$$\sigma_T = K\varepsilon_T^n \tag{3.3}$$

where K is strength coefficient and n is work-hardening exponent (Callister & Rethwisch, 2007). Both K and n vary depending upon material type, fabrication method and condition. For mild steel, K is approximately 1000MPa and n can range from 0.1 to 0.5. Take the common logarithm of both sides of equation 3.3,

$$log\sigma = n \cdot log\varepsilon + logK \tag{3.4}$$

It can be seen that n is the gradient of log true stress vs. log true strain plot up to the maximum load. Thus n can also be written as

$$n = \frac{\Delta log\sigma}{\Delta log\varepsilon} = \frac{log\sigma_F - log\sigma_U}{log\varepsilon_F - log\varepsilon_U} \qquad (3.5)$$

$$log\sigma_F = n(log\varepsilon_F - log\varepsilon_U) + log\sigma_U \qquad (3.6)$$

where subscript 'F' indicates stress/strain at fracture and 'U' indicates stress/strain at the peak. From Bull's tests with strain-rate of 0.002/min, σ_U= 157.80kN/mm^2, ε_U= 0.025 and ε_f= 0.407. Using equation (3.6),

$$log\sigma_F = n(log0.407 - log0.025) + log157.80$$

Based on 'Handbook of Workability and Process Design' by Dieter et al. (2003), for 0.6% Carbon Steel, quenched and tempered at 540°C a value of n = 0.1 and K = 1572MPa is given. According to BS EN ISO 898-1: 2013 (BSI, 2013), tempering temperature for Class 8.8 structural bolt is 425°C, which is reasonably close to 540°C, so that the above n and K can be used in this case to generate the value of stress at fracture (final point on the true stress-strain curve)
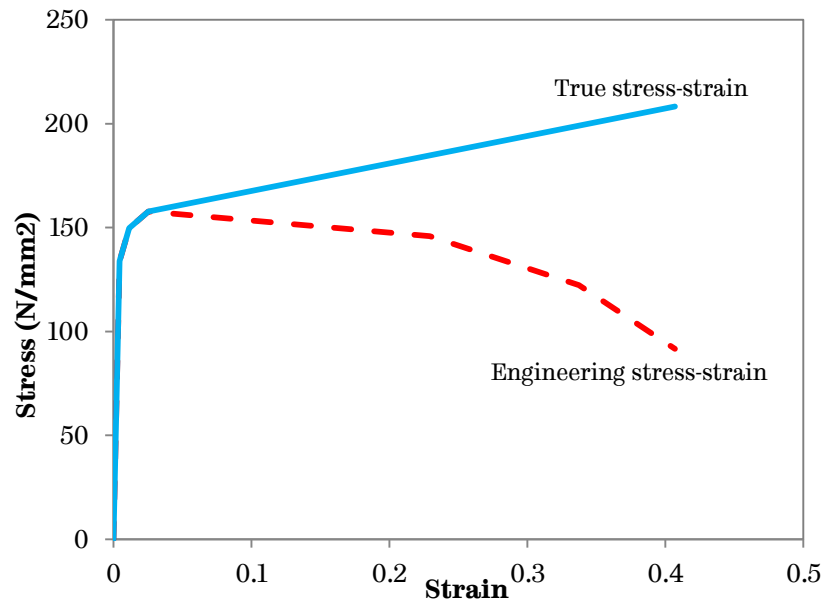
Figure 3-12 Class 8.8 M20 bolt true stress-strain relationships at 550°C

$$\sigma_F = 208.22 kN/mm^2$$

A comparison of the engineering stress-strain and the 'corrected' true stress-strain curves for Grade 8.8 structural bolts at 550°C is plotted in Figure 3-12. It can be noticed that the true stress-strain curve here provides a better presentation of material behaviour including the necking effect.

3.3.2.3   Interaction

Contact elements were adopted to accommodate complex interactions between parts. General surface-to-surface contact has been selected with 'Penalty' friction formulation and a friction coefficient of 0.3. Pressure-overclosure was set to 'hard' contact with 'separation after contact' allowed. The above contact elements have been applied to the following surface groups and are illustrated in Figure 3-13:

- Column flange – Bolt heads (———)
- Column flange – Bolt shanks (———)
- Column flange – Endplate (———)
- Endplate – Bolt shanks (———)
- Endplate – Washers (———)
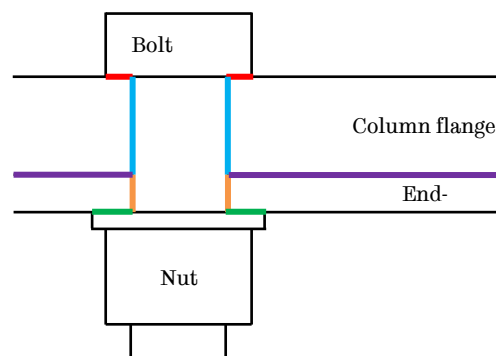
Figure 3-13 Contact surface groups

The Explicit Dynamic Solver was adopted to help overcome convergence problems with multi-surface contacts in this simulation.

3.3.2.4   Constraints

Three types of constraints were used in this model: "Tie', 'Rigid body' and 'Coupling'.

A 'Tie' constraint binds two parts together so that they behave as one piece. It has been used for the following part groups:

- Column flange – Rigid plate

  A strip of the column flange at its inner edge was tied to a rigid plate which acts as half of the column web.

- Beam stub – Endplate

  Welds were assumed to be infinitely stiff in this simulation and modelled using a tie constraint between the beam stub and the endplate.

- Beam stub – Loading block

  Loadings were applied on the loading block at the end of the beam stub, which helps to distribute loading evenly across the cross-section of the beam stub. A tie constraint was used here to make sure no relative movement occurred between the beam stub cross-section and the loading block.

A 'Rigid body' constraint was applied to the loading block to stop it from deforming. A 'Rigid Body' constraint confines the movement of the loading block to the movement of its reference point, thus the

relative motion of the loading block remains unchanged during the analysis. By defining the loading block as a rigid body, load applied to the connection can be distributed evenly and deformation from the loading block can be eliminated.

A 'Coupling' constraint allows motion of a node or a surface to follow the motion of a reference node. In this model, the 'Coupling' constraint was used to simulate the 3-bar articulated loading system and the pin connection between the furnace bar and the loading block, as described in detail below:

- Furnace bar – Link bar – Jack bar

  The ends of the three bars were linked using the 'Coupling' constrains to simulate the central pin connection. The central pin linked the translational movements of the ends of the bars. By using this constraint, when the jack bar was pulled downwards by the applied displacement control, the central pin would move downwards to mimic its behaviour in tests.

- Furnace bar – Loading hinge reference point

  This 'Coupling' constraint linked the other end of the furnace bar to the reference point of the loading hinge, which is the hole on the loading block to which the furnace bar was attached. The loading block reference was located in the centre of the loading hole. This pin connection enabled the load to be transferred to the loading block so the loads can be distributed further.

- Loading hinge reference point – Loading hinge

The last 'Coupling' constraint was applied to the loading hinge reference point and the loading hinge, as illustrated in Figure 3-14. This constraint enabled the motion of the entire loading block to be the same as the reference point translationally but rotationally free from the confinement of the reference point.
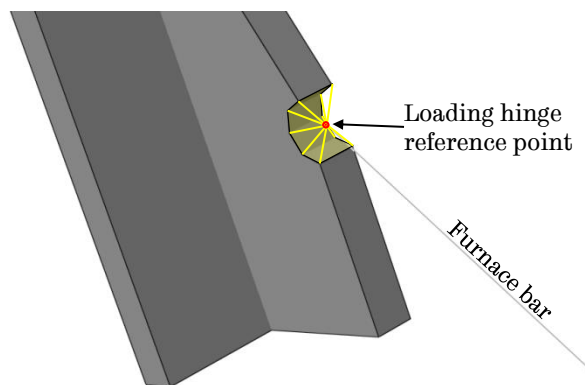
Figure 3-14 The 'Coupling' constraint around the loading block

3.3.2.5   Boundary conditions

Geometrical symmetry of the connection was represented in the model by assigning axial boundary conditions to the plane of symmetry through the centre of each part. These parts consist of the column flange, the endplate and the beam stub. The rigid plate was restrained both axially and rotationally to mimic the rest of the column.

The wall end of the link bar was restrained translationally but allowed rotational movements, to resemble the pin connection between the link bar and the wall during the test.

Displacement control was applied to the bottom end of the jack bar to simulate the movement of the loading jack in the test. This end was allowed to move vertically downwards and to rotate.

3.3.2.6 Mesh

Three element types were used in this model: solid elements, shell elements and wire elements. Different mesh elements were assigned to these parts, including an eight-node brick mesh type (C3D8R) for the solid elements, a four-node (R3D4) mesh type for the rigid shell elements and a two-node (B31) mesh type for the wire elements. The characteristics of these elements are shown in Table 3-5 (ABAQUS, 2012).

3.3.2.7 Mesh sensitivity check

If a suitable mesh size is chosen computational time can be reduced dramatically whilst still obtaining reliable results. A starting global

Table 3-5 Characteristics of *ABAQUS* mesh element C3D8R, R3D4 and B31

C3D8R		
C	Continuum stress/displacement	
3D	Three-dimensional	
8	8 nodes	
R	Reduced integration for computational effectiveness	
R3D4		
R	Rigid element	
3D	Three-dimensional	
4	4 nodes	
B31		
B	Beam element	
3	Three-dimensional	
1	Linear interpolation formulations	
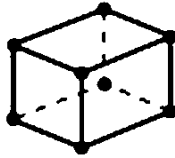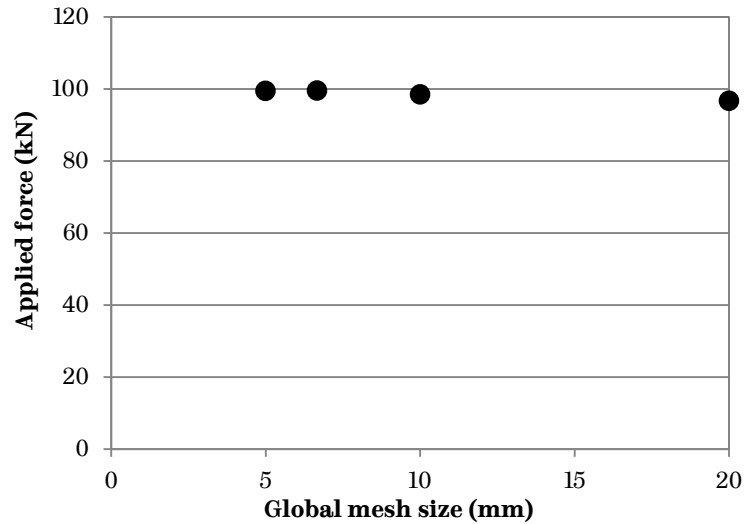
Figure 3-15 Mesh sensitivity check results

mesh size of 10mm was chosen for all parts apart from the beam stub, the loading block and the three bars, followed by a series of decreased mesh sizes of 6.67mm, 5mm and a coarser mesh of 20mm. A constant coarser mesh size of 30mm was used for the beam stub, the loading block and the three bars for all cases as these parts were not the main concern of this simulation, while their impact on the results is very small so can be ignored. As indicated in Figure 3-15, reducing mesh size from 6.67mm to 5mm, the results remained very close. Therefore, it is reasonable to state that a 6.67mm mesh size can produce reliable results with significant savings in computational time.

3.3.3   Results and discussion

The overall and detailed deformation comparisons between the test and finite element simulation results are presented in Figure 3-16 and Figure 3-17. It can be seen that the results from modelling are reasonable replications of the tests both globally and locally.

In order to generate the applied force against connection rotation plot of this simulation to be compared to the results recorded in the test, an understanding of the connection rotation is essential. In steel beam-to-column connections, rotation deformation includes contributions from a range of components. These include the bolt assemblies, the endplate and the column flange. The beam, however, was designed to be very stiff in this set of tests, thus its deformation was ignored in the calculation of the connection rotation. With considerations above, the overall connection rotation, φ, can be represented as $\varphi = \theta_b - \theta_c$. The rotations of beam (θ_b) and column (θ_c) can be calculated from the vertical displacements on the displacement transducers, labelled as D1 to D4 as shown in and Table 3-6.

Beam and column rotations can then be expressed as

$$\theta_b = \tan^{-1}\left(\frac{|\delta_{D1}| - |\delta_{D2}|}{l_b}\right) \tag{3.7}$$

$$\theta_c = \tan^{-1}\left(\frac{|\delta_{D3}| + |\delta_{D4}|}{h_c - t_{fc}}\right) \tag{3.8}$$

where l_b is the length of the beam segment, h_c is the height of the column and t_{fc} is the thickness of the column flange and the values used in this particular test were 400mm, 620mm and 17.3mm respectively. Since only half of the connection was simulated, the applied force data generated from *ABAQUS* simulation needed to be doubled to provide correct values.

Figure 3-16 Overall deformation comparison
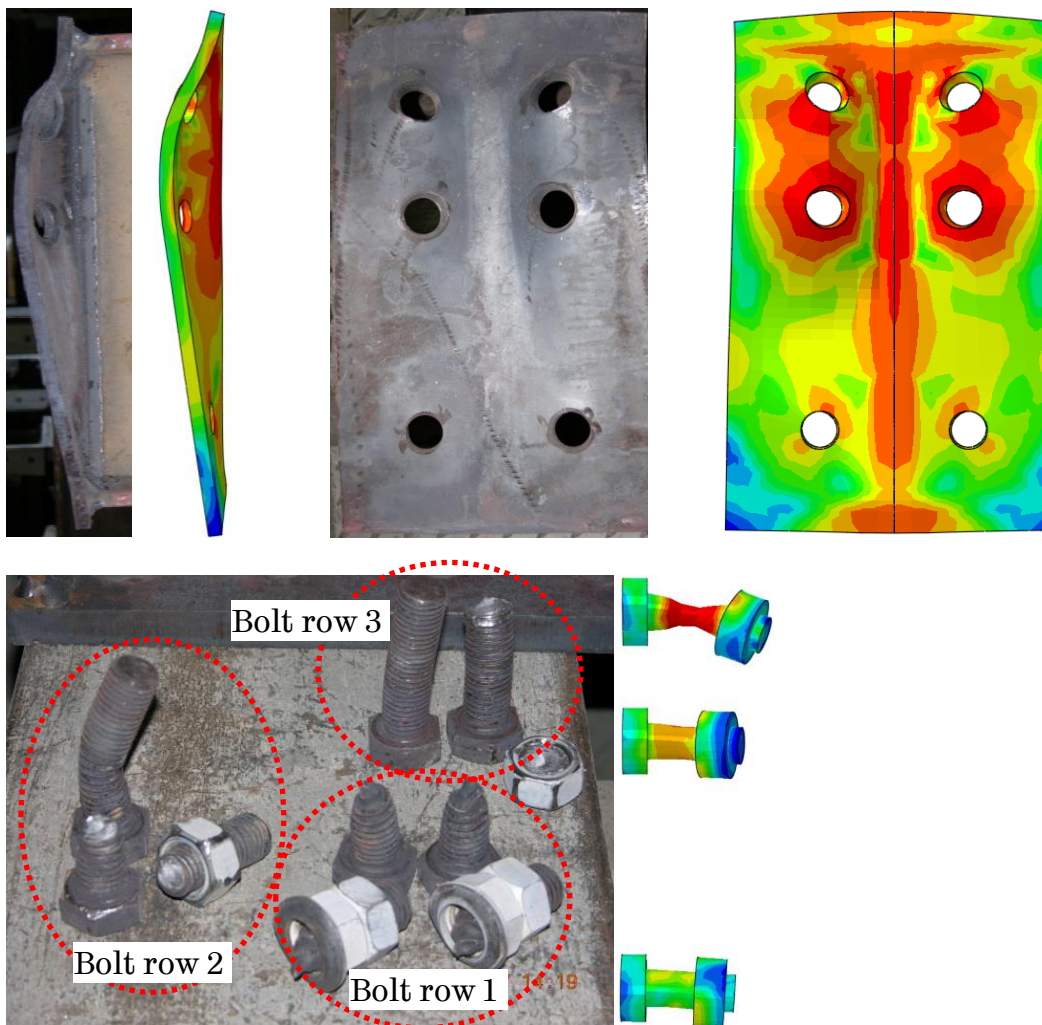
Figure 3-17 Endplate and bolt assemblies deformation comparisons
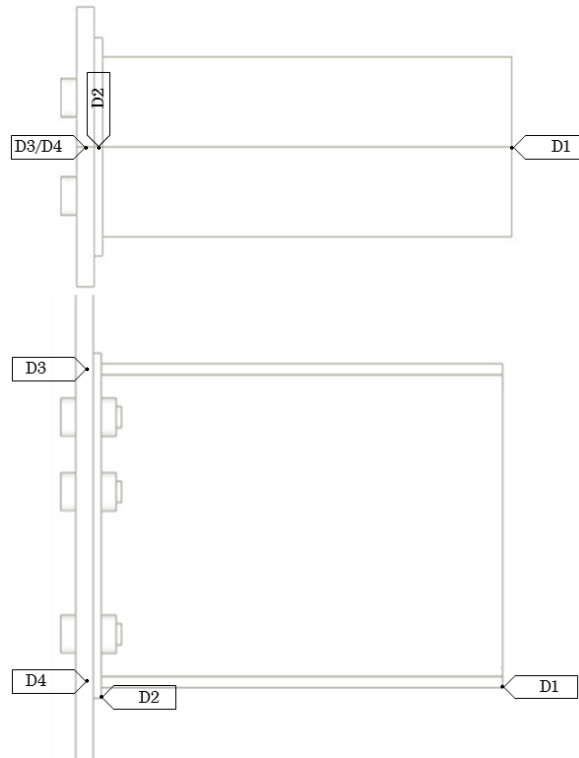
Figure 3-18 Location of displacement transducers

Table 3-6 Locations and purposes of displacement transducers D1 to D4

Displacement transducer ID	Location	To Measure the vertical displacement at
D1	Centre of the beam end next to the loading device	Beam end
D2	Centre of the endplate bottom surface	Endplate
D3	Centre of the column flange in line with the centreline of the beam top flange	Column flange
D4	Centre of the column flange in line with the centreline of beam bottom flange	Column flange
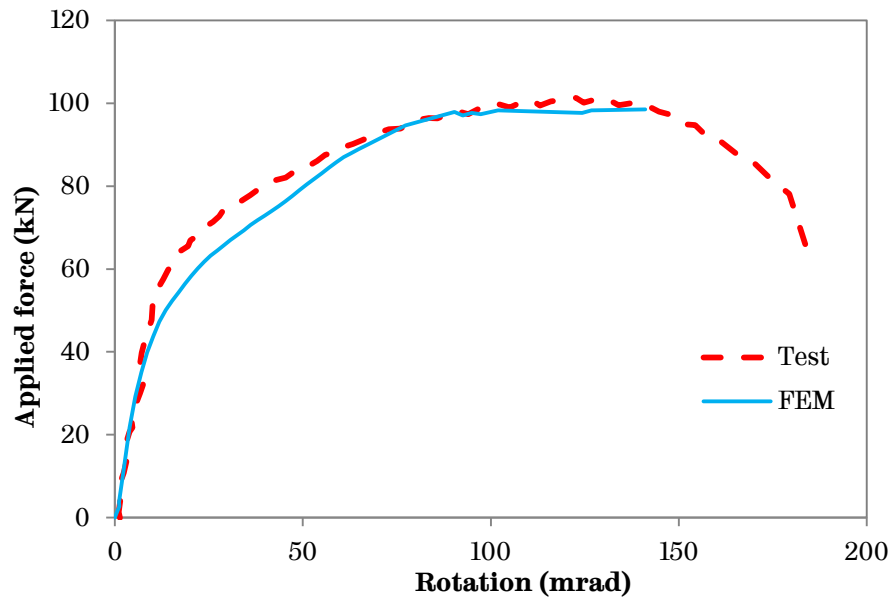
Figure 3-19 Simulated applied force-rotation relationship compared with the test results for the flush endplate connection

Figure 3-19 shows the applied force against the connection rotation comparison between the test and the finite element simulation. It can be seen that the general agreement has been achieved in initial elastic stiffness and load bearing capacity. However, it should be acknowledged that this current model is only trustworthy up to the maximum principle strain of the top bolt row, which was 0.41. Besides, even though the finite element models in *ABAQUS* can provide reliable simulation results, this detailed flush endplate connection simulation was very time consuming to run. As time cost is a key factor when analysing a multi-connection frame model, it needs to be taken into consideration before conducting full-scale simulation.

3.3.4 Influence of bolt material properties

From Figure 3-16 and Figure 3-17 it can be seen that the failure mode of the flush endplate connection presented in this section was bolt

fracture with endplate yielding (Failure Mode 2). Therefore the relative material properties of the bolts and the endplate in the *ABAQUS* modelling play a very important role in determining the overall load capacity of the connection. The stress-train characteristics of Grade 8.8 bolts and the S275 structural steel have been studied intensively, however the data under steady-state elevated temperature were limited. For the S275 structural steel, Renner's test results and reduction factors (Renner, 2005) were adopted as explained in Section 3.3.2.2. In this section, a study was carried out on the same model as that in Section 3.3.2 with a range of stress-strain characteristics of Grade 8.8 bolts to investigate the effects of different material properties on the overall simulation results of flush endplate under a combination of shear and tying forces.

In total five Grade 8.8 stress-strain relationships at elevated temperature were used in this study: BS EN 1993-1-2 (CEN, 2005b), Hu et al. (2007) and three from Bull (2014). According to BS EN 1993-1-2, the bolt elevated temperature strengths are calculated by applying prescribed reduction factors (Table D.1 in BS EN 1993-1-2) to the bolt nominal ambient temperature strength (CEN, 2005b). These strength reduction factors were generated based on Kirby's research on Grade 8.8 bolts (Kirby, 1995). Hu (2007) carried out a series of tests with a strain-rate of 0.001-0.003/min on Grade 8.8 bolts and produced another set of recommended strength reduction factors, shown inFigure 3-20 together with the reduction factors prescribed in BS EN 1993-1-2. More
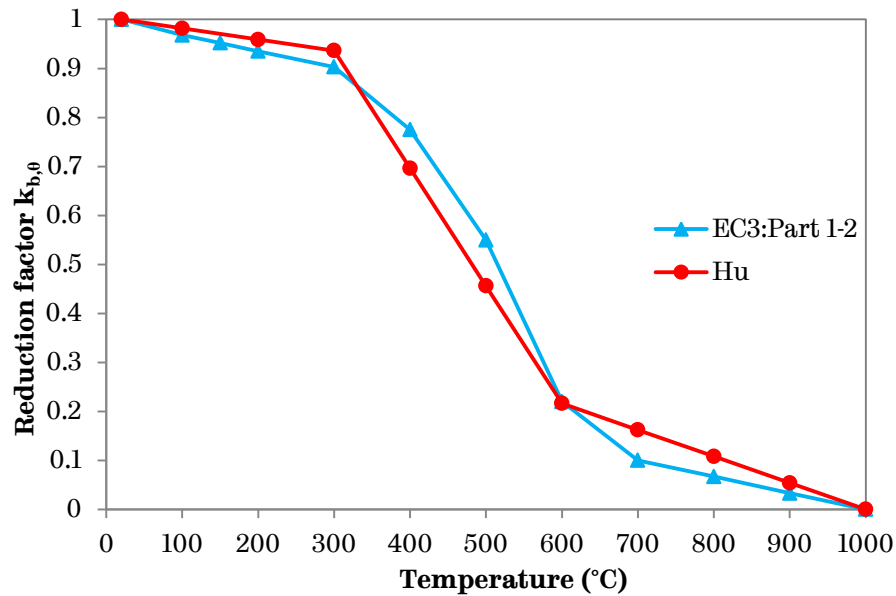
Figure 3-20 Bolt Strength reduction factors recommended by BS EN 1993-1-2 (CEN, 2005b) and Hu (2007)

recently, Bull (2014) conducted multiple tensile tests on Grade 8.8 bolts with various strain-rates (0.02/min, 0.01/min and 0.002/min) at high constant temperatures (550°C, 620°C and 700°C). It was highlighted that the ultimate tensile strengths obtained from the tests (Figure 3-21) were significantly lower than the nominal ultimate tensile stress given in BS EN ISO 898-1 (800MPa) with the BS EN 1993-1-2 reduction factor (0.385) applied (BSI, 2013; CEN, 2005b), which is also shown in Figure 3-21. It has also been concluded that the strain-rate has great effects on the stress-strain behaviour of bolts under elevated temperature (Bull, 2014).

The *ABAQUS* model used in Section 3.3.2 was adopted for this study. Despite the material properties of the bolt assemblies, the rest of the input data were kept unchanged. Five simulations in total were conducted with various bolt stress-strain relationships. For the two models using strength reduction factors by BS EN 1993-1-2 and Hu, as
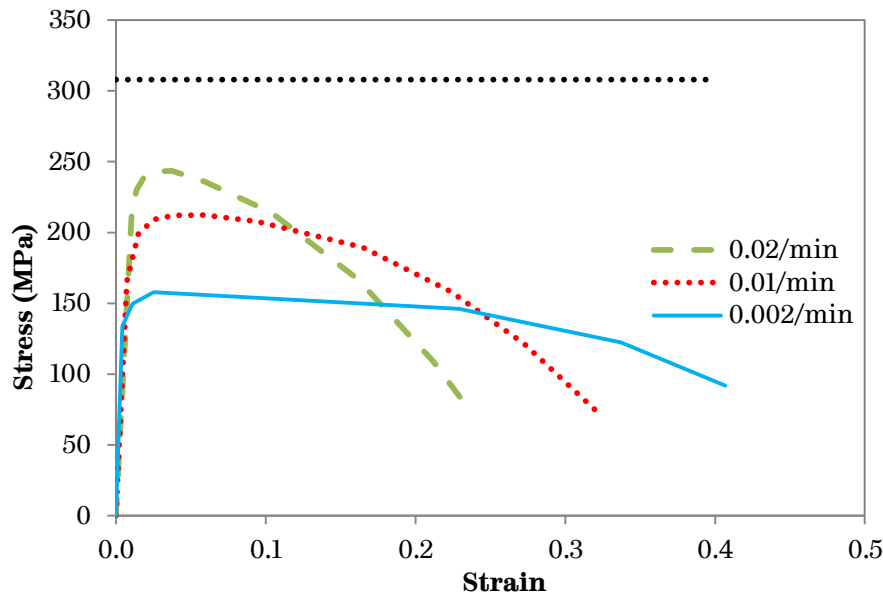
Figure 3-21 Grade 8.8 bolt engineering stress-strain relationships obtained in tests at 550 °C at various strain-rates, by Bull (2014)

only 500°C and 600°C reduction factors were provided, the average bolt tensile resistance from tests done by Yu (2009a), which was 224kN to generate the input bolt stress-strain relationships. For the three models conducted with Bull's test data, the engineering stress-strain curves were converted into true stress-strain curves based on the method introduced in Section 3.3.2.2 and are shown in Figure 3-22.

The comparisons of the applied force versus connection rotation with the above bolt material properties are plotted in Figure 3-22. Based on these results, the following observations can be made:

- Figure 3-22 shows that, apart from Model Bull-0.002/min, the other models had higher load capacity compared to the test results. This was caused by the higher bolt ultimate stress in the other models with the exception of Model Bull-0.002/min.
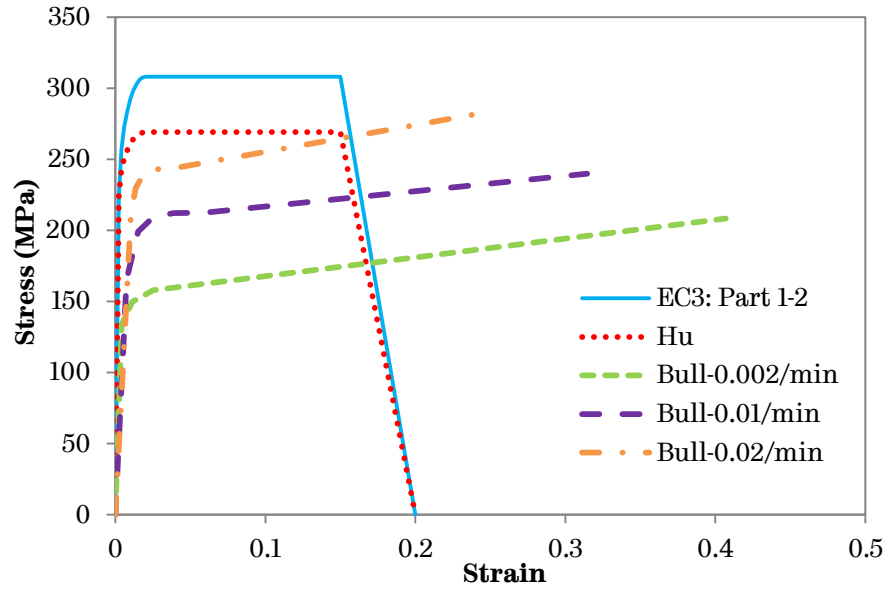
Figure 3-22 Bolt assemblies true stress-strain at 550°C based on strength reduction factors by BS EN 1993-1-2 (CEN, 2005b) and Hu (2007), and at various strain-rates based on Bull (2014)
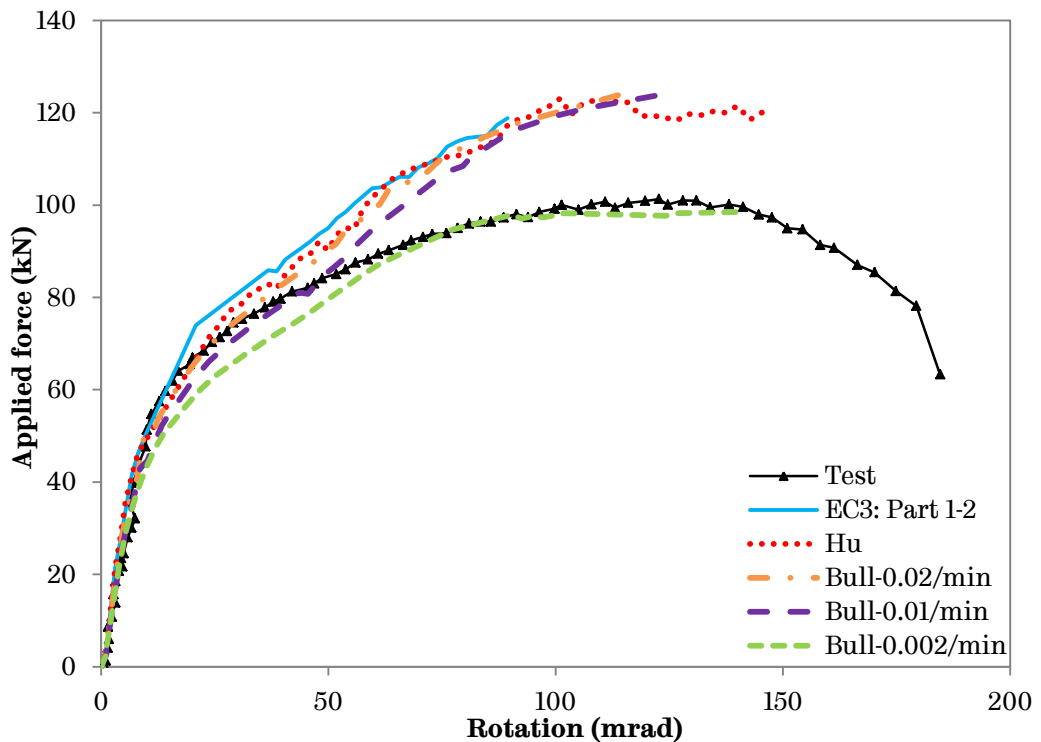
Figure 3-23 Applied force-rotation relationships of flush endplate connections with various bolt stress-strain relationships

- Among these results, only Model Bull-0.002/min and Model Bull-0.01/min models had the same failure mode as the test, which was top bolt row fracture accompanied by yielding of the second bolt row and the endplate (Figure 3-16 and Figure 3-17). The other models had a failure mode of endplate fracture around the top bolt holes, as shown in Figure 3-24, which was the result of the bolt ultimate strength at 550°C being higher than that of the endplate.
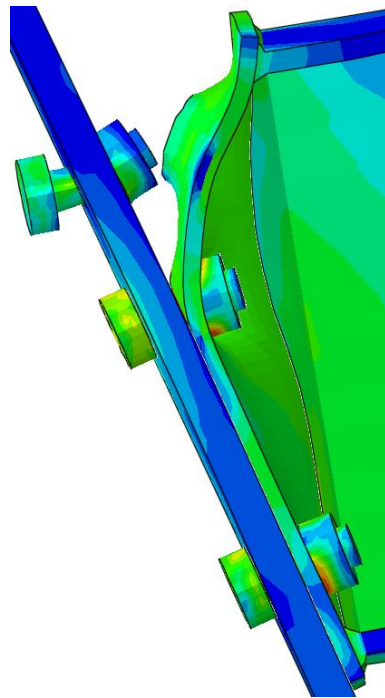
Figure 3-24 Failure mode: endplate fracture with bolts bending

- The finishing point of each simulation was chosen based on its failure mode. For the two models with the failure mode of bolt fracture, the maximum principal strain of the top row bolt shanks was used as the key criteria which corresponded to the test that it was stopped after the fracture of the top bolt row.

This value was set to be 0.41 for Model Bull-0.002/min and 0.32 for Model Bull-0.01/min. These two values were in-line with the maximum strain of the bolt stress-strain relationships. For the other three models, the failure mode was controlled by the endplate, therefore a maximum plastic strain of 0.40 (the average of the maximum strain at 500°C and 600°C of the endplate from Figure 3-11) was adopted.

- The effect of strain-rate on the stress-strain relationship of the bolts was investigated in Bull's research and is shown in Figure 3-21. Together with the strain-rate of Hu's and the simulation results shown in Figure 3-23, it can be summarized that by using the stress-strain relationship from the material tests with similar strain-rate, better correlation can be achieved.

3.4   Chapter conclusion

In this chapter, steel beam-to-column flush endplate connections were modelled using Finite Element simulation packages *VULCAN* and *ABAQUS*. Two groups of simulations were conducted to investigate (a) the differences between the two connection modelling approaches in *VULCAN* research and commercial versions – the Ordinary Spring Element Method and the Component Based Method; and (b) the feasibility of using *ABAQUS* as a tool to model flush endplate connections and whether the results from *ABAQUS* are suitable for

validation purpose when no test data is available. A parametric study on the influences of the bolt tensile properties on the connection behaviour was also performed. Based on these studies, the following conclusions can be drawn:

- In the current version of *VULCAN* research version, when used for steel beam-to-column connection simulations, Ordinary Spring Element Method does not take the non-linearity of the connection's axial and rotational characteristics into consideration.

- Frame analysis which uses the Component Based Method modelling approach for the steel beam-to-column flush endplate connections provides more conservative solutions compared to models using Ordinary Spring Element Method. However, the Component Based Method in the current research version of *VULCAN* cannot deal with flush endplates with more than five bolt rows. This limits the current research version of *VULCAN* from being used in the simulations of long-span structures with deep beam sections, which would require more than five bolt rows.

- When simulating flush endplate connections in *ABAQUS*, if the column section is much stronger compared to the beam section, only modelling the column flange attached to the endplate is adequate to provide reasonably accurate results.

- The model created in this chapter using *ABAQUS* can be used as a tool for flush endplate connection simulation to provide reliable

results, which is very useful especially when test data is not available.

- *ABAQUS* simulation is very time consuming due to the number of elements in each model and the complexity of contact elements, hence it is not feasible to be adopted for frame analysis when multiple connections are present.

- The bolt tensile characteristic at elevated temperature has a significant effect on the behaviour of flush endplate connections, based on a parametric study conducted in *ABAQUS*. Depends on the tensile strength of the bolts relative to the bending strength of the endplate, the failure mode might be altered when using different bolt properties. When choosing the high temperature bolt stress-strain characteristic, strain rate should be considered as it affects both the ultimate stress and the ductility of the bolts (Bull, 2014).

- Even though the Component Based Method in the *VULCAN* research version is not as time consuming as detailed *ABAQUS* simulation for frame analysis with connections, it still requires extensive computational time considering the frame used in Section 3.2 only consisted of a set of very basic structural elements.

Among these conclusions, the deficiencies of *VULCAN* and *ABAQUS* need to be highlighted. Even though the existing Finite Element packages, like *VULCAN* and *ABAQUS*, can be used to simulate the behaviour of steel flush endplate connections at elevated temperature

and can provide reliable results, their deficiencies cannot be neglected. As discussed, the current *VULCAN* commercial version can only model the connections using Ordinary Spring Element Method which is less conservative than desired; the current *VULCAN* research version using the Component Based Method is only capable of modelling flush endplate connections up to five bolt rows; there is no certain restrictions on the use of *ABAQUS* for connection modelling, but due to the significant time cost it is not feasible to adopt *ABAQUS* for frame analysis with numerous connections. As the numbers of high-rise and long-span buildings increase rapidly in recent decades, there is a need for a more universal and faster modelling approach for steel connections. This desired modelling approach should satisfy the following requirements:

- It should be able to provide reliable simulation results for multi-connection frame analysis under fire conditions;

- It should be suitable for all sizes of flush endplate connections disregard of the number of bolt rows;

- It should be relatively time efficient compared to the Component Based Method in the *VULCAN* research version and the detailed *ABAQUS* simulation.

In order to meet the above requirements, an innovative modelling approach was developed and will be introduced in Chapter 4.

4

Development of a Simplified Spring Connection Modelling Approach

Page Intentionally Left Blank

4.1   Chapter introduction

As presented in Chapter 3, steel beam-to-column connections can be simulated using a detailed finite element modelling approach in *ABAQUS* or a component based modelling approach in *VULCAN*. These approaches can provide a reasonably accurate representation of connection behaviour, but they are not very time efficient, especially in frame analysis where multiple connections are presented. Connections with more than five bolt rows are not included in the current research version of *VULCAN*, which limits the usage of *VULCAN* for modelling realistic sized connections for long-span frames. Furthermore, the existing commercial version of *VULCAN* includes the effects of translational and rotational springs *separately*; using this approach the behaviour of steel connections cannot be simulated accurately because the interaction of the effects is not modelled.

In order to combat the drawbacks of the above two modelling approaches, a simplified spring connection modelling approach will be introduced in detail in this chapter. The development was based on a flush endplate connection with six bolt rows and the development procedure is summarised in Figure 4-1.
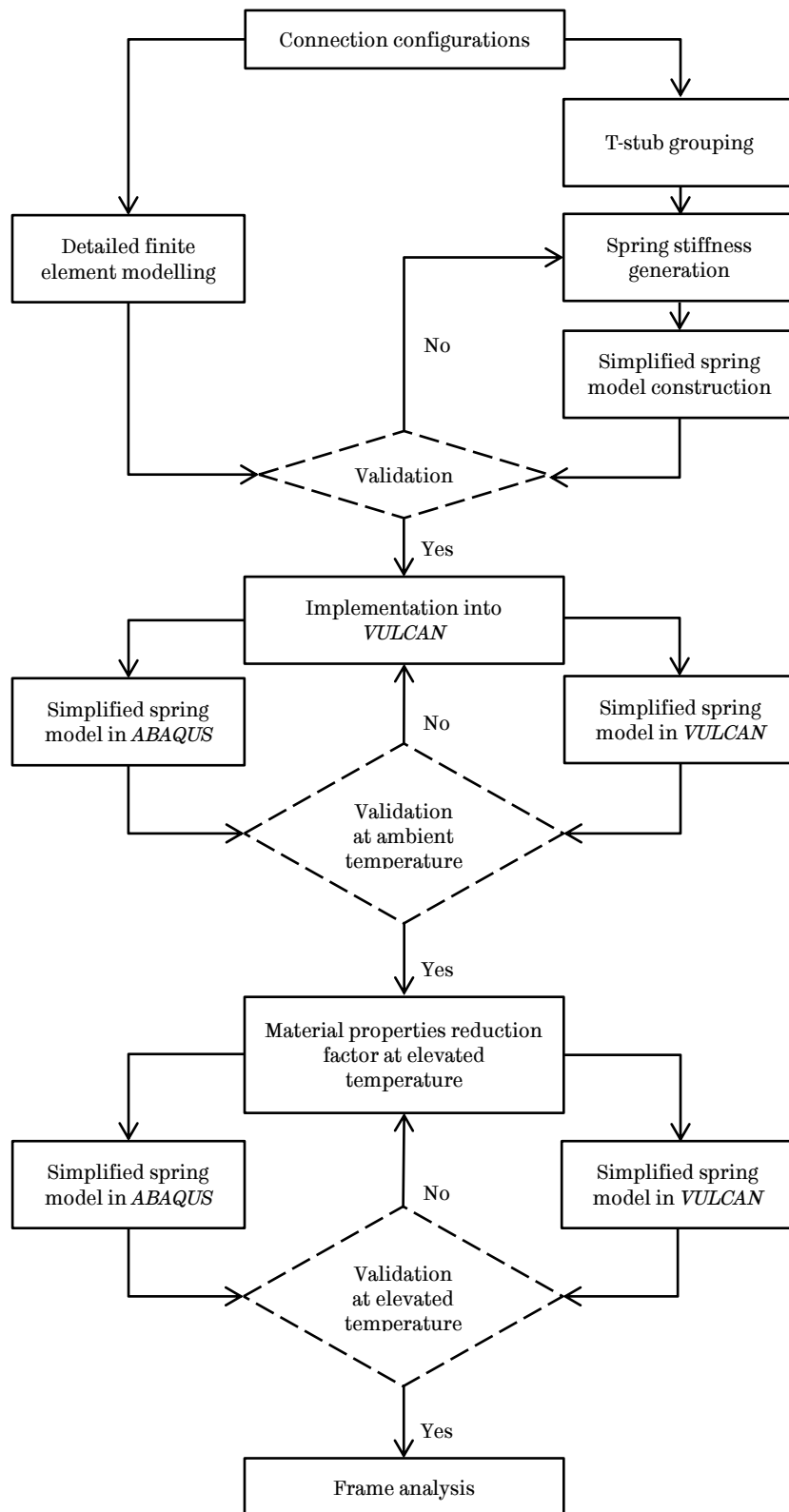
Figure 4-1 Flowchart of the development procedure

4.2 Development of a simplified spring connection model for realistic sized connections

4.2.1 Connection configurations

A standard flush endplate connection for realistic sized long-span (e.g. 18m) steel frame was created and its detailed geometry information is shown in Figure 4-2. The endplate was in structural steel grade S275 as recommended in Joints in Steel Construction: Moment-resisting Joints to Eurocode 3 (the Green Book) (UK Connections Group, 2013). All other steel sections were also in grade S275 to simplify the input parameters. A UB686×254×152 section was used for the beam while a UC356×406×287 was used for the column. In total six rows of M24 structural bolts were adopted again as recommended in the Green Book (UK Connections Group, 2013). The chosen grade of bolts was Grade 12.9 instead of 8.8 recommended in the Green Book in order to achieve Failure Mode 2 (bolt fracture with endplate yielding) which provides the most ductility. This choice was helpful at this stage so that both the behaviour of the bolts and endplate can be validated in the following studies. The length of the beam stub is assumed to be 1000mm and the height of the column is 1500mm. The connection can be loaded axially or rotationally, or a combination of both. The axial resistance of the connection was calculated to be 2284kN based on a method shown in the Green Book (UK Connections Group, 2013).
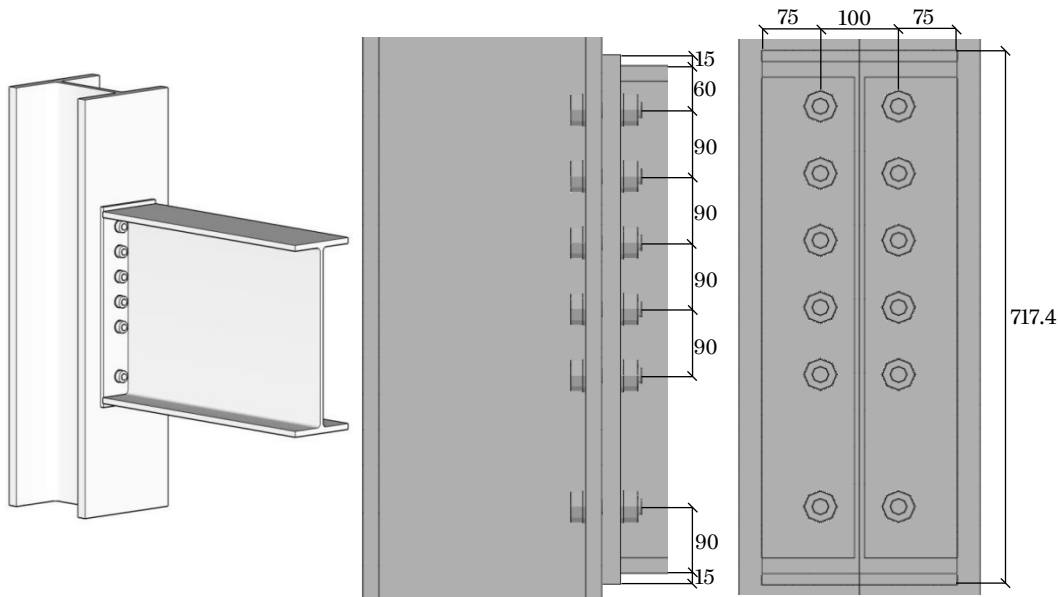
Figure 4-2 Flush endplate geometry (unit: mm)

4.2.2 Detailed finite element modelling of the connection

The model created is based on a previous model discussed in Section 3.3, therefore for certain sections only brief overview will be provided with essential details or changes made.

4.2.2.1 Model geometry

A 3D model of the connection shown in Figure 4-2 was constructed in the finite element package *ABAQUS*, as shown in Figure 4-3. Thanks to the symmetrical geometry of the connection, only half of the connection was modelled thus saving computational time. The model includes: a beam stub, a column flange, a full length flush endplate, six bolt assemblies, a rigid plate and a loading block.

Similar to the *ABAQUS* model presented in Section 3.3.2.1, only the column flange was modelled and the bolt assemblies were assumed to be one integrated part.
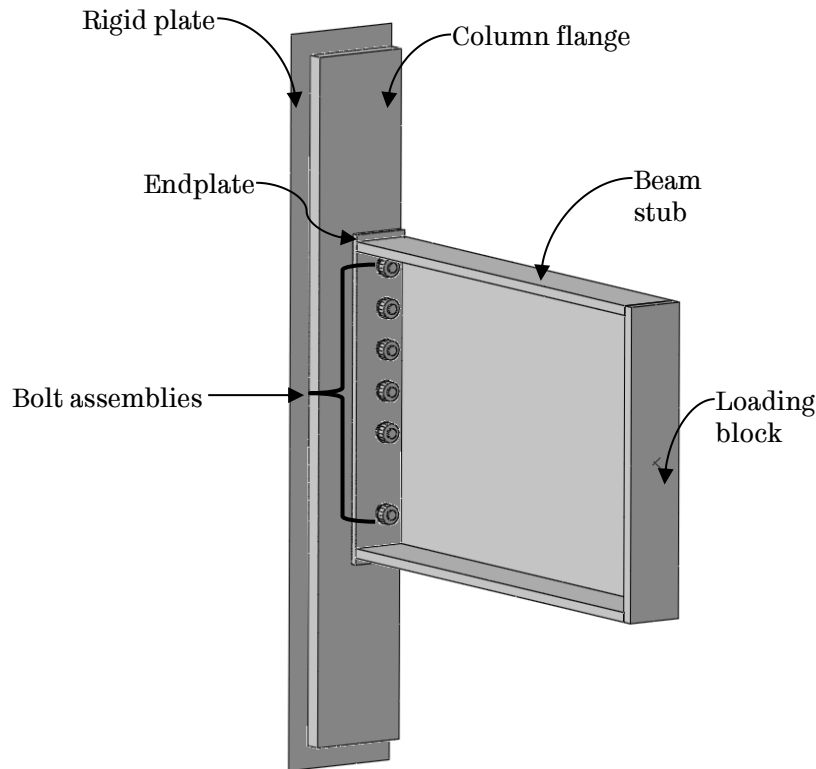
Figure 4-3 3D flush endplate connection model in *ABAQUS*

4.2.2.2   Material Properties

For both the beam stub and the column, S275 structural steel was used. Material properties were adopted from BS EN 1993-1-1 and BS EN 1993-1-2 (CEN, 2005a; CEN, 2005b) as shown in Table 4-1. M24 Grade 12.9 bolt assemblies were used for the six bolt rows in the proposed flush endplate connection. As each bolt assembly was modelled as one integrated element, identical material properties were used across each assembly. These properties are presented in Table 4-2 based on ISO 898-1 (BSI, 2013) .

Table 4-1 Material properties of S275 structural steel from Eurocode 3

Yield strength f_y, ultimate tensile strength f_u and corresponding plastic strain ε_{pl}			
Nominal thickness of the element t (mm)	$t \leq 40$ mm	40 mm $< t \leq 80$ mm	ε_{pl}
f_y (N/mm^2)	275	255	0
f_u (N/mm^2)	430	410	0.15
Density of structural steel			
$\rho = 7850$kg/m^3			
Modulus of elasticity			
$E = 210000$N/mm^2			
Poisson's ratio in elastic stage			
$\nu = 0.3$			

Table 4-2 Material properties of Grade 12.9 structural bolt assembly

Yield strength f_y, ultimate tensile strength f_u and corresponding plastic strain ε_{pl}		
		ε_{pl}
f_y (N/mm^2)	970	0
f_u (N/mm^2)	1200	0.15
Density of structural steel		
$\rho = 7850$kg/m^3		
Modulus of elasticity		
$E = 210000$N/mm^2		
Poisson's ratio in elastic stage		
$\nu = 0.3$		

4.2.2.3   Interaction

The same contact elements and pairs were adopted as mentioned in Section 3.3.2.3 and also listed below:

- Column flange - bolt heads

- Column flange - bolt shanks

- Column flange - endplate

- Endplate - bolt shanks

- Endplate - washers

The Explicit Dynamic Solver was also used.

4.2.2.4   Constraints

Two types of constraints were used in this simulation: 'Tie' and 'Rigid body'. These constraints have been discussed in details in Section 3.3.2.4 and the same approach was adopted for this model. 'Rigid body' constraint was applied to the loading block only. 'Tie' constraints were applied to the following part groups:

- Column flange - rigid plate

- Beam stub - endplate

- Beam stub - loading block

4.2.2.5   Boundary conditions

Same boundary conditions as discussed in Section 3.3.2.5 were adopted in this model in order to model the symmetricity of the connection.

4.2.2.6   Mesh element type

Both solid and shell elements were used in this simulation, and the characteristics of the mesh types of C3D8R and R3D4 have been discussed in Section 3.3.2.6 in details.

4.2.2.7   Mesh sensitivity check and results

Mesh sensitivity check was done using the same method mentioned in Section 3.3.2.7, with the starting mesh of 10mm (equivalent to 0.1/mm) followed by a series of decreased mesh sizes of 8mm, 6.67mm, 5.71mm and 5mm. A constant coarser mesh size of 50mm was used for the beam stub and the loading block. It is indicated in Figure 4-4 that reducing mesh size from 10mm to 5mm, the results remained very close. Therefore, it is reasonable to state that a 10mm mesh size can produce reliable results with significant savings in computational time.
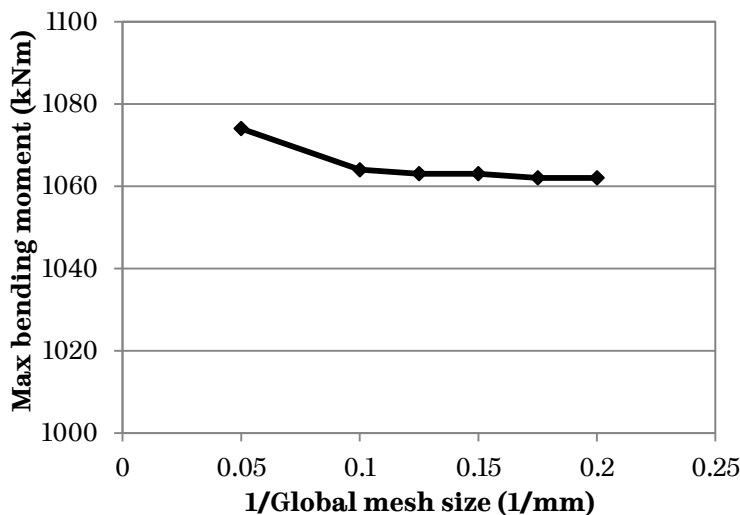
Figure 4-4 Mesh sensitivity check results

It has been shown in Chapter 3 that detailed connection finite element models conducted in *ABAQUS* can produce reliable results. From the simulation with a mesh size of 10mm (except for the beam stub and loading block), the maximum bending moment the connection resisted was 1064kNm and its rotational behaviour is shown in Figure 4-5. The

deformation shapes (Figure 4-6) were as expected in terms of global deformation and localized deformation.
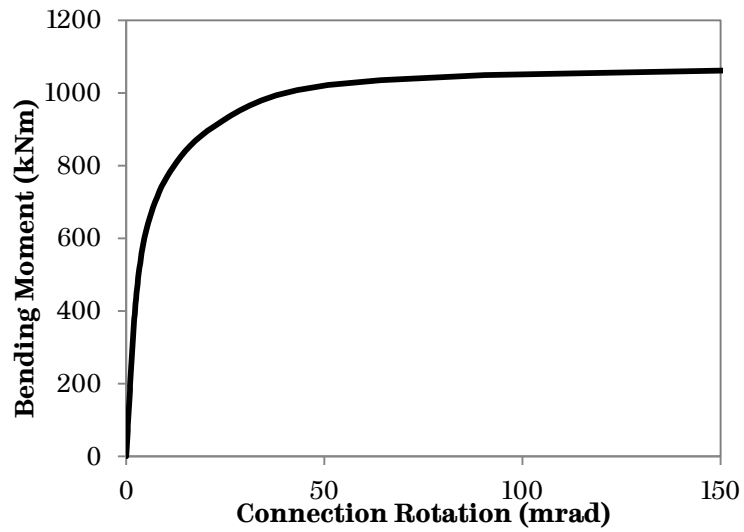
Figure 4-5 Connection rotational behaviour

(a) Full connection　　(b) Endplate　　(c) Bolt rows
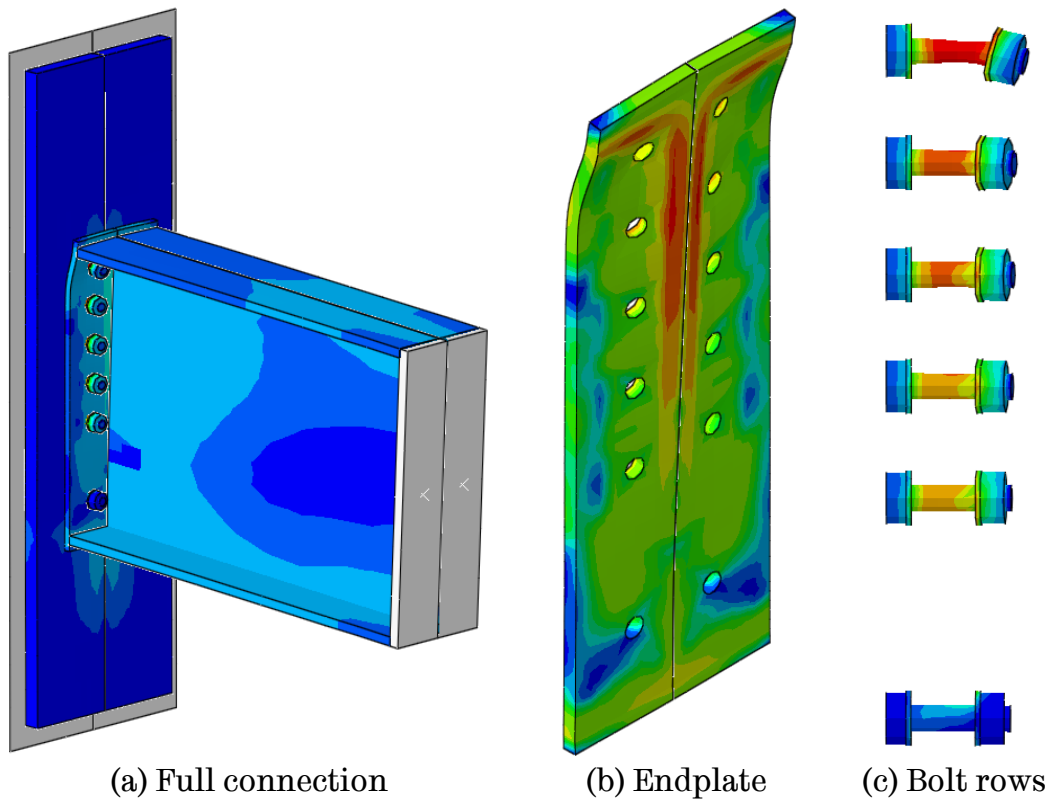
Figure 4-6 Connection deformation

4.2.3   Spring stiffness generation for T-stubs

In order to create the proposed simplified spring connection model, the connection was divided into 3 T-stubs to be modelled separately to generate corresponding spring force-displacement characteristics. This step involves (1) grouping multiple bolt rows into single T-stubs and then (2) conducting finite element modelling on each T-stub to generate the desired spring stiffness curve. The above steps were carried out based on the connection configuration presented in Section 4.2.1.

To make sure grouping was conducted correctly for the tensile bolt rows (shown in Figure 4-7), a detailed connection model (as presented in Section 4.2.2) was loaded under bending moment only to investigate the force-displacement response of each tensile bolt row. It can be seen from Figure 4-7 that bolt rows 2 to 5 behaved very similarly under pure bending while bolt row 1 was stiffer and stronger than all of the rest. This was caused by the beam top flange within the zone of bolt row 1. When the connection was loaded, forces passed from the beam to the endplate through the welds, which were modelled as 'tie' constraints. The beam top flange brought extra stiffness to the bolt row, thus the difference shown in Figure 4-7. Therefore the whole connection was divided into three T-stubs and is illustrated in Figure 4-8. T-stub 1 included bolt row 1, the beam top flange and the corresponding endplate and column flange. T-stub 2 encompassed bolt rows 2 to 5 and the corresponding beam web, endplate and column flange. T-stub 3

incorporated bolt row 6, the beam bottom flange and the corresponding

endplate and column flange.
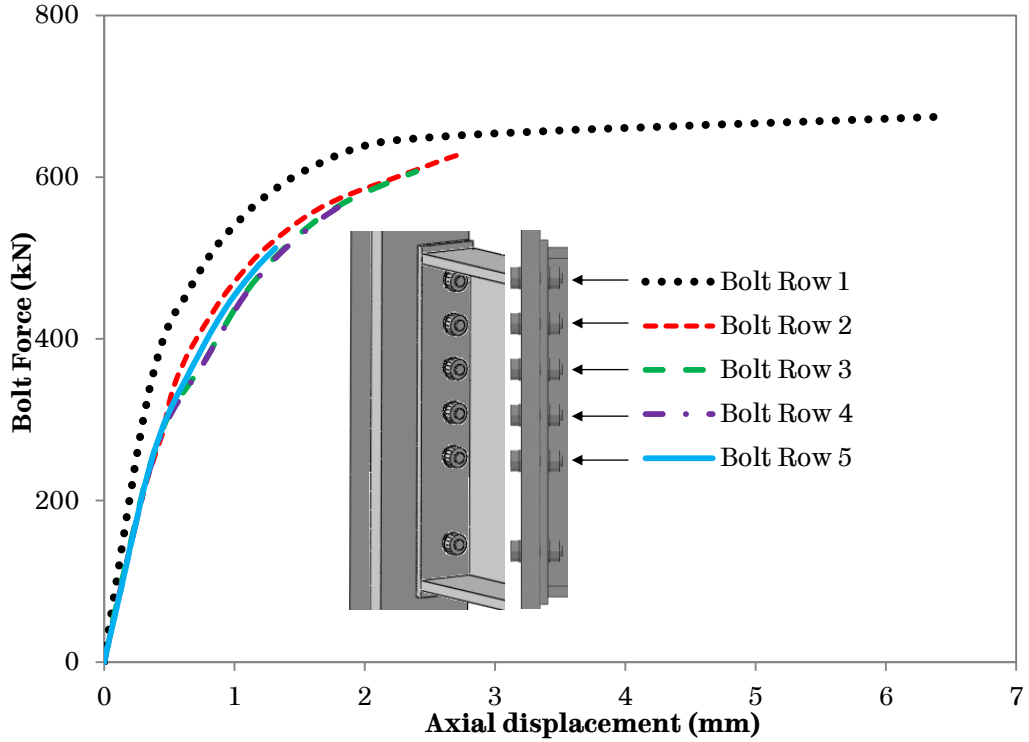
Figure 4-7 Bolt force of tensile bolt rows 1 to 5 under pure bending
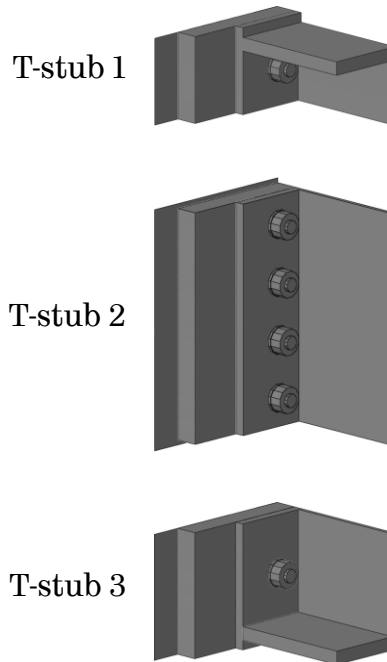
Figure 4-8 T-stub grouping configurations

Once the T-stub grouping arrangement was finalised based on the bolts' moment-rotation behaviour, the force-displacement curve for each T-stub were generated by loading them under pure tension and pure compression. This was achieved by applying displacement control on the end of the beam cross-sections. Each case was modelled until any element reached 0.20 strain. To avoid excessive deformed beam elements, the beam was assumed to be very stiff (E_{beam}= 2100GPa) to ensure deformation happened at the connection.

Force-displacement curves both in tension (positive) and compression (negative) for the three T-stubs are shown in Figure 4-9. To satisfy the input requirement of *VULCAN*, all curves in the tensile region have been converted into 5-node multi-linear curves, while in the compressive region they have been converted into 3-node bi-linear curves. When the T-stubs were in tension, it can be noticed that T-stub 1 and T-stub 3 have very similar behaviour, this is caused by the fact that they have almost identical geometry. Both T-stubs include the beam flange and the only difference is the bolt edge distance; a detailed study of the effect of edge distance on the T-stub force-displacement characteristic will be presented in Section 4.2.4. Coming to the compressive region, it can be noticed that although having almost identical geometry, results of T-stub 1 and 3 are apart. Compressive behaviour of T-stubs is controlled by the compressive length (the length of column web in compression in these models), thus T-stub 3 has a higher compressive capacity than T-stub 1. However for T-stub 2, even

though it has the longest compressive length, without the benefit of the contribution of the beam flanges its compressive capacity is lower than the other two. Data from Figure 4-9 was implemented into *VULCAN* research version in order to capture the complexity of a detailed whole connection model in a much simplified spring model.
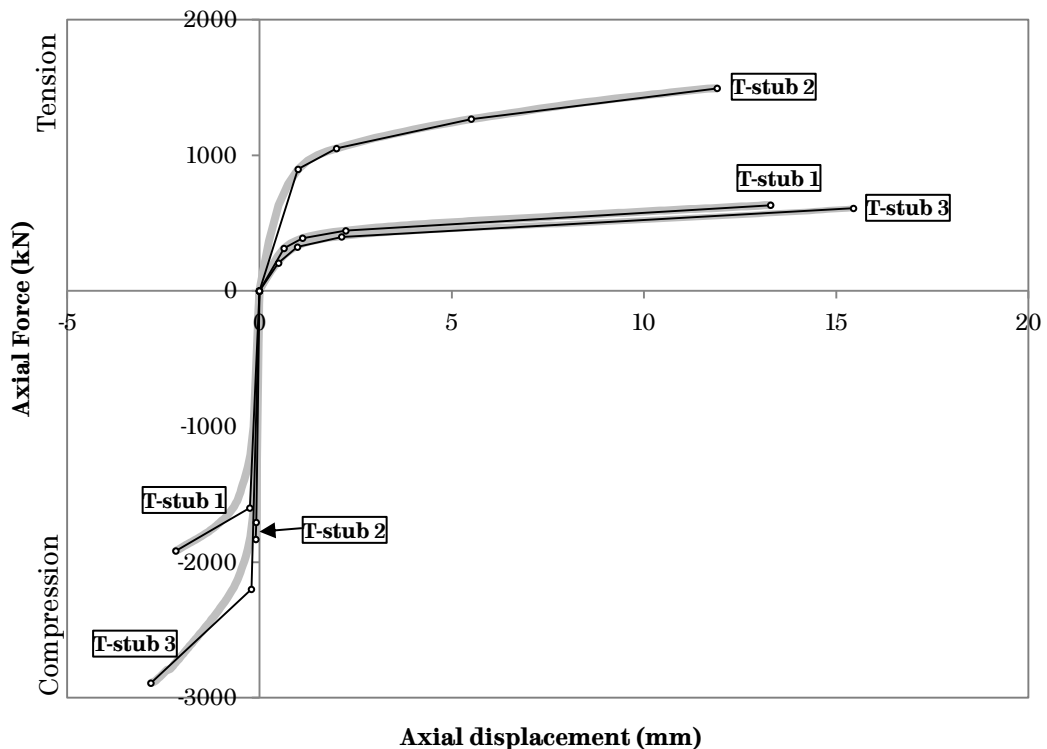
Figure 4-9 T-stub force-displacement curves

4.2.4   End distance study

As discovered in the last section, the distance from the centre of the bolt to the beam flange exterior surface can affect a T-stub's force-displacement behaviour. As shown in Figure 4-10, this distance, h_b, is part of the end distance, e, of the connection. Therefore, investigation was undertaken to establish the relationship between h_b and force-displacement behaviour of T-stubs. Configurations of T-stub 1 were

chosen to be the base model. The only parameter that was changing is h_b, as indicated in Figure 4-10. It varied from 60mm to 90mm at intervals of 10mm. Each model was loaded under pure tension and compression to provide results shown in Figure 4-12.

Figure 4-12 shows three key points with increasing h_b. First of all, axial ductility of the T-stubs increased from 12.0mm for 60mm to 15.5mm for 90mm. Secondly, the axial capacity decreased from 679.7kN for 60mm to 608.9kN for 90mm. The first two points were caused by the increased bending length of the endplate. This increase provided extra ability for the endplate to deform hence the whole T-stub's ductility was increased. Finally, axial ductility and capacity in compression were almost identical for all cases due to the compressive length remaining unchanged.
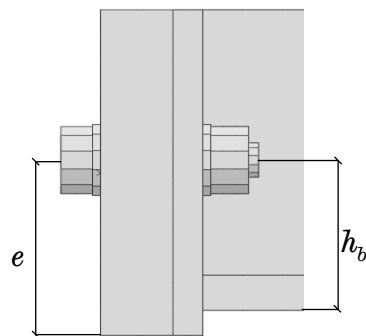
Figure 4-10 End distance e and bolt centre to the exterior surface of the beam flange h_b
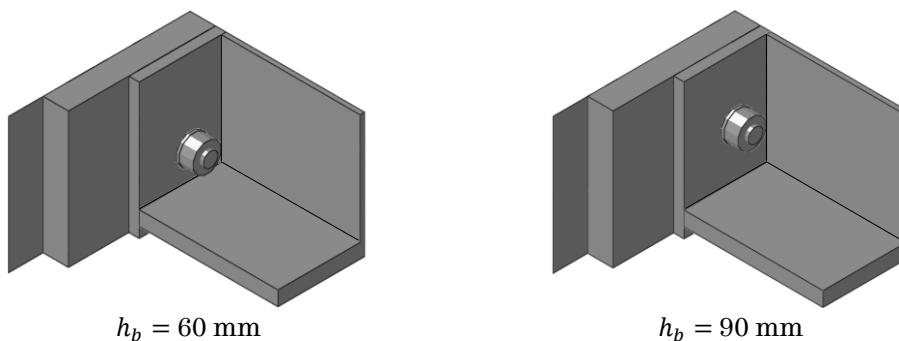
$h_b = 60 \text{ mm}$ $h_b = 90 \text{ mm}$

Figure 4-11 60 mm and 90 mm T-stub configurations
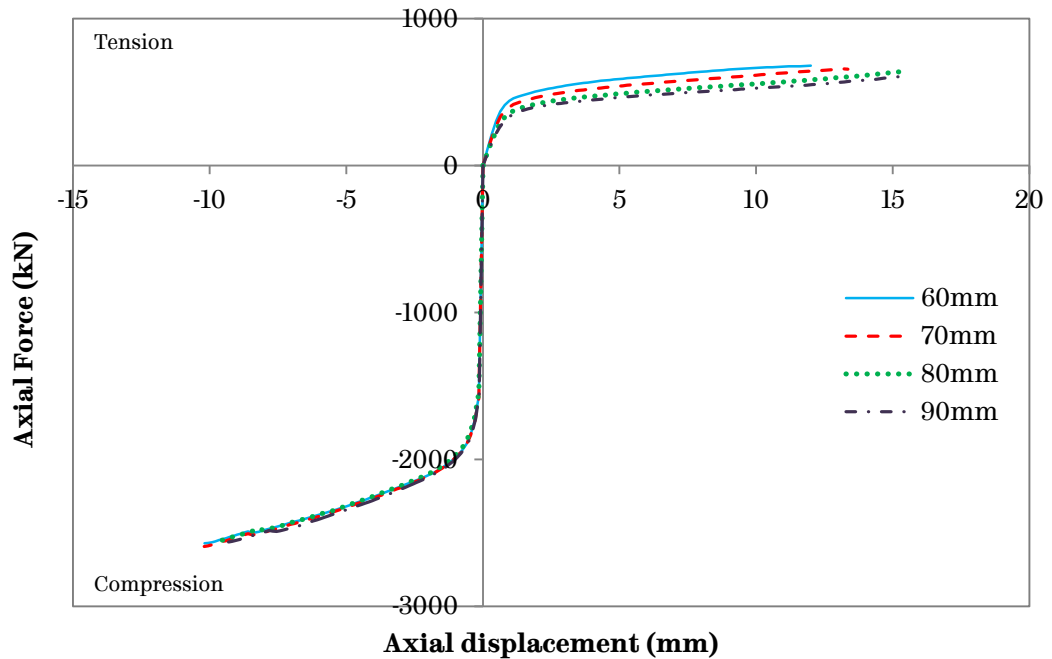
Figure 4-12 Force-displacement curve comparisons of the T-stub with various bolt centre to near surface of beam flange h_b

4.2.5 Simplified spring model construction

An *ABAQUS* finite element model was built to validate the simplified spring approach proposed; this is illustrated in Figure 4-13. The three components of the connection were represented by two outer springs, each composed of a tensile T-stub and a compressive T-stub with different lever-arms based on the configuration of the connection, together with a central component which was a tensile T-stub. Each of the outer springs utilized only one of its pair of T-stubs at any time, depending on the sense of its force. These springs were attached to two panels; representing the column web (Panel 1) and the beam end cross-section (Panel 2). Both panels were modelled as rigid plates to ensure no deformation occurs on them, so that they could act
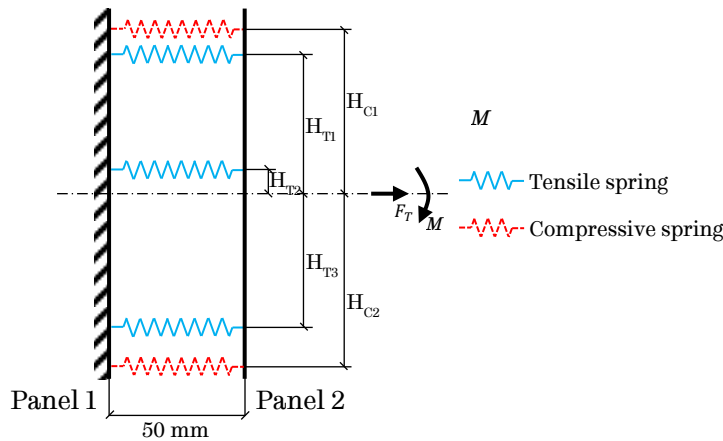
Figure 4-13 Simplified spring *ABAQUS* validation model

solely as load distributors. The distance between them was set to be 50mm, which allowed the springs to deform into the compressive region if they needed to. The whole model was fully fixed at Panel 1, while Panel 2 was free to move horizontally and to rotate. The positions of the top and bottom tensile springs were in-line with the first and the last bolt rows respectively, while the middle tensile spring was located at the horizontal centreline of T-stub 2. The two compressive springs were located at the centrelines of the beam's top and bottom flanges. The model was then loaded by an axial tensile force, F_T, and/or a bending moment, *M*, which was applied to Panel 2, to generate a force-displacement curve to be compared with detailed connection *ABAQUS* simulation results presented in Section 4.2.2.

It can be seen from Figure 4-9 that the spring stiffnesses used for this simulation were all non-linear. However, non-linear spring stiffness cannot be defined in *ABAQUS* interface version directly, which led to modifications in its code based input file. Firstly an input code file of the model containing linear spring stiffnesses was generated. Then in

this input code file, these linear spring stiffnesses were replaced by non-linear ones for each corresponding spring. Finally the code-based model was re-run to produce desired results in *ABAQUS*.

By constructing connection models in this manner, rotational behaviour of the connections is generated as a result of combinations of translational springs. This modelling method can provide more realistic simulation of the connections compared with modelling the connections using linearly connected axial and rotational springs (OSE).

4.3 Validations of the simplified spring model against detailed finite element simulation

4.3.1   Validation results

The connection simulated in Section 4.2 was adopted for validating the proposed simplified spring connection modelling approach. The connection was transformed into an assembly of panels and springs, which is illustrated in Figure 4-14. The comparison against the detailed finite element model result presented in Section 4.2 is shown in Figure 4-15. It can be seen that good agreement was reached, which leads to the conclusion that the proposed simplified spring connection modelling approach is capable of representing the behaviour of the connections accurately.
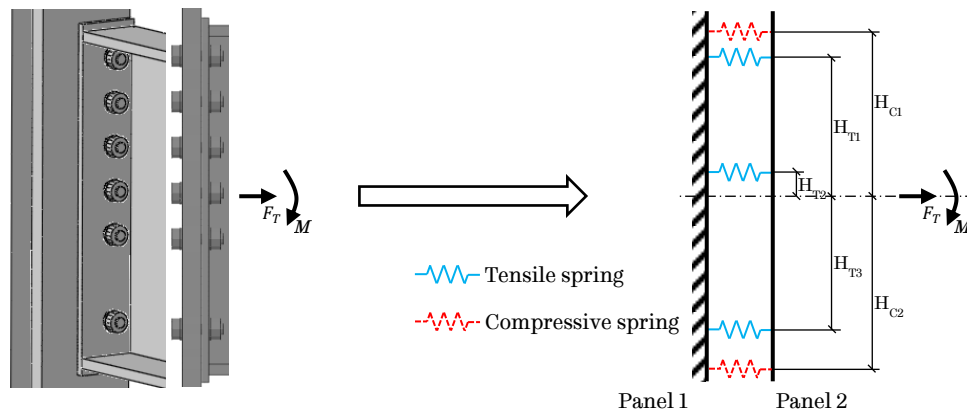
Figure 4-14 A connection transformed into a simplified spring connection model
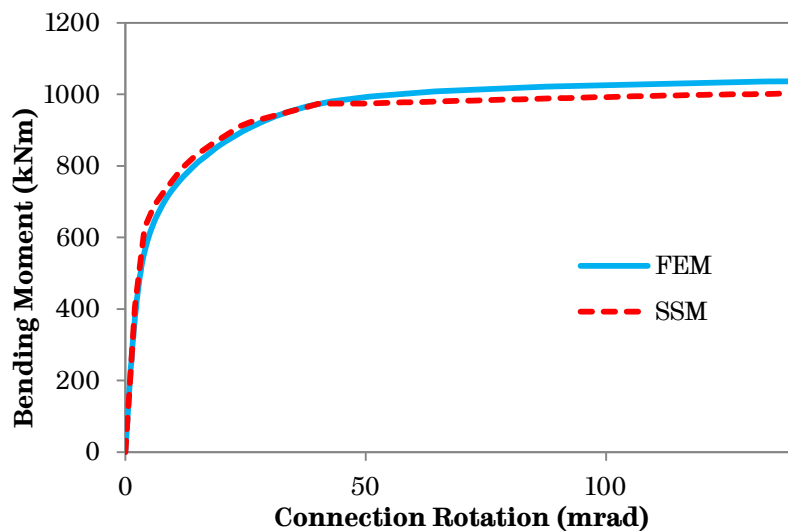
Figure 4-15 Simplified spring model (SSM) validating against FEM

4.3.2 Validation against isolated tests by Simões da Silva et al. (2004)

Bending moment is often considered to be the main loading that affects the behaviour of steel beam-to-column connections. However, an increasing number of studies on the effects of axial force have confirmed that the presence of axial load can greatly impact on the behaviour of the joints under certain scenarios and therefore cannot be neglected (Simões da Silva, et al., 2004). An experimental study of the effects of combined bending moment and axial force on flush and

extended endplates has been conducted at the University of Coimbra (2004). This study highlighted that axial force can affect the connection's rotational stiffness and capacity. The test results have been utilised here to validate the proposed simplified spring model for flush endplate connections.

4.3.2.1 Model geometry and loading conditions

The configuration of the flush endplate connection used in the above experiments is shown in Figure 4-16. The sections for the beam and the column were IPE240 and HEB240 respectively. Undoubtedly, the size of the sections and the connections are not ideal because the simplified spring connection model was developed for use with larger sections. However, due to the lack of test data on combined loadings conditions (axial force and bending moment) on long-span structures, this group of tests was chosen for validation. The specimens were loaded under various levels of constant tensile or compressive axial force expressed as a percentage of the beam plastic resistance, N_{pl}, followed by a clockwise bending moment up to failure. Three tests results were chosen to validate the simplified spring model, with details shown in Table 4-3.

It can be seen that this connection is symmetrical about its centreline and it only has two bolt rows. Again, it is not ideal to use the results from these test to validate the proposed simplified spring model because of the difference in the number of springs generated but due to

the lack of similar experiments on the effects of combined bending moment and axial force, this set of tests were chosen.
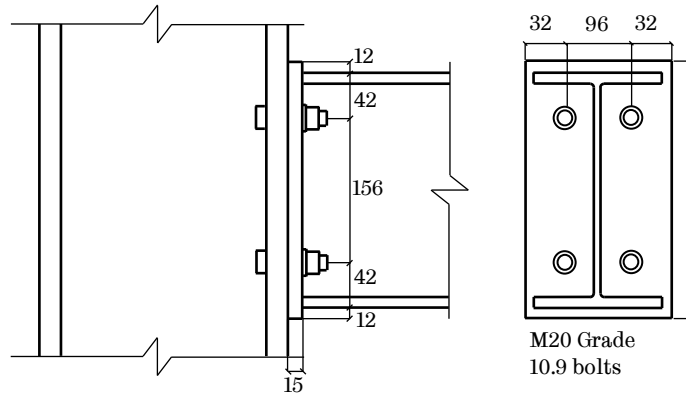
Figure 4-16 Flush endplate connection configuration

Table 4-3 Test information (Simões da Silva, et al., 2004)

Test	Axial force as percentage of N_{pl}	N (kN)
FE1	0	0
FE5	20% compression	-265
FE8	10% tension	130.6

4.3.2.2 T-stub stiffness generation

Similar to the model presented in Section 4.2.2, this flush endplate has been separated into two identical T-stubs, and only half of the T-stub (Figure 4-17) has been modelled due to its symmetricity. Due to the simplicity of the configuration of the connection, the locations of the springs are as shown in Figure 4-18. Force-displacement curves for this T-stub in both tension and compression are shown in Figure 4-19.

4.3.2.3 Validation results

Results of the simplified spring approach are presented in Figure 4-20 together with experimental results and detailed *ABAQUS* modelling
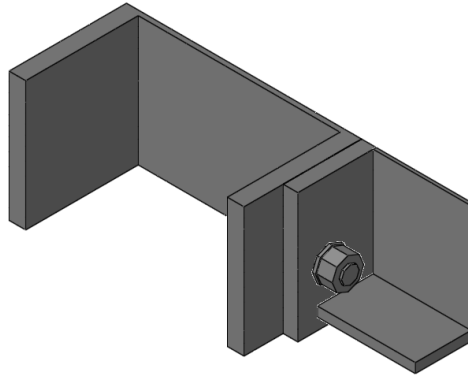
Figure 4-17 Detailed FE model for T-stub stiffness generation
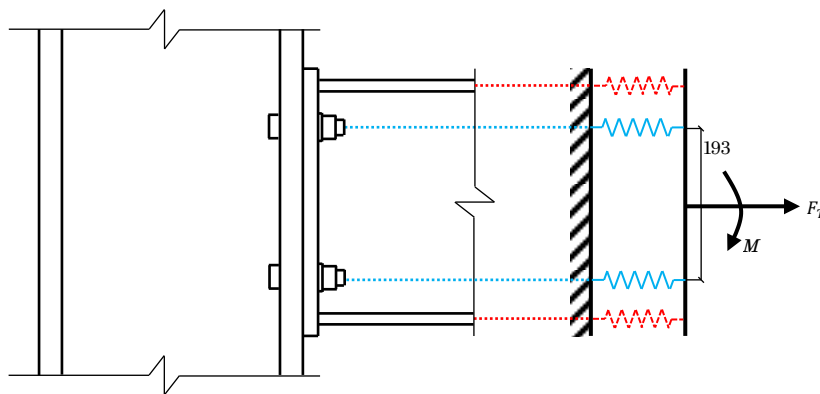
Figure 4-18 Simplified spring model transformation
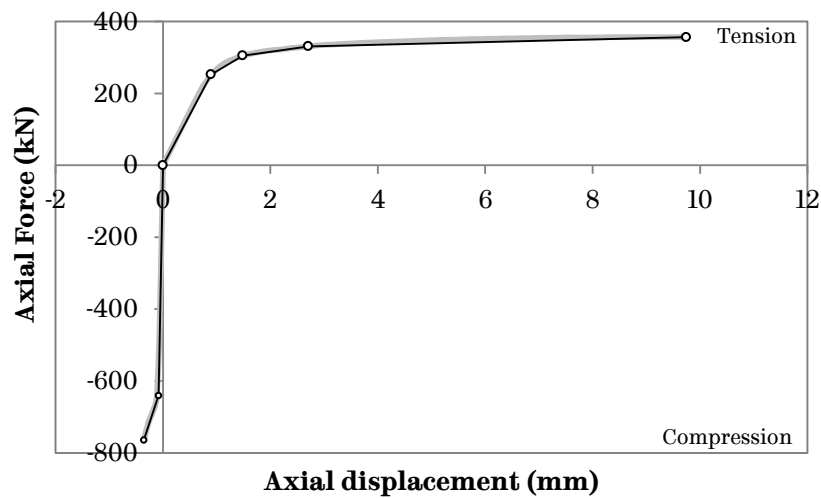
Figure 4-19 T-stub force-displacement curves

results for three tests mentioned in Table 4-3. It can be seen that for all

three tests, the simplified spring model can provide reasonably close

results compared to both the experimental results and the detailed
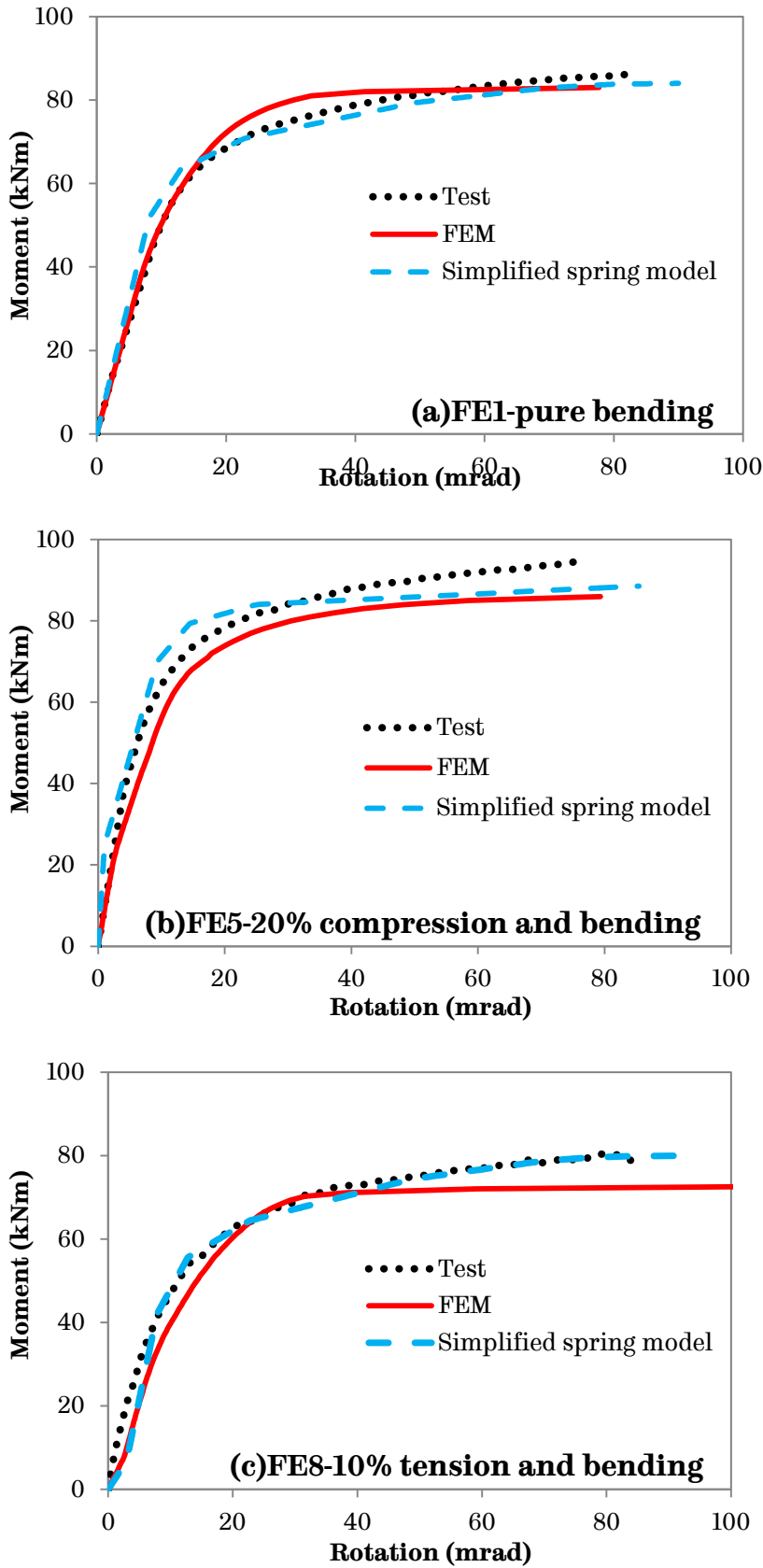
Figure 4-20 Validation results of FE1, FE5 and FE8

finite element modelling results. Therefore, the proposed simplified spring approach can be used to model steel beam-to-column connections under pure bending moment combined with tensile or compressive axial force.

4.4   Implementation of the simplified spring model into *VULCAN*

4.4.1   Existing spring model by Sun and further development

A spring connection model was proposed by Sun et al. (2015) in the research version of the finite element software *VULCAN*. This approach was used to simulate ductility of two types of steel beam-to-column connections and thus investigate their impact on the entire frame under elevated temperature. The simulations were conducted on two-dimensional multi-storey frames with assumptions made on restraints from adjacent frames and slabs. As the characteristics of each type of connections vary, the stiffness of springs was defined to reflect these differences by assumptions. Each connection model is made up of five springs, of which three are tensile springs, and the other two are compressive springs, as illustrated in Figure 4-21. Each tensile spring consists of three components, which are defined by their force-displacement characteristics entered by users. The overall stiffness of each tensile spring is then calculated as for components connected in series. The current version of the model only allows the same characteristic for each component of a certain type (column flange, bolt

or endplate), and therefore the axial characteristics of the springs are identical. The rotational stiffness of the whole connection is a result of the combination of the axial springs. This model is capable of modelling frames containing whole beams with connections on both ends of the beams. With this existing connection model, previously generated T-stub force-displacement relationships in Section 4.2.3 can be implemented into *VULCAN* with adjusted lever arms as described in Section 4.3.1 for modelling of different types of connections.
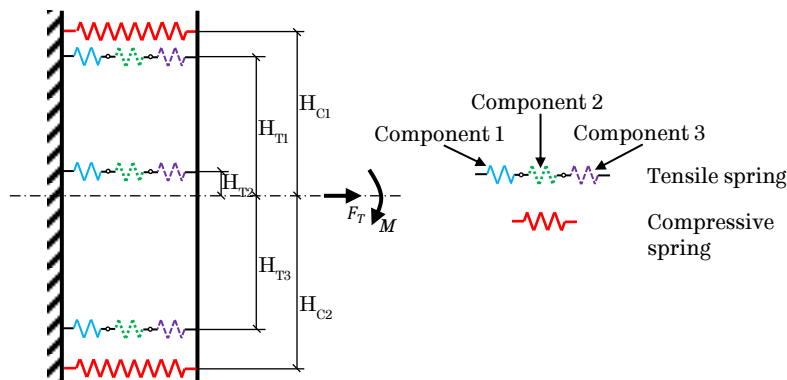
Figure 4-21 Spring connection model proposed by Sun et al. (2015)

Due to the limitation of the above spring connection model that all three of the tensile springs are identical, there was a need to modify the existing code to implement the simplified spring connection model into *VULCAN*. In effect, the spring characteristics were taken directly from full T-stub assemblies, and so it was unnecessary to consider the three components individually. To implement this, one component of each spring was selected to represent the T-stub, and the other two components were set to be very stiff and strong. Since the local conditions around the outer and middle springs are different, different

stiffnesses can be assigned to them according to location. With the modifications described above, the simplified spring connection model illustrated in Figure 4-13 was implemented into *VULCAN*. Before investigating the effect of various connections on frame behaviour, the proposed simplified spring connection model was validated against *ABAQUS* results at both ambient and elevated temperatures.

4.4.2   Validation at ambient temperature

Figure 4-22 presents the 2D rugby goalpost frame used for validation of the simplified spring connection *VULCAN* model against the *ABAQUS* spring model. The beam span and elevated height of the frame were 7.5m and 3.6m respectively, and its section information and material properties were the same as described in Section 4.2.2. The column bases were fully fixed while the tops were only allowed to move vertically, to mimic the restraint provided by the upper structure. A vertical point load, F=1500kN, was applied at the centre of the beam. Figure 4-23 represents the details of the spring model used for beam-to-column connections on both ends of the beam. A same model was also produced in *ABAQUS* to be used as the control results, which has been validated previously in Section 4.3.1.

As illustrated in Figure 4-24, results produced by *VULCAN* and *ABAQUS* have a good correlation. It shows that the proposed simplified spring connection model is robust and can be used to model flush endplate connections at ambient temperature.
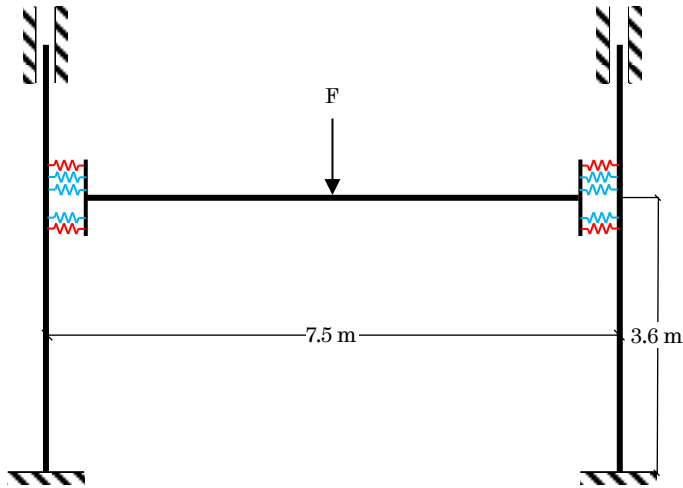
Figure 4-22 2D frame model used in *VULCAN* and *ABAQUS*
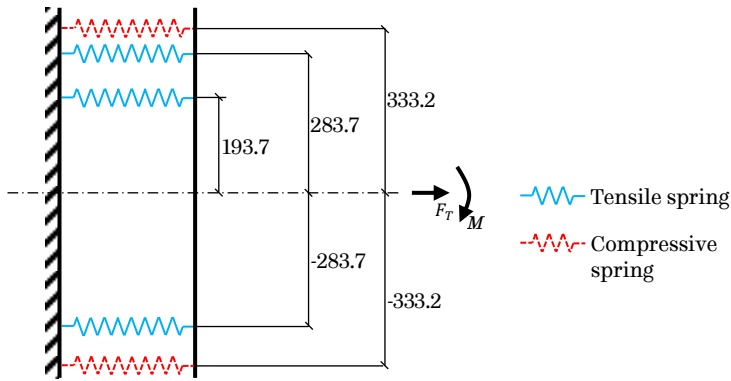
Figure 4-23 Simplified spring connection model (unit: mm)
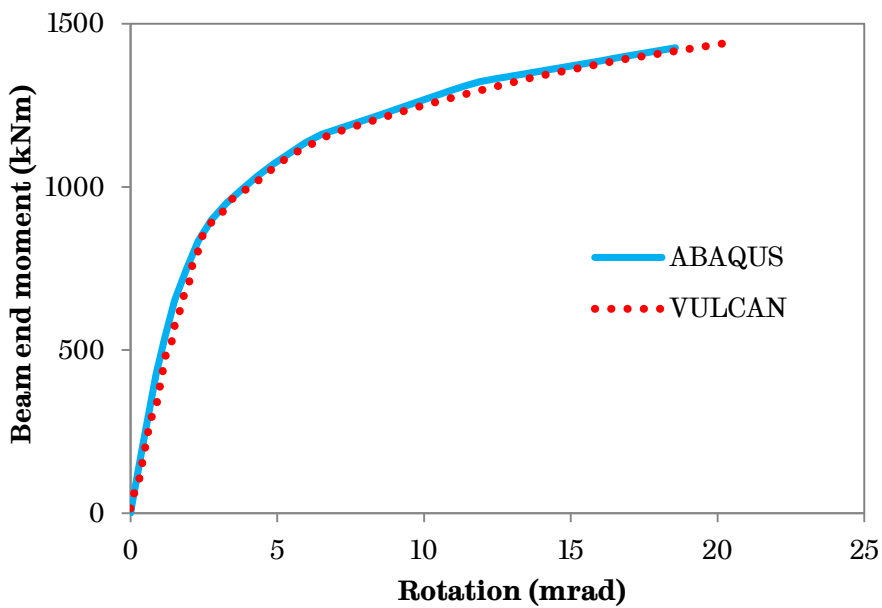
Figure 4-24 Validation of the simplified spring model in *VULCAN* and *ABAQUS* at ambient temperature

4.4.3   Validation at elevated temperature

The same models used for ambient temperature validation in Section 4.4.2 were adopted, with changes made on temperature data. The frame was assumed to be heated in ISO 834 standard fire (ISO, 1999). To make sure the models in *ABAQUS* and *VULCAN* were exactly the same, the model frame in *ABAQUS* was loaded up to desired level first and then heated up.

The heating process was achieved in *ABAQUS* by adding a pre-defined temperature field and in *VULCAN* by adding a temperature data block in its input file. The temperature profiles for elements in the frame are presented in Table 4-4. The reduction factors were used to apply to ISO 834 standard fire curve (Figure 4-25) to generate temperature profile for each element. The beam was heated directly from the bottom flange, thus the temperature of bottom flange and web were assumed to be the same as the fire temperature. The top flange, on the other hand, was assumed to be slightly cooler due to the presence of the concrete slab. The columns are normally protected, thus a reduction factor of 0.7 was applied to the fire temperature. The connection was assumed to be the same temperature as the columns because normally connections are protected and due to its complex composition, it should heat up slower than bare steel. *VULCAN* research version is capable of dealing with the spring stiffness degradation with increasing temperature automatically;

hence the deduction in stiffness and strength of the connections can be simulated.
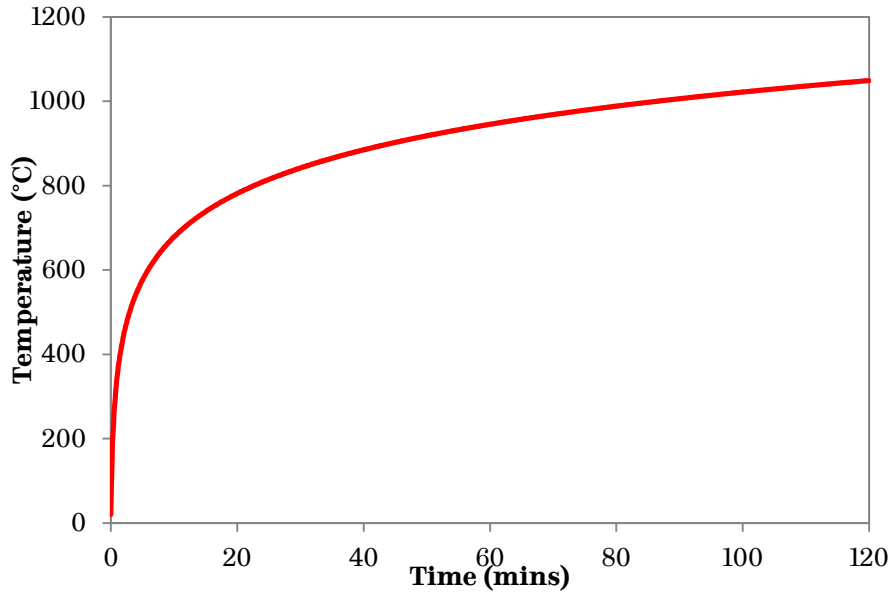
Figure 4-25 ISO 834 standard fire curve

Table 4-4 Element temperature profile in two dimensional validation frame

Element	Temperature profile type	Reduction factor applied on ISO 834 standard fire curve
Beam	Flange – Web – Flange	0.8 – 1.0 – 1.0
Column	Uniform	0.7
Connection	Uniform	0.7

550°C is commonly regarded as the failure temperature for structural steel as the material yield strength reduced to about 60%. Therefore two temperatures at 500°C and 600°C were chosen for the elevated temperature validation. As the moment capacity of the connections reduces with increasing temperatures, the point loads in these two models were set at 1500kN for the 500°C case and 1000kN for the 600°C case.

The validation results of the proposed simplified spring approach against *ABAQUS* simulation are represented in Figure 4-26 and Figure 4-27. It can be seen that the ultimate moment capacities agree well using two methods for both 500°C and 600°C. Thus it can be concluded that the proposed simplified spring connection modelling approach can be used under both ambient and elevated temperatures.

4.5 Chapter conclusion

In this chapter a simplified spring connection modelling approach has been presented along with explanation of the detailed development procedures. It has been validated against existing isolated test data and *ABAQUS* modelling results. Based on the validation results, it can be concluded that the proposed simplified spring modelling approach is suitable to be used under both ambient and elevated temperature in *VULCAN* for simulating the behaviour of steel flush endplate connections. From the studies which have been performed in this chapter, the following conclusions can be drawn:

- Bolt row(s) are strengthened when located closer to beam flanges. When grouping the bolt rows, their locations need to be taken into consideration.

- End distance has effects on the tensile strength of the T-stubs, but compressive strength was not affected.
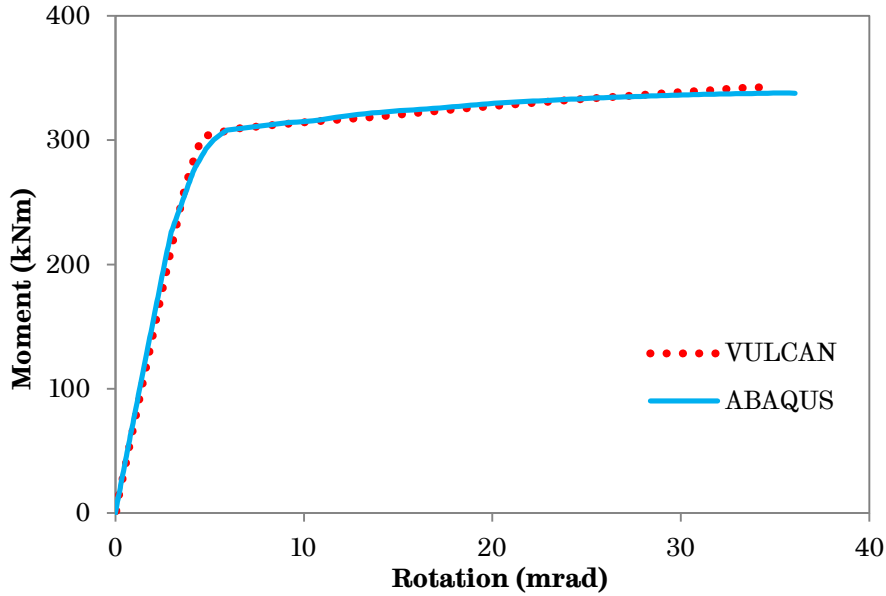
Figure 4-26 Validation of the simplified spring model in *VULCAN* and *ABAQUS* at 500°C
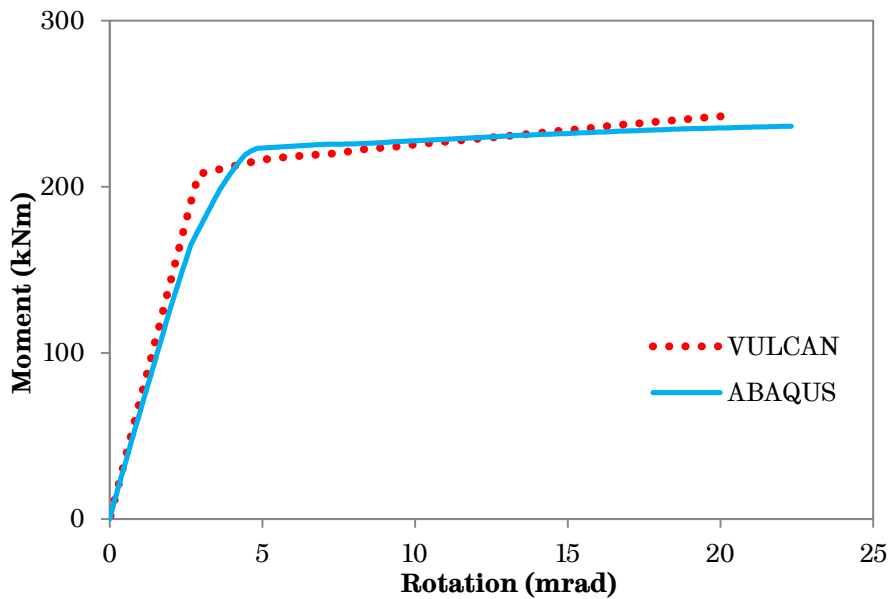
Figure 4-27 Validation of the simplified spring model in *VULCAN* and *ABAQUS* at 600°C

- A simplified spring modelling approach can accommodate various combinations of axial force and bending moment and can produce reasonably accurate simulation results both at ambient and elevated temperatures.

- The proposed simplified spring connection modelling approach can also be used for shallower connections which need only two tensile springs and two compressive springs to provide good agreement with experimental results.

The successfully developed simplified spring connection modelling approach can be used in frame response analysis which will be conducted in Chapter 5.

Page Intentionally Left Blank

5

Performance of 2D Steel and 3D Composite Frames in Fire

Page Intentionally Left Blank

5.1 Introduction

The importance of steel and composite beam-to-column connections has been emphasised in both full-scale fire tests at Cardington (Newman, et al., 2006) and real life disasters, for instance, the collapse of WTC 7 (FEMA, 2002a, 2002b). Traditionally the connections are assumed to be able to withstand fire attack because of their lower temperature and slower heating rate compared with the structural members they are linked to. However, the above evidence has shown that the connections are actually the most vulnerable structural members under fire conditions. Connections are typically designed for the ultimate limit state at ambient temperature. However, the force scenario changes significantly under elevated temperature and becomes much more complex.

Conventionally, the connections in frame simulations are usually assumed to be either rigid or pinned for ease of modelling, due to the simplicity of modelling the connections in this way. In some situations, these assumptions are made to save computational and/or time costs because the existing Component Based connection models require extensive computational and time costs. The simplified spring connection modelling approach proposed and validated in Chapter 4 can provide an accurate and reliable way to include both the axial and the rotational ductility in frame analysis much more efficiently.

In this chapter, two sets of investigations have been conducted to demonstrate the importance of incorporating connection axial and rotational ductility in frame analysis. A set of 2D internal steel frame models with varying beam spans, from a relatively short length (6m) to long-span (18m), have been studied first. These models have been chosen as continuations of the 2D isolated rugby goalpost models adopted in the previous chapters. Following which, a range of 3D composite frame models with increasing secondary beam spans has been conducted to include the effect of the concrete slab and composite action. The effect of load ratio on connection ductility demand in 3D composite frames has also been investigated. This chapter provides an insight of frame response with more realistic, ductile connection models compared with traditional rigid or pinned choices.

5.2   Influence of connection ductility on 2D steel frames

5.2.1   2D steel frame model details

An internal bay of a 2D 2-storey frame has been selected to investigate the influence on frame behaviour when including connection ductility compared with conventional rigid or pinned assumptions. The beam spans vary from 6m to 18m to provide an insight of the effects of the length of the beam on the ductility demands on the connections.

5.2.1.1   Geometrical configurations and loadings

Figure 5-1 illustrates the 2D frame and connection details adopted in this study. The bay of interest is assumed to be the middle one of a 3-bay frame as depicted in Figure 5-1(a). The beam lengths, L, vary from 6m to 18m in increments of 3m. The factored uniformly distributed line load at ambient temperature is 28.86kN/m (equivalent to a factored area load of 9.62kN/m^2). This load gives a line load at the Fire Limit State of 18.9kN/m and the load ratio (R) is assumed to be 0.4 for all cases. The beam sizes according to the beam span and the actual load ratio are shown in Table 5-1; a UC305x305x198 is selected as the column for all cases. Structural steel grade S355 is used for both the beams and the columns, with ambient temperature yield and ultimate strengths of 355N/mm^2 and 470N/mm^2 respectively.

To imitate the axial restraint provided by the adjacent cold structures, one linear elastic spring is placed on each side of the investigated bay as indicated in Figure 5-1(b), which are referred to as the 'support spring' in this section. The 'support springs' link this bay to a fixed end support. The rotational flexibility of the 'support springs' are ignored in this study and are therefore assumed to be rotationally rigid. The stiffnesses of these 'support springs' are affected by either (a) the combined lateral stiffness of the upper and lower cold columns in the adjacent bay, or (b) the sum of the axial resistance of the beams and the connections next to the cold column. In this study, the elastic stiffness of the 'support
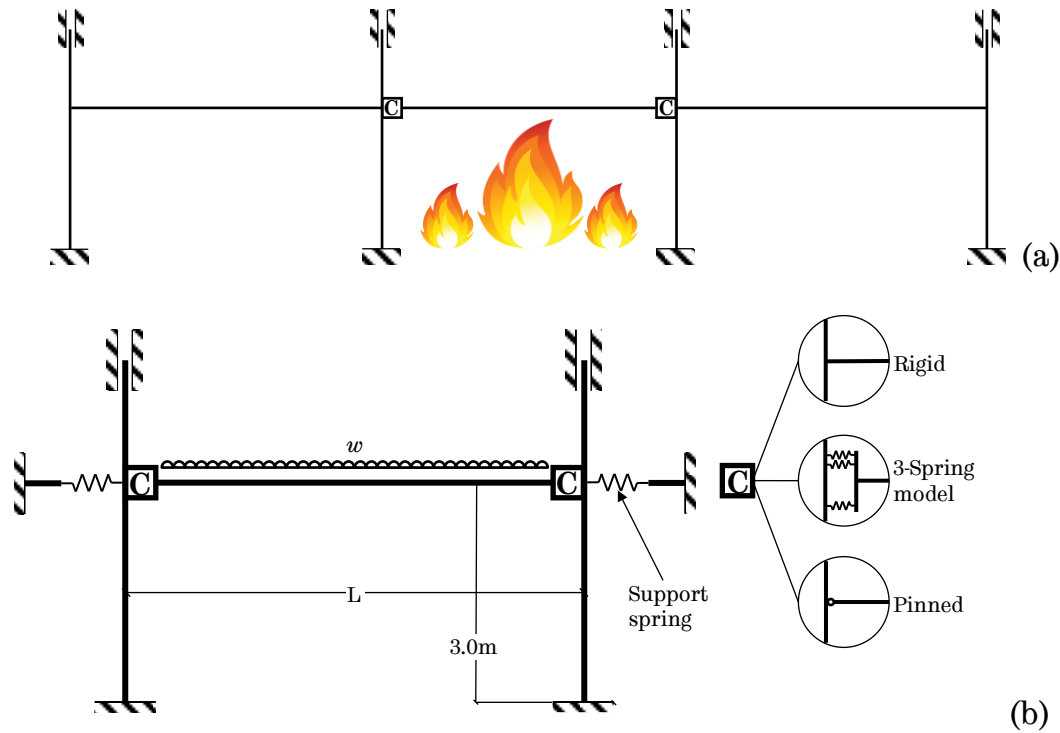
Figure 5-1 2D steel frame model and connection details

Table 5-1 Beam section selection

Model ID	Beam span (m)	Beam section	Actual load ratio, R
2D-6	6	UB305×127×42	0.39
2D-9	9	UB406×178×67	0.40
2D-12	12	UB533×210×92	0.41
2D-15	15	UB686×254×125	0.39
2D-18	18	UB762×267×147	0.43

springs', K_L, are assumed to be calculated based on the aggregate lateral stiffness of the adjacent cold columns as:

$$K_L = \sum_{i=1}^{n} K_{l,i} \tag{5.1}$$

$$K_{l,i} = \frac{12EI_{i,c}}{L_c^{\,3}} \tag{5.2}$$

where n is the number of adjacent columns; $K_{l,i}$ is the combined lateral stiffness of ith adjacent cold column; E is the Young's modulus of the column at ambient temperature, which is assumed to be 210kN/mm^2 in

this study; $I_{i,c}$ is the second moment area of the column section selected and finally L_c is the height of the column (Sun, et al., 2015). For this study, the investigated bay is assumed to be the middle bay of a 3-bay frame, thus the axial stiffness of the 'support springs' is calculated to be 47.5kN/m. The employment of the 'support springs' is a simplification of the actual lateral restraint provided by the cold adjacent structures to the hot bay, but this method is chosen because it can produce approximation with ease of both calculation and simulation.

5.2.1.2   Connection details and spring stiffness generation

For each beam span, three types of connection rigidities were assigned to the beam-to-column connections: (1) rigid connection (axially and rotationally rigidly connected), (2) simplified spring connection (axially and rotationally semi-rigidly connected) and (3) pinned connection (axially rigidly connected and rotationally free).

The rigid and pinned connection cases can be achieved in *VULCAN* by amending the corresponding spring type. For the simplified spring connection case, the simplified spring connection model developed in Chapter 4 was used. The simplified spring connections were assumed to be flush endplate and the design details according to SCI P398 (UK Connections Group, 2013) for each frame size are shown in Figure 5-2. All endplates were in structural steel grade S275, and all bolts were in Grade 8.8. The same pre-processing steps were conducted according to Chapter 4: (1) each of the connections was divided into three T-stubs

(indicated in grey dash lines in Figure 5-2) followed by (2) the generation of their tensile and compressive stiffnesses using *ABAQUS*. These stiffnesses were then inputted into *VULCAN* as the stiffnesses of the three springs so that the simplified connections were implanted into each model. The spring stiffnesses of each of the connections are presented in Figure 5-2 next to the connection details.

The size of the beam mesh element depends on the span of each frame. Due to the restriction of the current version of *VULCAN* research code only six elements (13 nodes) are allowed for each beam when the simplified spring connection models are included. Thus the size of the beam mesh element is one-sixth of the span of the beam.

5.2.1.3   Boundary conditions

As illustrated in Figure 5-1(b), the column bases of the 2D frame are fully fixed, while the tops of the columns are only allowed to move vertically. Restraints provided by the adjacent cold structures are simulated as axial elastic springs as explained in Section 5.2.1.2.

5.2.1.4   Temperature data

The fire protection scheme adopted in this study is presented in Figure 5-3. The beam is left un-protected and the temperature profile selected is flange-web-flange, where the reduction factors on the standard fire curve are 0.9-1.0-1.0. The lower columns are assumed to be protected therefore a uniform temperature distribution with a reduction factor of 0.7 on the standard fire curve is selected. The upper columns are
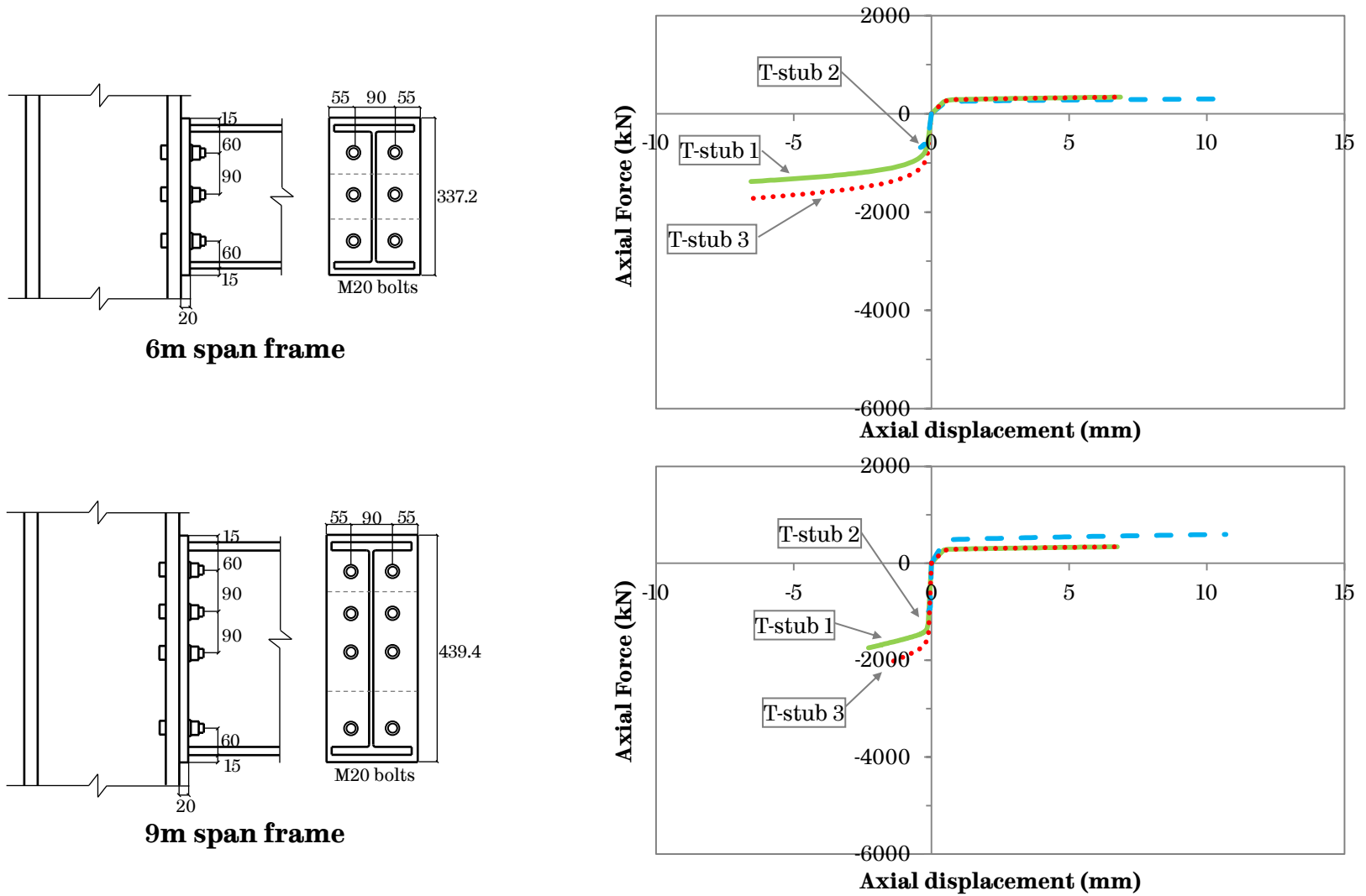
Figure 5-2 Flush endplate connection details and T-stub stiffnesses
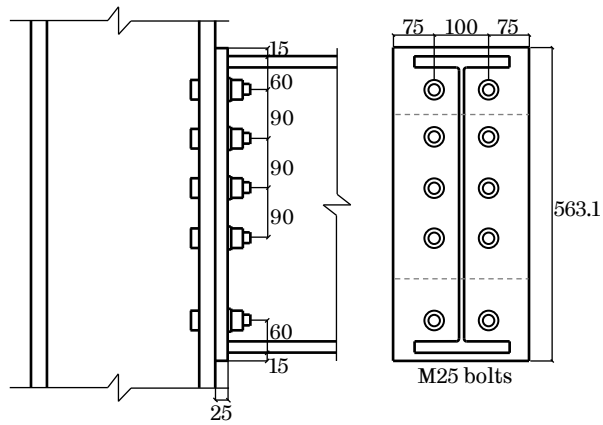
12m span frame
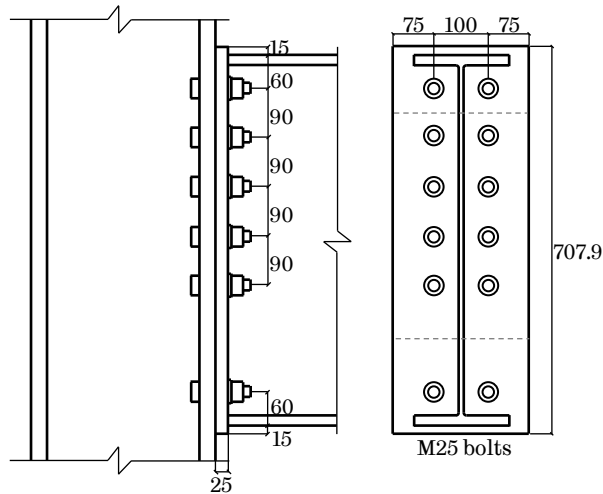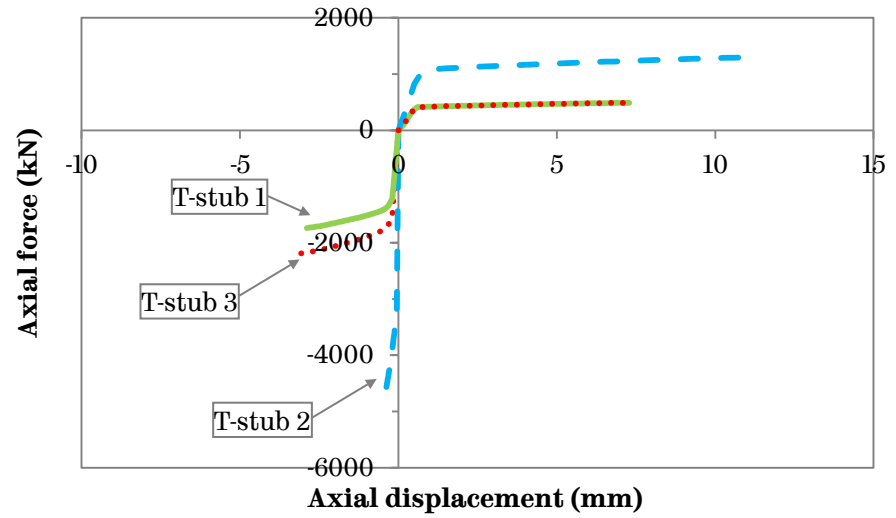
15m span frame
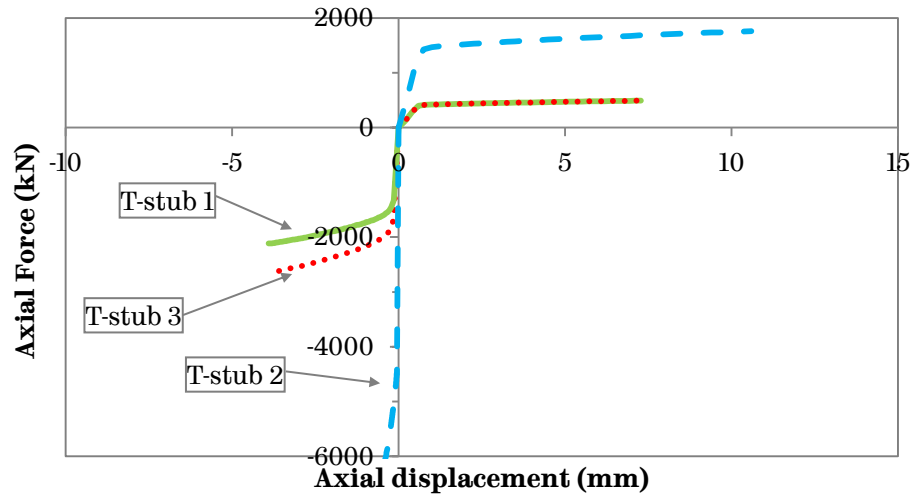
Figure 5-2 (continued) Flush endplate connection details and T-stub stiffnesses
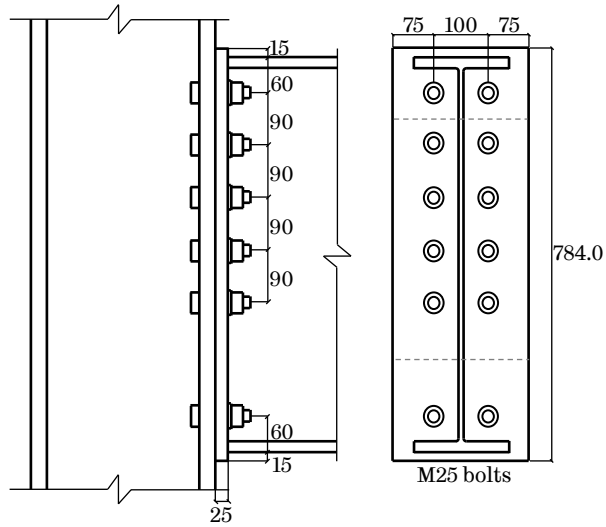
18m span frame

Figure 5-2 (continued) Flush endplate connection details and T-stub stiffnesses
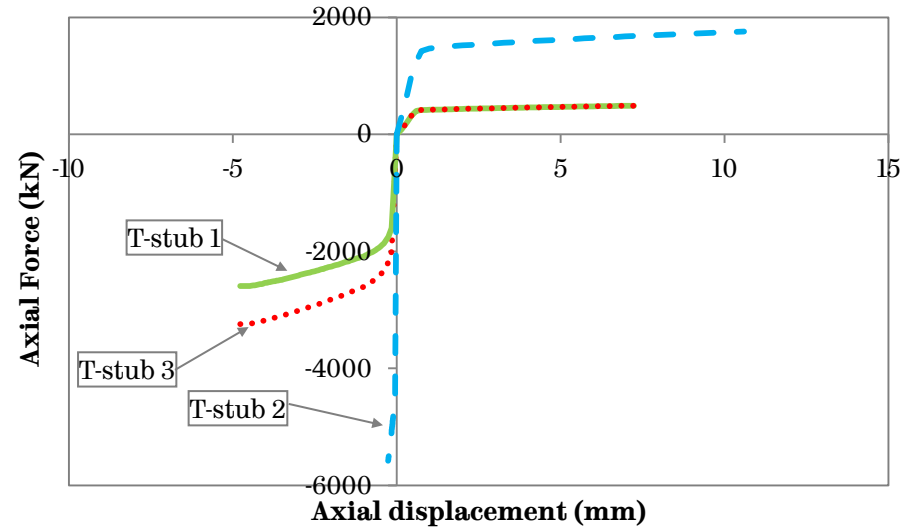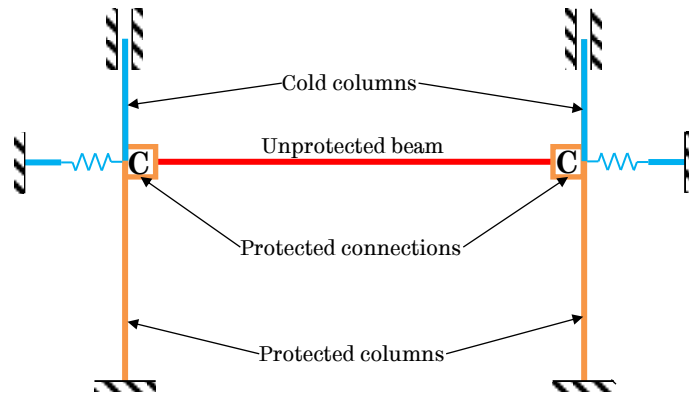
Figure 5-3 Fire protection scheme
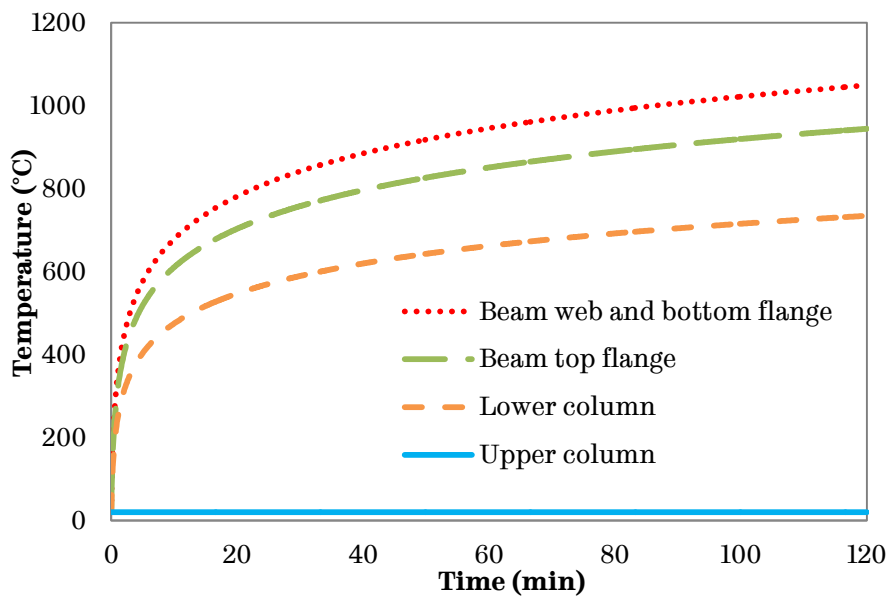
Figure 5-4 Member temperature up to 120 minutes

assumed to stay at an ambient temperature of 20°C, together with the supporting structures. Since the connections are generally protected and are greater in mass due to their complexity in composition, the same temperature distribution as the lower columns is adopted. The temperatures of the members are shown in Figure 5-4.

5.2.2   Results and discussion

Figure 5-5 presents the axial force at the connections versus the beam temperature for various beam spans. The scales of the axes are kept

consistent for ease of comparisons. Table 5-2 summarises the maximum axial force for the different spans, with the axial forces in the simplified spring and the pinned connection scenarios shown both in the actual force values and in the percentage values of the axial force in the rigid connection scenario.

The axial force in the restrained beams (models with the rigid and the pinned connections in the study) usually goes through three stages in fire. With rising temperature, the axial compressive force develops and increases because of the restrained thermal expansion, with a limited amount of deflection. The ends of the beam push outwards on the connected column. During this stage, the material properties are initially elastic but degrade as the members get hotter during the fire. The axial force generated in the beam/at the connections reaches a peak compression, which is when the first stage finishes. In the second stage, the beam deflection increases which leads to a reduction in the axial compressive force in the beam. As temperature increases still further, the axial force eventually reduces to zero, which denotes the end of the second stage. In the third stage (often referred to as the catenary action stage) the axial force in the beam/at the connections enters the tensile force region resists the tensile forces resulting from the beam hanging like a cable between the two connections. The axial tensile force grows until peaking at the maximum tensile force, which is followed by a reduction in the axial tension until the end of the simulation.
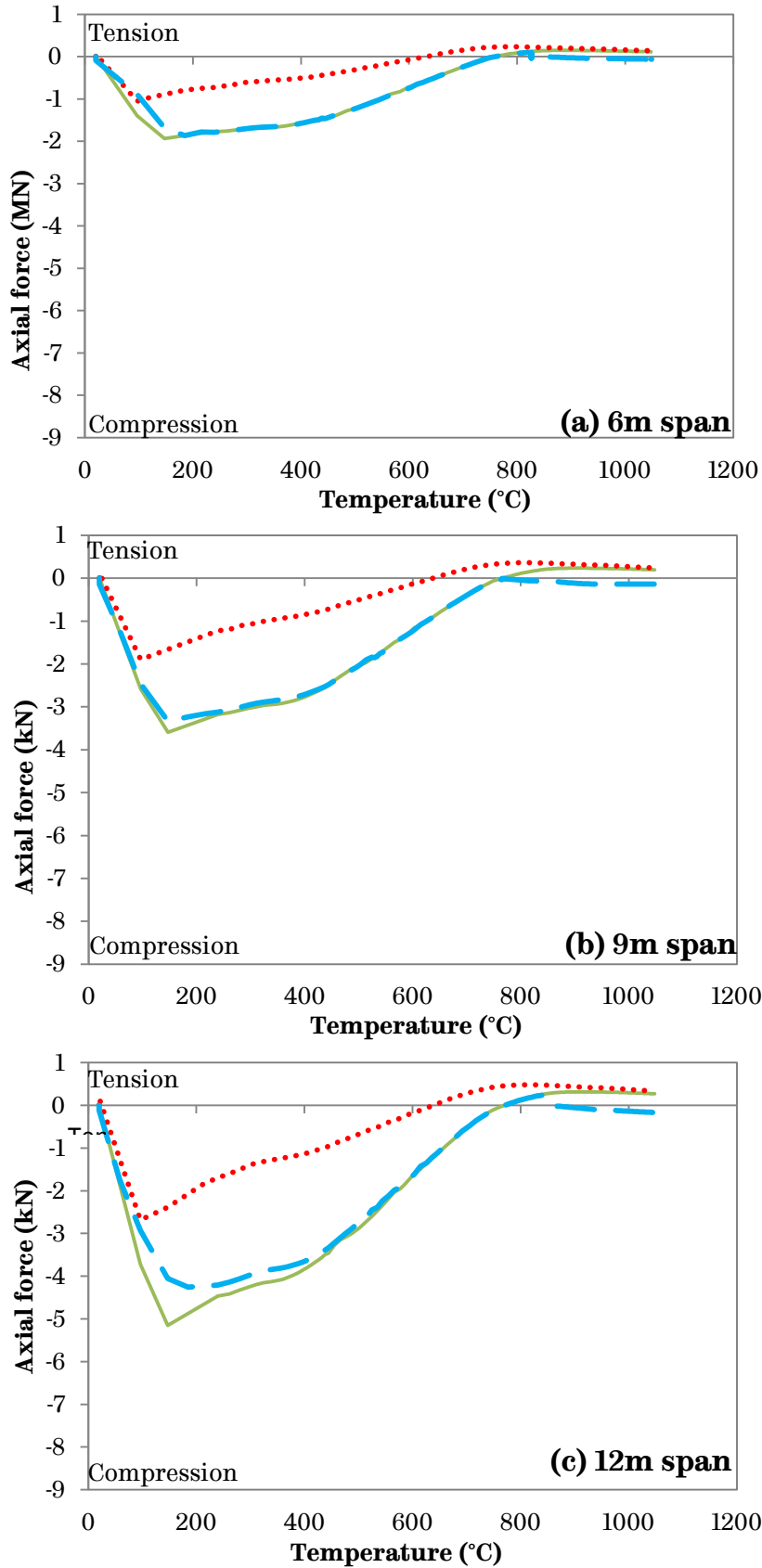
Figure 5-5 Axial forces at connections for various spans of the beam

(d) 15m span

(e) 18m span
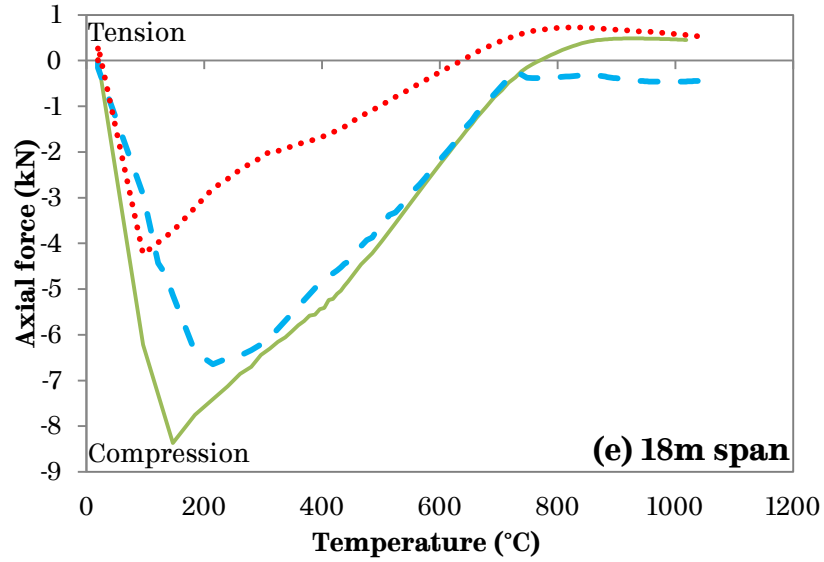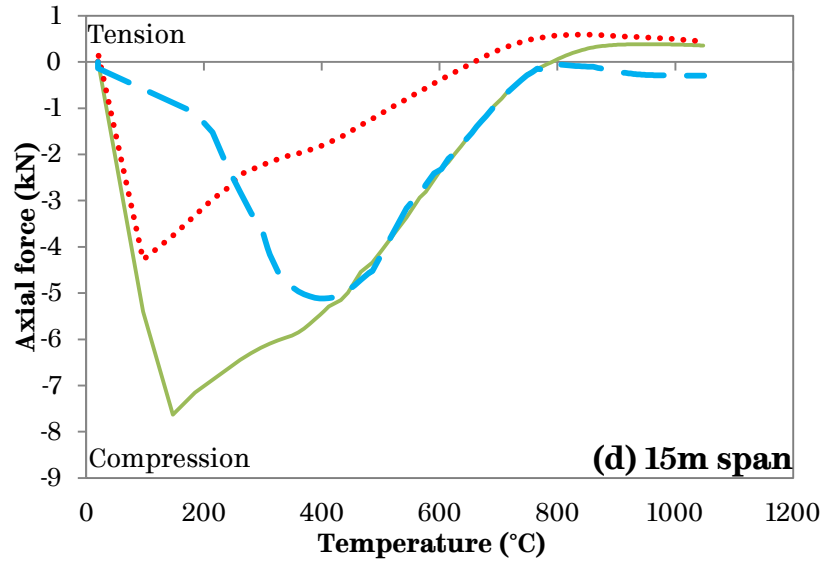
——— Rigid connection   – – – Simplified spring connection   ········· Pinned connection

Figure 5-5 (continued) Axial forces at connections for various spans of the beam

Table 5-2 Maximum axial force at the connections comparisons

Beam span (m)	Axial force in the rigid connection case(kN)	Simplified spring connection case		Pinned connection case	
		Axial force (kN)	Percentage of the rigid case (%)	Axial force (kN)	Percentage of the rigid case (%)
6	1939	1868	96	1054	55
9	3593	3339	93	1895	53
12	5153	4258	83	2688	52
15	7634	5120	67	4280	56
18	8370	6646	79	4232	51

When the axial ductility is included, for example by including the simplified spring connection model in this study, the axial force response changes correspondingly. It can be seen from the plots that, at short spans (6m), the axial force at the connection is almost identical for the rigid and the simplified spring connection cases, but the differences get more obvious with the increase of the beam span. The percentage values of the simplified spring connection case for different spans in Table 5-2 also indicate that the longer the span the more reduction of the axial force at the connection when spring ductility is included. This finding articulates that in common practice simulations when the connections are simply assumed to be rigid both axially and rotationally, the axial forces at the connection are very possibly over-estimated especially for long-span structures.

For the pinned connection scenarios, comparing the maximum axial forces with the rigid connection scenarios, the percentage values are not affected much by the span of the beam, staying between 50-55%. The reductions in the axial force at the connections are the result of the released rotational degrees of freedom in the pinned cases. The rotational flexibility permits the thermal expansion to be accommodated by thermal bowing. Therefore the compressive forces exerted on the connections by the beam are reduced dramatically. However, by comparing the actual force values with the simplified spring connection scenarios, it can be observed that the differences become smaller with increasing span. This observation leads to a

deduction that in common practice simulations by simply assuming the connections to be axially rigid but rotationally free the resulting axial forces acting on the connections may be under-estimated, especially for smaller spans. For the longer span cases, the pinned connection assumptions provide similar maximum compressive force as the simplified spring connection assumptions, but the axial force responses are not as ductile.

It is indicated in Figure 5-5 that the peaks of the axial force curves with the simplified spring connection cases are smoother than those of the pinned and the rigid connections cases. This variation is caused by the axial ductility that the simplified spring connection model provides. With the axial flexibility in the connections, the end of the beams can move inwards or outwards when the connections experience tension or compression, closely simulating the axial ductility the connections have in reality.

In this section, the benefits of including connection ductility both axially and rotationally have been studied. Conventionally assumed rigid or pinned connections with no axial ductility either over- or under-estimate the axial forces at the connections, or fail to capture the ductile transition of the axial forces during heating.

5.3   Influence of connection ductility on 3D composite frames

5.3.1   Composite frame simulations in *VULCAN*

Finite element modelling software *VULCAN* can be used for modelling steel structures in fire as shown in previous chapters, and it can also be used to simulate the behaviour of three-dimensional composite structures under elevated temperature by considering the composite frames as assemblies of the beam (including the column), connection and layered floor slab elements. When modelling composite structures, the local reference plane is assumed to be fixed and coincide with the mid-surface of the concrete slab as illustrated in Figure 5-6. The positions of the other nodes of the above elements are decided by offsetting from the local reference plane, which ensures that the beam top flanges are in contact with the composite slab bottom surface, and the connection elements are located in the centre of the beam depth.

The composite slab is simulated as a collection of finite plate elements, which represent either concrete or reinforcement steel mesh layers. The slip between the plain concrete layers and the reinforcement mesh layers were assumed to be non-existent. Therefore the bond between the reinforcement meshing bars and the concrete surrounding them are assumed to be perfect. The orthogonal reinforcement steel mesh layers were modelled using smeared steel layers, which have uniaxial stiffnesses along the directions of the reinforcement meshing. The user has the freedom to decide the amount of the reinforcement meshing
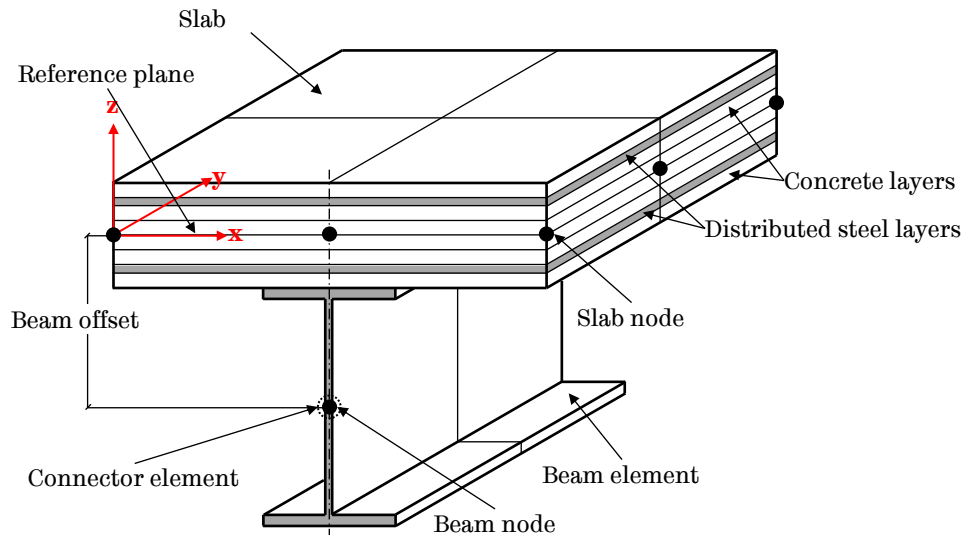
Figure 5-6 Division of composite structure into beam and slab elements
(Huang, et al., 2004)

layers by altering the thickness of them, which is equivalent to the total area of the rebar in the corresponding direction. Based on research done by Huang et al. (1999), it is suggested that the reinforced concrete slab should be divided into 10-20 layers when modelling its behaviour in fire conditions, depending on its overall thickness.

The composite interaction between the concrete slabs and the steel beams can be modelled by shear connector elements. These elements have zero length and are formed by linking two nodes, one on the beam and one on the slab. If full bond between the concrete slabs and the steel beams is assumed, the shear connector elements can be replaced by sharing nodes between the slab and the beam elements.

The temperature profile applied to the composite slab cross-section is slightly more complicated than that applied to steel elements alone. There are five types of the temperature profile for slab elements available in *VULCAN*, which are (1) uniform distribution, (2) linear

distribution, (3) bi-linear distribution, (4) tri-linear distribution and (5) user defined. Lin et al. (1989) reported, based on the results of fire tests on reinforced concrete slabs, that the temperature increment of the top surface of the slab was approximately 13.5% of the bottom surface due to the poor thermal conductivity of concrete. *VULCAN* provides the flexibility for the user to define the temperature of each layer if test data or other reliable resources are available, or the user can use the above recommendation to produce a temperature profile.

5.3.2   Composite frame model details

5.3.2.1   Geometrical configurations

The models consist of a typical internal bay from a steel-concrete composite frame. Extra strips of composite slab, together with their downstand steel beams, located on each side of the bay are included in the models to mimic the effect of the adjacent bays and will be discussed further in detail in Section 5.3.2.3. Five frame sizes are chosen for this study, and the general layout is shown in Figure 5-7. The length of the primary beam (L_{prm}) is kept unchanged at 6m while the lengths of the secondary beams (L_{sec}) are changed from 6m to 18m with intervals of 3m. The design of the structural members are according to BS EN 1994-1-1 (CEN, 2005d) and BS EN 1994-1-2 (CEN, 2005e) with up to 60 minutes of fire resistance, and are shown in Table 4-3. For all three groups of models, other design details are kept unchanged, including:

- Column section: UC305 × 305 × 198;

- Height of column: 3m above and 3m below slab panel;

- All steel sections are in S355;

- Light-weight concrete with a trapezoidal profiled decking - ComFlor60 with 1.0mm thickness (see Figure 5-8);

- The slab was divided into 13 layers including two layers of reinforcement mesh;

- Reinforcement mesh: A193;

- Single shear stud per trough;

- Permanent and variable loads: 3.5kN/m^2, resulted in a factored combined load of 9.62kN/m^2.

5.3.2.2   Connection details and spring stiffness generation

For each frame size, three types of connection rigidities are used for the eight secondary beam-to-column connections (shown as ■ in Figure 5-7): (1) rigid connection, (2) simplified spring connection and (3) pinned connection. The four secondary beam-to-beam connections and the eight primary beam-to-column connections (shown as □ in Figure 5-7) are kept as pinned connections throughout the entire study. Secondary beam-to-beam connections normally adopt fin-plate connection in practice (as this makes construction safer) and for the purpose of this group of parametric studies, the primary beams are assumed to be connected to the web of the columns using fin-plate connections, so it is reasonable to consider these connections as pinned connections.
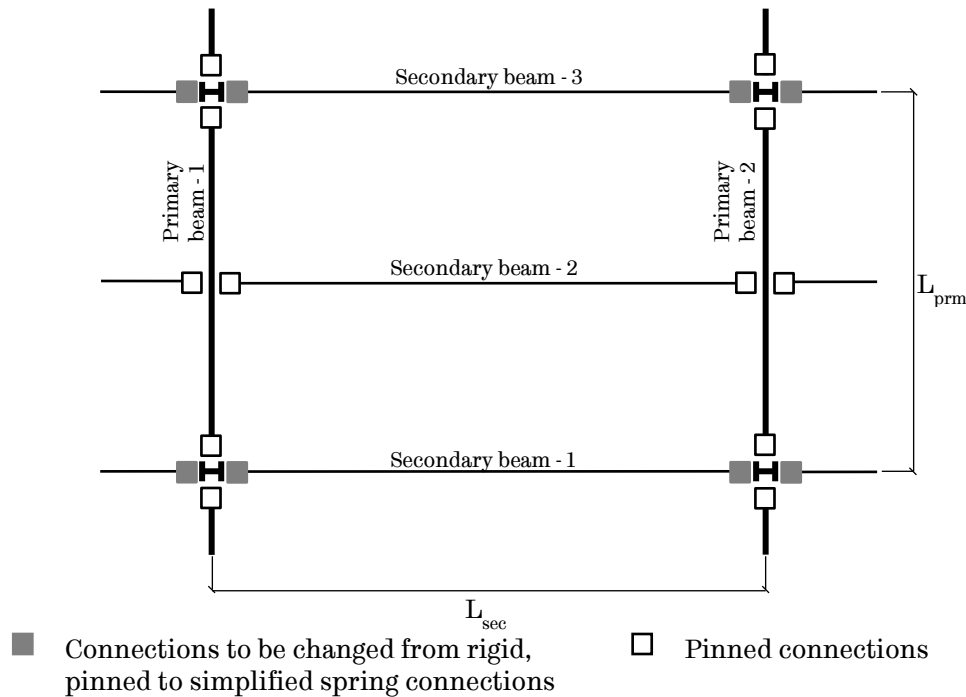
Figure 5-7 General floor layout

Table 5-3 Beam section sizes

Model ID	Frame size	Primary beam	Secondary beam
FS1	6m×6 m	UB356×127×33	UB254×102×25
FS2	6m×9 m	UB457×152×82	UB305 ×165 ×54
FS3	6m×12 m	UB457×151 ×74	UB457 ×152 ×82
FS4	6m×15 m	UB610×305×179	UB533×210 ×122
FS5	6m×18 m	UB762×267 ×197	UB686×254 ×140
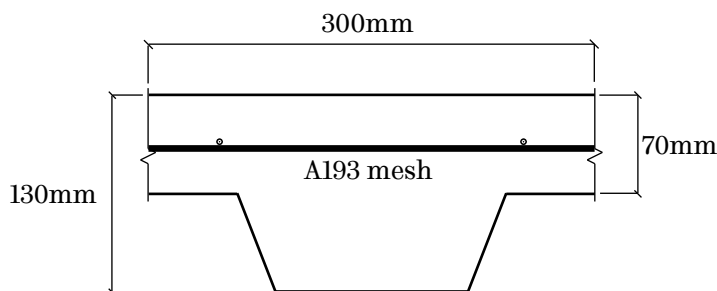
Figure 5-8 Reinforced concrete slab cross-section with ComFlor60 steel decking and A193 mesh

The rigid and pinned connection cases can be achieved in *VULCAN* by amending the corresponding spring type. For the simplified spring connection case, the simplified spring connection model developed in Chapter 4 is used. The simplified spring connections are assumed to be

flush endplate and the design details according to SCI P398 (UK Connections Group, 2014) for each frame size are shown in Figure 5-9. All endplates are in structural steel grade S275 and all bolts are in Grade 8.8. The same pre-processing steps were conducted according to Chapter 4: (1) each of the connections was divided into three T-stubs followed by (2) the generation of their tensile and compressive stiffnesses using *ABAQUS*. These stiffnesses are then inputted into *VULCAN* as the stiffnesses of the three springs so that the simplified connections are implanted into each model. The spring stiffnesses of each of the connections are presented in Figure 5-9 next to the connection details.

The sizes of the beam and slab elements depend on the span of each frame. Due to the restriction of the current version of *VULCAN* research code, only six elements (13 nodes) are allowed for each beam when the simplified spring connection models are included. The size of the beam element is $1/_6$ of the span of the beam. The width of the slab elements depends on the span of the primary beam, which is constant at 6m. Therefore the width of the slab elements stays at 1m. The length of the slab elements, on the other hand, varies according to the span of the secondary beams and again is $1/_6$ of the secondary beam span.

(a) 6m × 6m
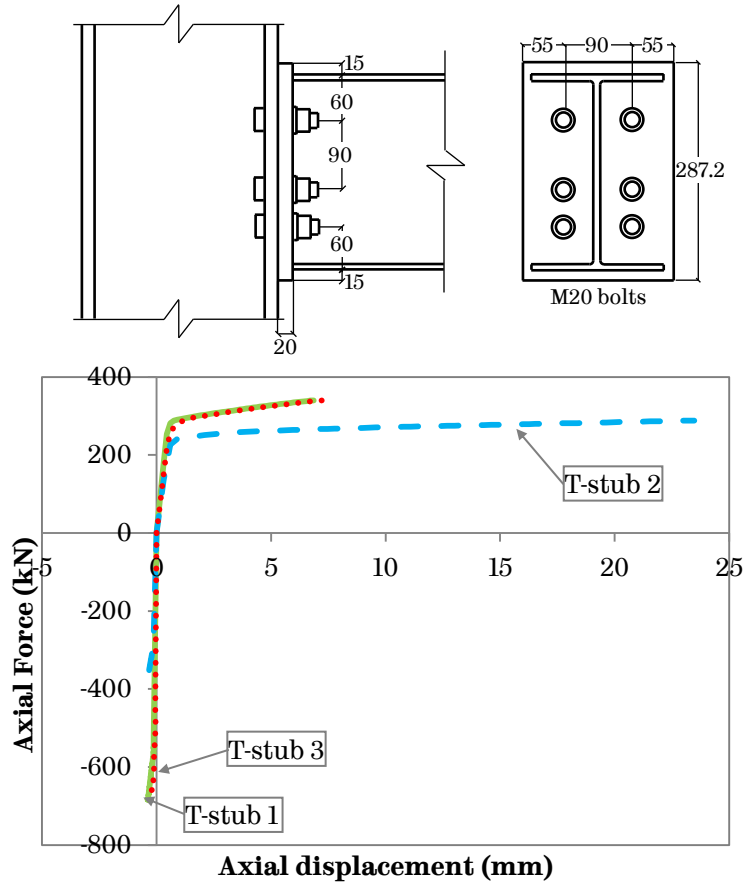
(b) 9m × 6m
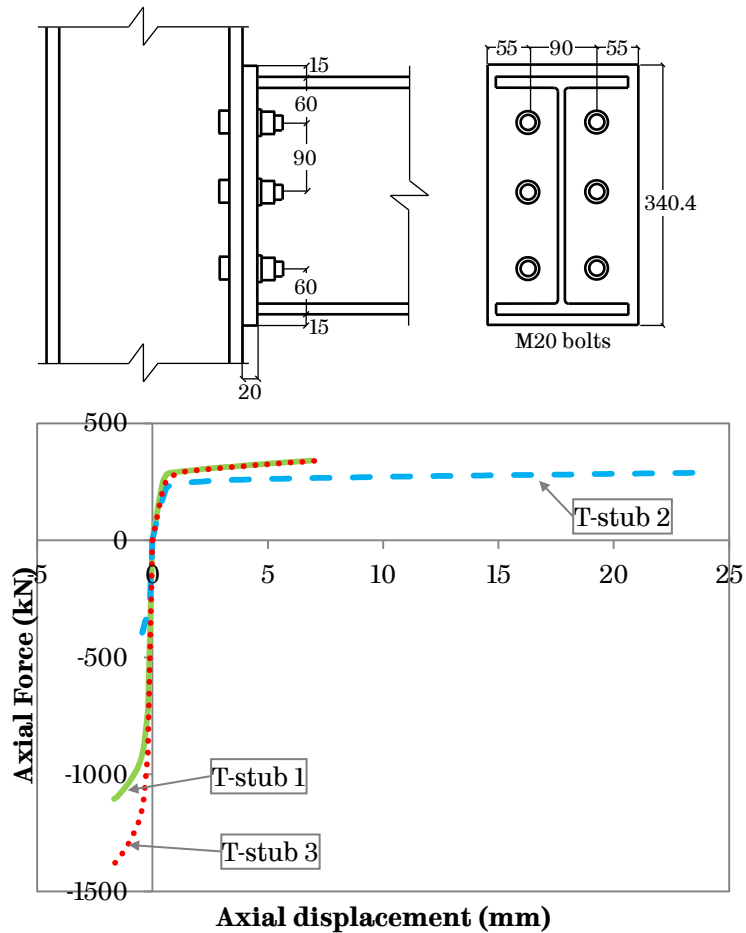
Figure 5-9 Flush endplate connection details and T-stub stiffnesses

(c) 12m × 6m

M20 bolts

(d) 15× 6m

M25 bolts
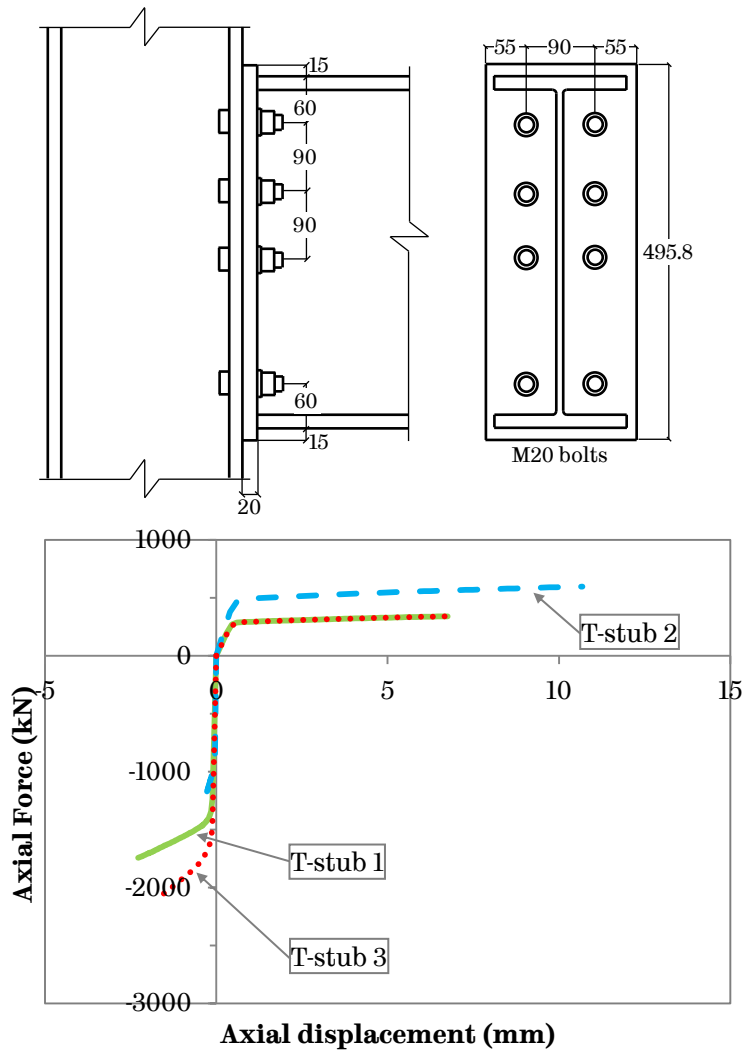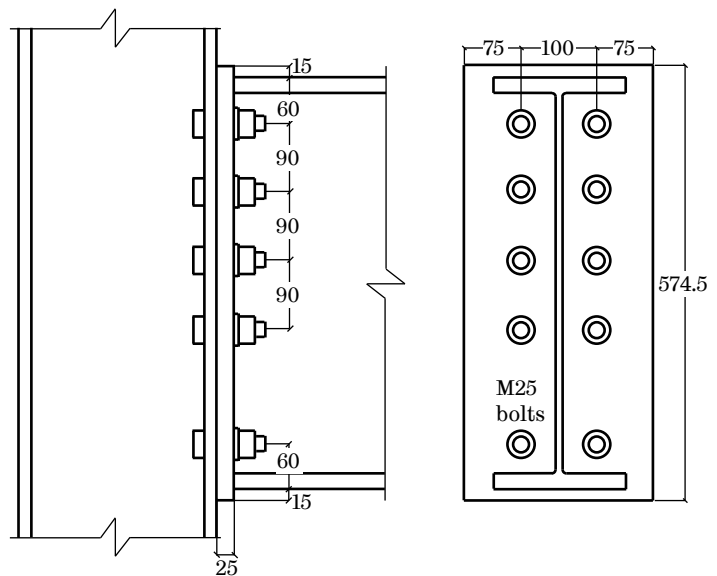
Figure 5-9 (cont'd) Flush endplate connection details and T-stub stiffnesses
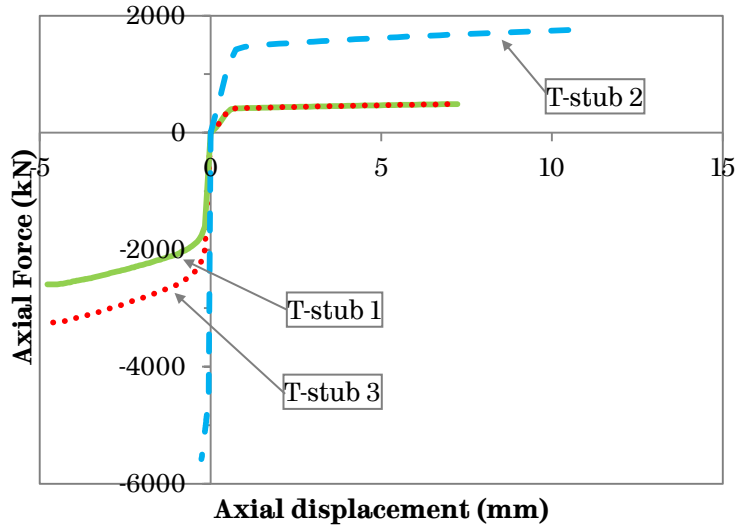
(e) 18× 6m
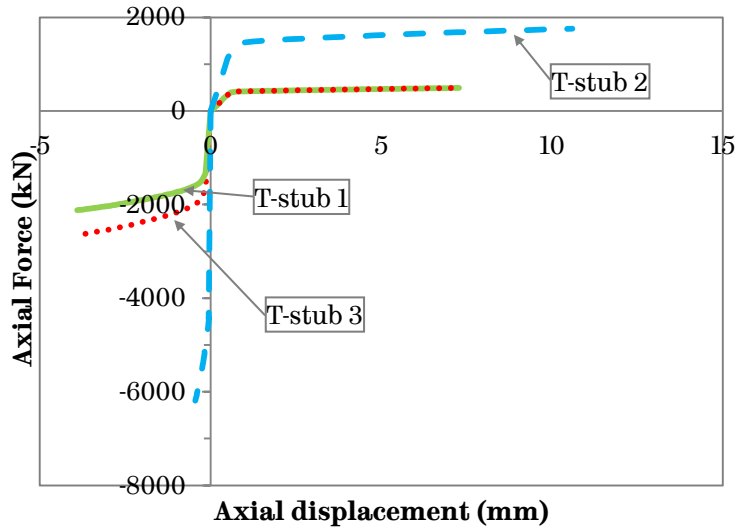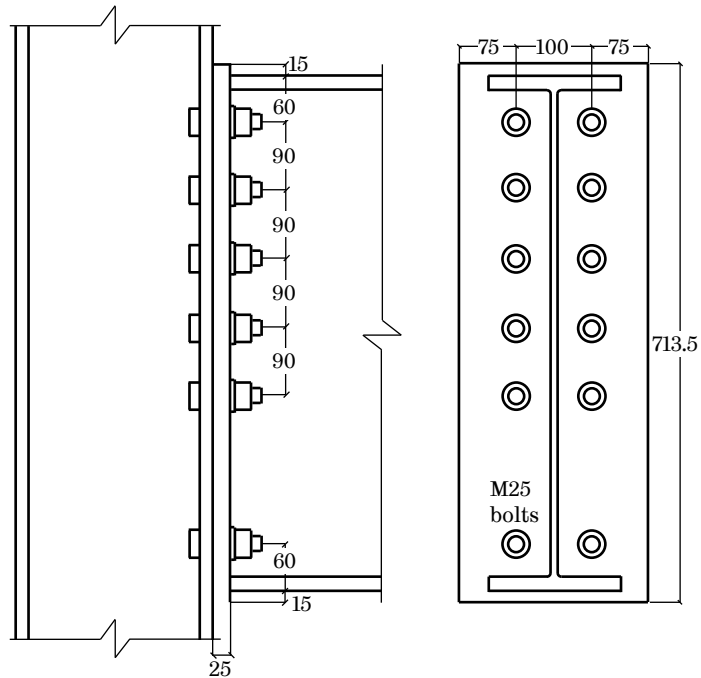
Figure 5-9 (cont'd) Flush endplate connection details and T-stub stiffnesses

5.3.2.3   Boundary conditions

To reliably mimic the restraint provided by the adjacent slab panels to the bay this study is interested in, four strips of composite slabs together with their downstand steel beams are modelled as shaded in red in Figure 5-10 and will be referred to as 'slab fringes' in this study. It needs to be highlighted that by adopting this approach the simulation results would not be as realistic as the results from modelling all of the adjacent eight bays, however this approach is chosen for the following reasons: (a) when including the simplified spring connection models, the current version of *VULCAN* research code must have complete beams with two simplified spring connections on both ends; and (b) computational time can be significantly shortened as the number of elements is massively reduced.
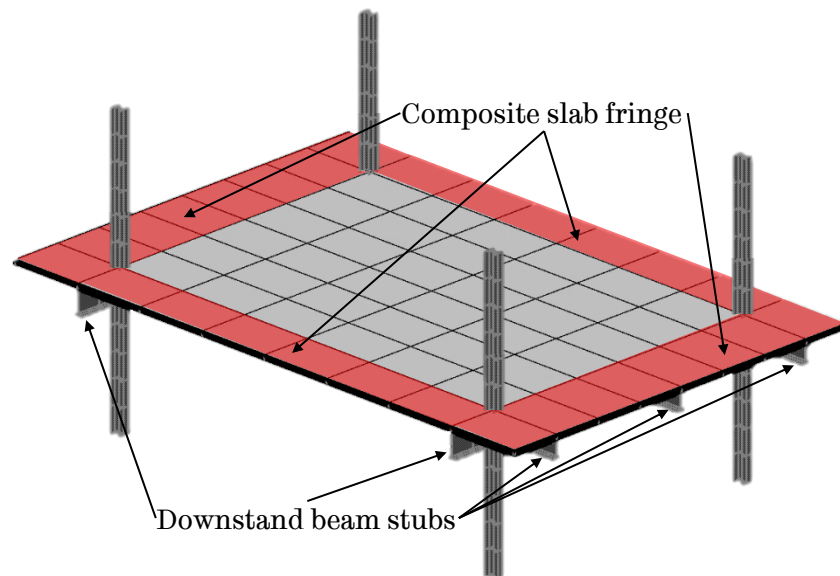
Figure 5-10 Composite slab strips and downstand beam stubs in the frame models

For the frame, the bottoms of the columns are assumed to be fully fixed while the tops of the columns are allowed to move vertically and the rotation about its longitudinal axis is restrained. For the primary beams and the edge secondary beams, out-of-plane rotations are not allowed. The intermediate secondary beam is restrained by the slab and adjacent structures. Therefore, no boundary conditions are applied. The slab elements are restrained rotationally in the vertical direction only. The downstand beam stubs labelled in Figure 5-10 have the same constraints as the beam that they are a continuation of.

5.3.2.4   Loadings

As mentioned in Section 5.3.2.1, the assumed overall factored uniform distributed load is $9.62kN/m^2$, which is applied to the entire slab element surfaces as an area load. Conventionally, to include the loads from the adjacent bays, the primary beams would carry point loads where the intermediate secondary beams are located while the edge secondary beams would carry line loads. For this study, due to the inclusion of the slab fringes (shaded in red in Figure 5-10), reductions in the point loads and the line loads are considered. The two point loads applied at the centre of the primary beams indicated as F in Figure 5-11, are calculated as:

$$F = \text{Area load} \times 3m \text{ (width of the slab panel)} \times (\frac{2}{3} \times \frac{1}{2} \times \text{secondary beam span})$$

due to the width of the slab fringe was a third of half secondary beam span. Similarly, the line loads applied to the edge secondary beams indicated as UDL in Figure 5-11, are calculated as:

$$\text{UDL} = \text{Area load} \times 1.5\text{m (width of the slab panel)} \times \frac{1}{3} = 9.62 \times 1.5 \times \frac{1}{3} = 4.81\text{kN/m}$$

as the width of the slab fringe was two-thirds of half primary beam span.

For all cases, the area load (9.62N/m^2) and the UDL (4.81kN/m) stay unchanged while the only changing loads are the point loads due to change in the length of the secondary beams.
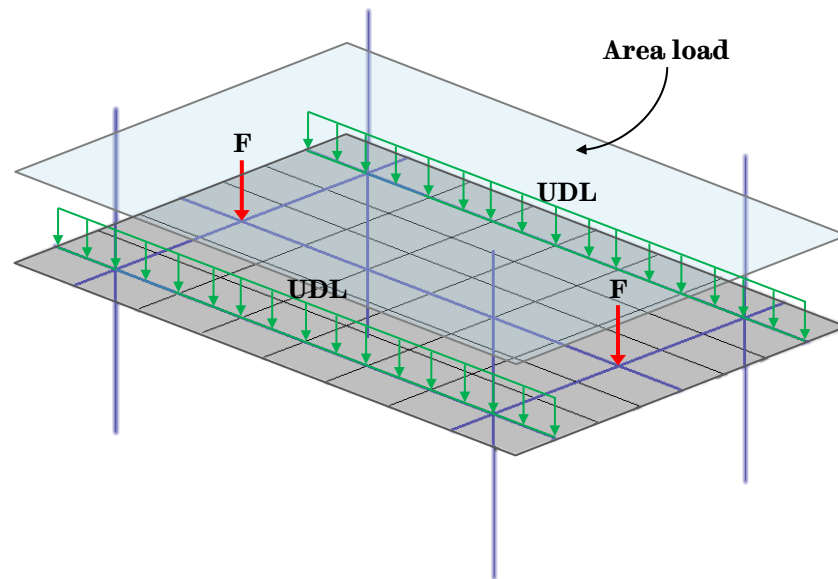
Figure 5-11 Loadings applied to the composite frame

5.3.2.5   Temperature data

The standard fire curve is adopted for this study. The edge primary and secondary beams and the columns are assumed to be protected, and the intermediate secondary beam is left un-protected. Three types of

temperature profiles for cross-sections are used: (1) top flange–web–bottom flange for the beams, (2) uniform distribution for the columns and (3) bi-linear distribution (bottom–middle–top) for the composite slabs and are presented in Table 5-4. Various reduction factors are applied to the standard fire temperature for each structural member to reflect their fire protection scheme (Figure 5-12) and the temperature curve for each reduction factor compared with the standard fire curve are presented in Figure 5-13.
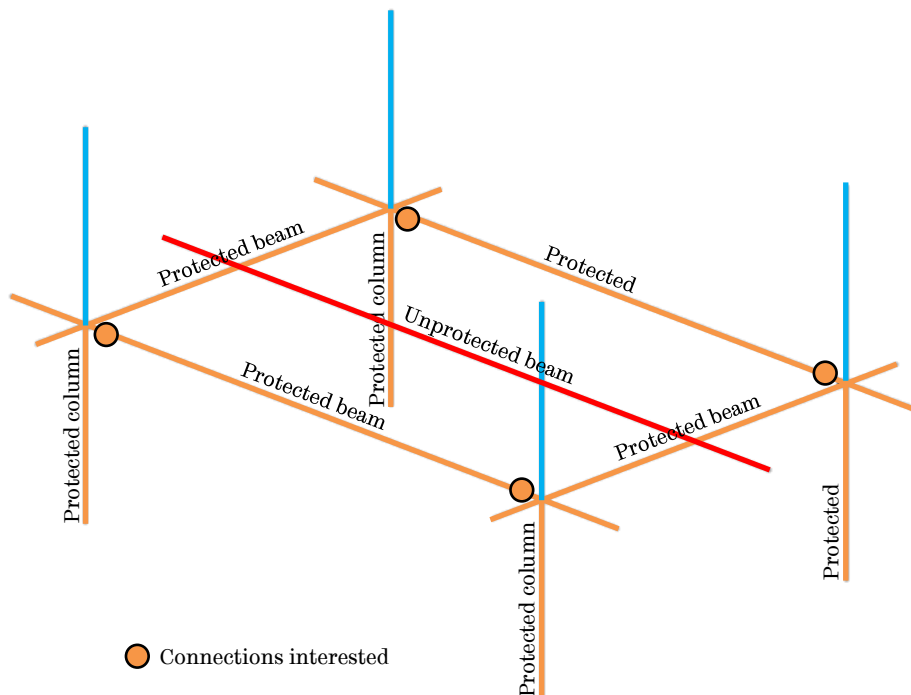
Figure 5-12 Steel frame protection scheme and locations of connections investigated in this study

Table 5-4 Structural member temperature profile with reduction factors

Structural member	Protection	Temperature profile	Reduction factor
Primary beam	Protected	Flange – web – flange	$0.6 - 0.7 - 0.7$
Secondary beam (edge)	Protected	Flange – web – flange	$0.6 - 0.7 - 0.7$
Secondary beam (intermediate)	Un-protected	Flange – web – flange	$0.9 - 1.0 - 1.0$
Column (below slab)	Protected	Uniform distribution	0.7
Column (above slab)	Protected	Uniform distribution	N/A (stayed at 20°C)
Slab	N/A	Bi-linear distribution	$1.0 - 0.3 - 0.2$
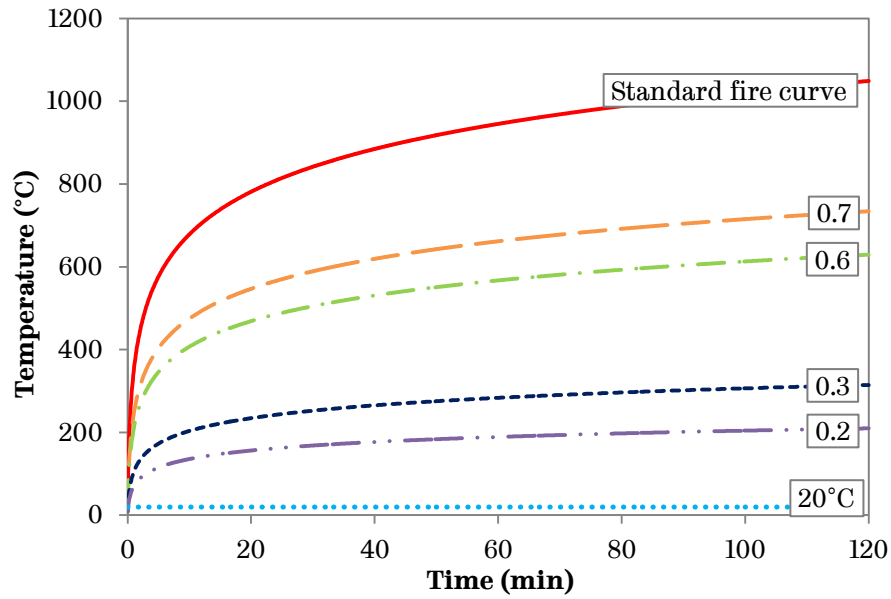
Figure 5-13 Factorised temperature compared with the standard fire temperature up to 120 minutes

5.3.3 Results and discussions

The deflections at the mid-span of the edge beam and the slab centre, and the axial force at the connection are shown in Figure 5-14, Figure 5-15 and Figure 5-18 respectively. Each plot includes results from three connection types. Due to the protection scheme of the frame discussed in the last section, following the standard fire temperature up to 120 minutes results in the temperature of the protected edge beam mid-span deflections (Figure 5-14) and the axial forces acting on the connections (Figure 5-18) being modelled up to 734°C while the slab central deflection (Figure 5-15) is modelled up to 1049°C as the un-protected intermediate secondary beam is not protected.

5.3.3.1   Deflections

Both the mid-span deflections and the slab central deflections for each slab dimension are very close despite the type of connections used, as can be seen from Figure 5-14 and Figure 5-15. These 3D composite frame models include concrete slabs and full composite action is assumed between the slabs and the beams. At ambient temperature, since the top of the beam flanges are fully attached to the bottom surface of the slabs, the vertical deflection is restricted due to the difficulty of deforming the concrete slabs when compared with the 2D steel frame models. At elevated temperature, the existence of the composite slabs produces tensile membrane action, which stretches the central area of the slab inducing a ring of compression to reduce the vertical deflection caused by the high temperature. The deflections from the rigid connection models are always the smallest among the three connection scenarios for each frame size. This is because with the rigid connections the beam end rotation is much smaller compared with the simplified spring and the pinned connections. This limited rotation generates smaller deflections compared with the other two scenarios. On the contrary, the deflections from the simplified spring connection models are the highest among the three connection scenarios for each frame size. This is caused by the axial ductility offered by the springs at the connections compared to the axially-restrained rigid and pinned connections, where the columns provide resistance to the axial
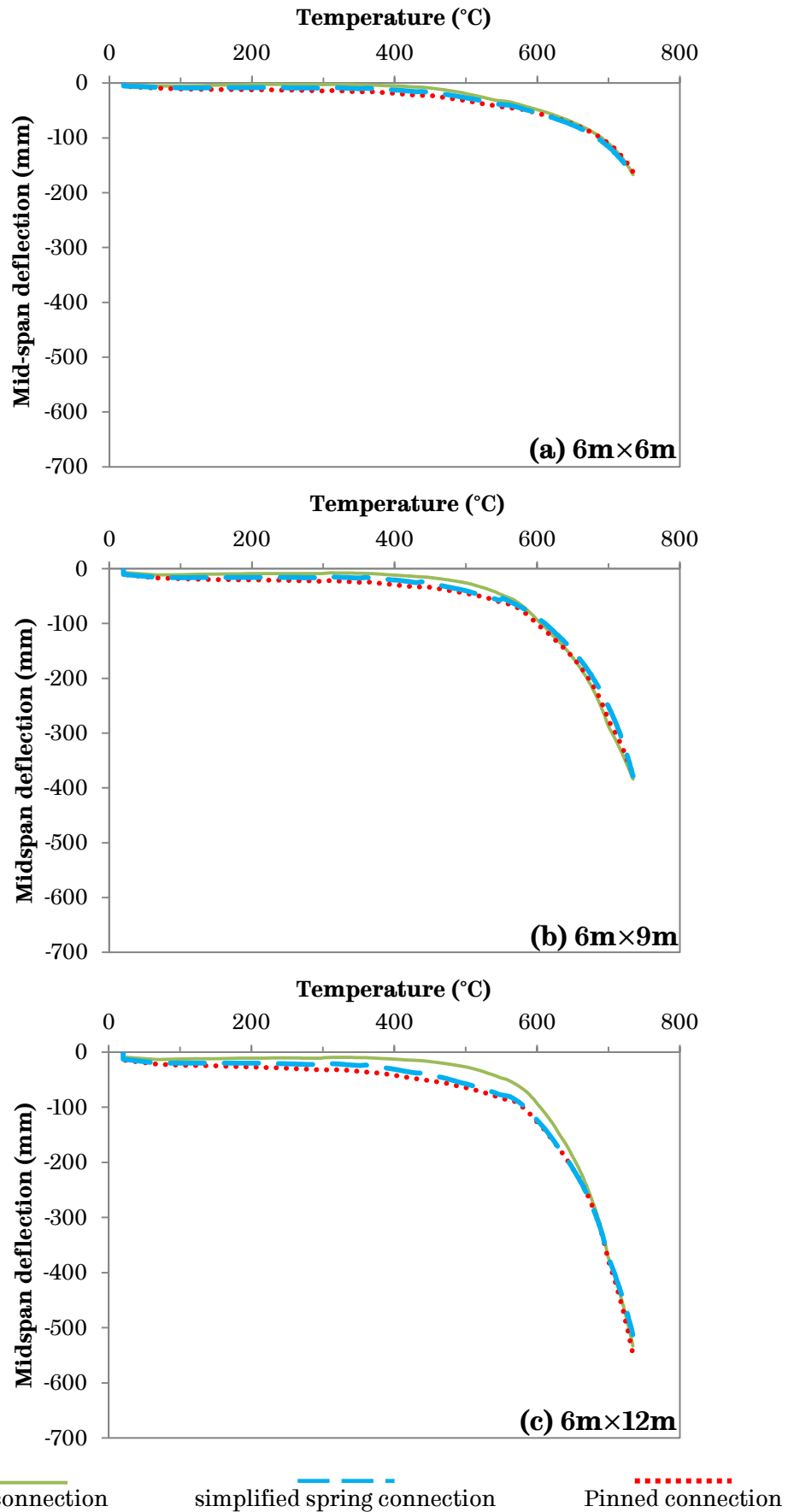
Figure 5-14 Edge secondary beam mid-span deflections

(d) 6m×15m

(e) 6m×18m

Rigid connection   simplified spring connection   Pinned connection
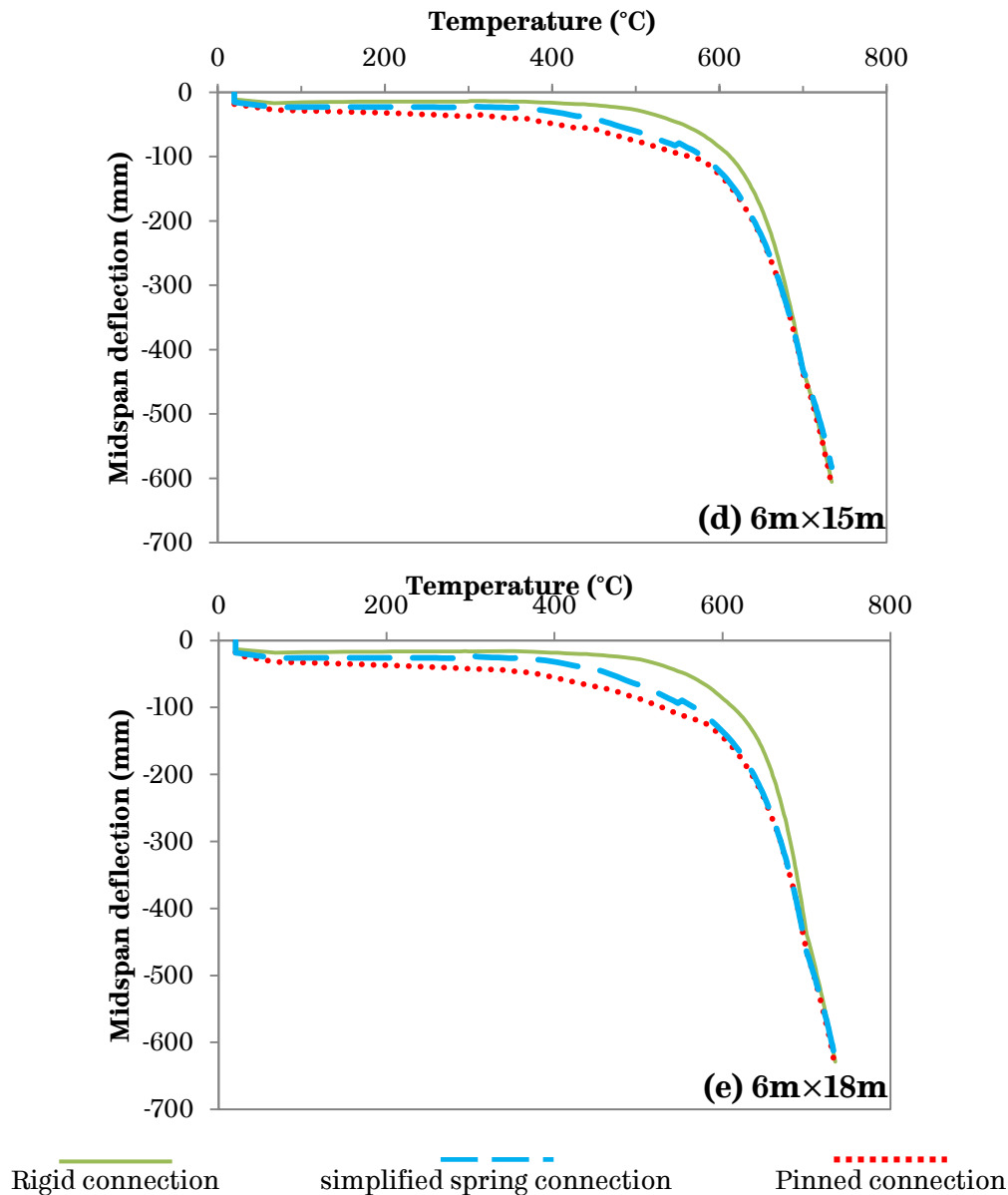
Figure 5-14 (cont'd) Edge secondary beam mid-span deflections

movement of the end of the beams. The plotted deflections are the combinations of the deflections in the springs and the beams.

5.3.3.2   Axial forces acting on the connections

In 3D composite frames, the axial forces show different patterns compared with those in the 2D steel frames. Since the connections which form the focus of this study are on the slab edge secondary
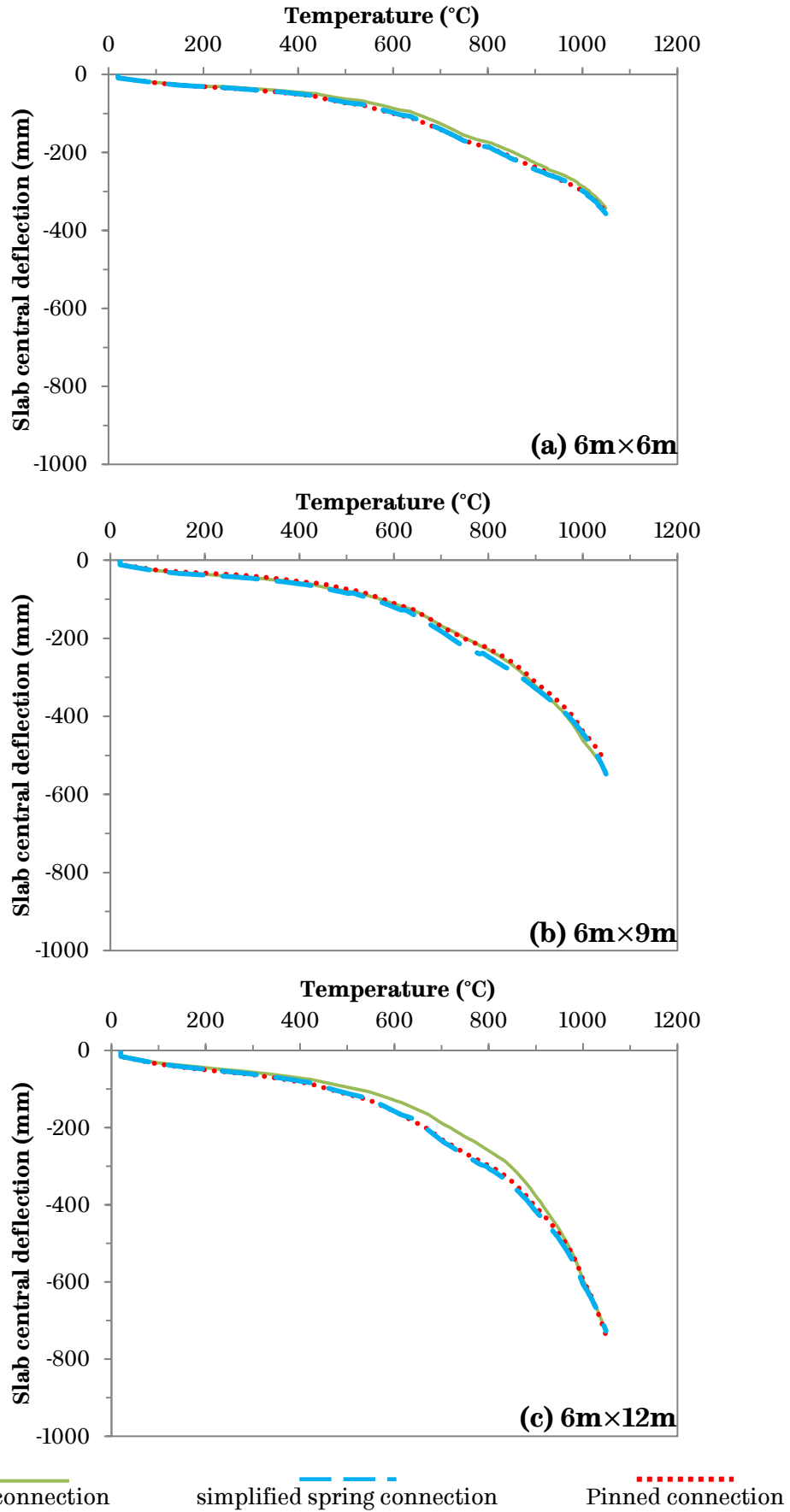
Figure 5-15 Slab central deflecitons
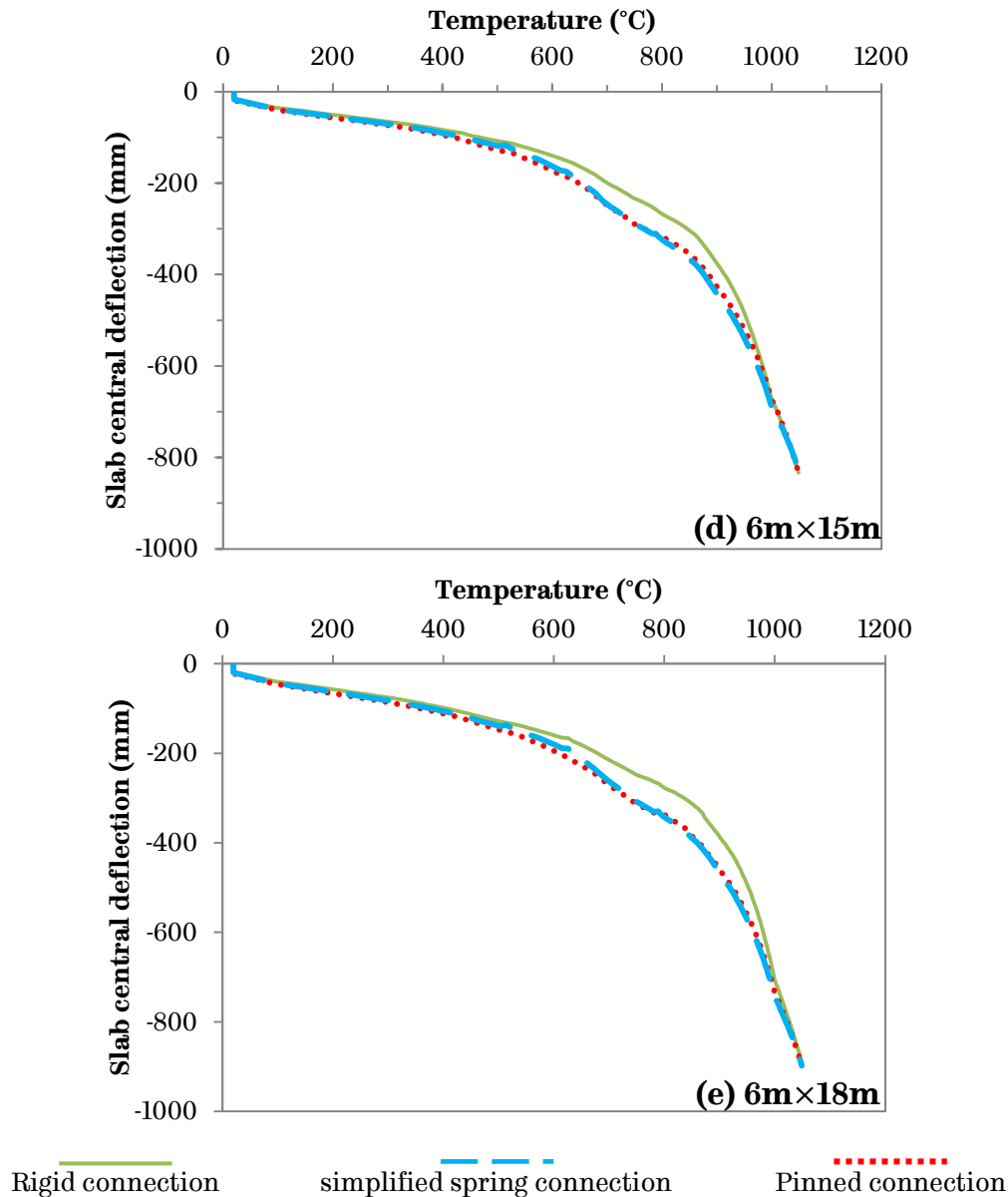
Figure 5-15 (cont'd) Slab central deflections

beams, which are protected and cooler than the un-protected intermediate secondary beam, the axial force distribution is more complex than in the 2D steel frame which has only one beam in the model. During the initial mechanical loading stage, the connections are in compression while the continuous concrete slabs on top of the connections are in tension. As temperatures increase, the axial forces acting on the edge secondary beam-to-column connections is divided

into three stages as illustrated in Figure 5-16 with the changes of axial force acting on the connections, ΔF_{ax}, shown in Figure 5-17:

Stage 1

During the initial heating stage, thermal expansion dominates the behaviour of the frame. The intermediate secondary beam heats up faster than the edge secondary beams, resulting in the intermediate secondary beam expands faster than the edge ones. The differential expansion rates leads to the hotter intermediate secondary beam pushes the primary beam outwards together with the columns, but is restrained by the adjacent structures which are represented by the composite slab strips around the heated bay. The compression the intermediate secondary beam exerts on the primary beam reduced the axial forces acting on the secondary beam-to-column connections from the initial compressive forces induced by the mechanical loading at ambient temperature. This stage continues until the protected edge secondary beam reaches around 400°C, which is around 570°C for the un-protected intermediate secondary beam.

Stage 2

When the temperature rises further, the material degradation becomes the dominating factor, causing the beams and the slabs to become softer, which results in large rotation occurring at the interface of the beam and the column. This reflects in Figure 5-16 as a dramatic increase to the peak compression, which happens around 500~550°C for the
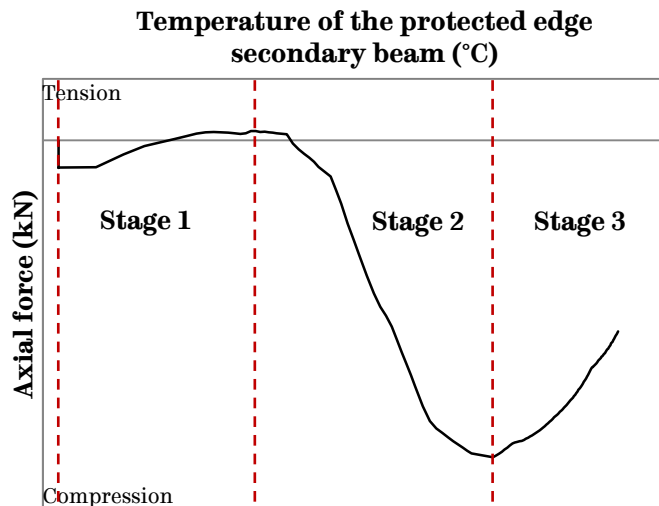
Figure 5-16 Typical axial force acting on the edge secondary beam-to-column connections in 3D composite frame
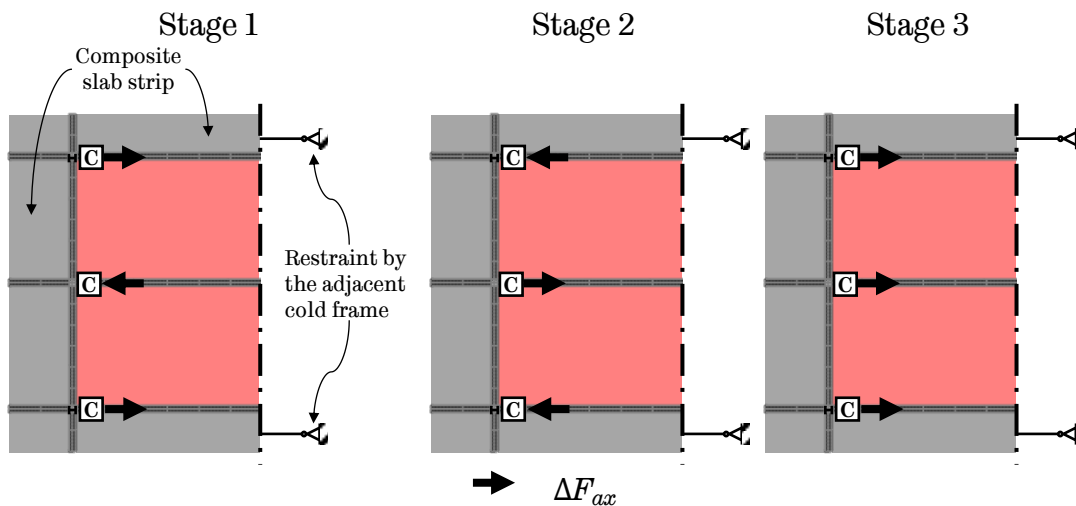
Figure 5-17 Typical changes in axial force, ΔF_{ax}, acting on connections

protected edge secondary beam and around 700~800°C for the un-protected intermediate secondary beam.

Stage 3

In this stage, the whole sub-frame becomes very hot. The intermediate secondary beam continues to lose its strength while the edge secondary beams start to soften, reducing the compression acting on the

connections. Therefore alleviation of the axial compressive force can be observed from Figure 5-16.

The axial forces acting on the connections are illustrated in Figure 5-18. It can be seen that by including the axial and rotational ductility of the connections into the 3D composite structure modelling the peak compressive forces acting on the connections are less than the conventional rigid or pinned connection assumptions. Within each frame size, it can be seen that the models with rigid connections suffer the highest compressive forces. This is as expected since the rigid connection assumption essentially stops the beam from any form of movement from the column flanges, the restrained beam end generates high axial forces acting on the connections. Similarly, the pinned connection assumption only frees the rotational degrees of freedom and brings reductions in the axial forces acting on the connections, however, because of the restrained axial movement the reduction is limited. With the more realistic simplified spring connection model which allows ductility both axially and rotationally, the reductions are more obvious. Table 5-5 provides a quantitative comparison of the maximum axial forces in the form of the actual values and as percentages of the highest case. By including the axial and rotational ductility in the 3D composite frame simulations, the maximum axial forces acting on the connections are lower than the rigid connection assumption. It also needs to be highlighted the amount of the reduction is the greatest with the bay size 6m×9m. The included axial ductility

allows the beam end to move without pulling or pushing the column flanges directly, but instead by deforming the connections. Once again it shows that by using the conventional connection assumptions, which ignore the axial and rotational ductility of the connections, the maximum axial forces acting on the connections are overestimated. The misrepresentation of the actual behaviour of the connections under fire conditions can lead to over designing structural members and an increase in costs.
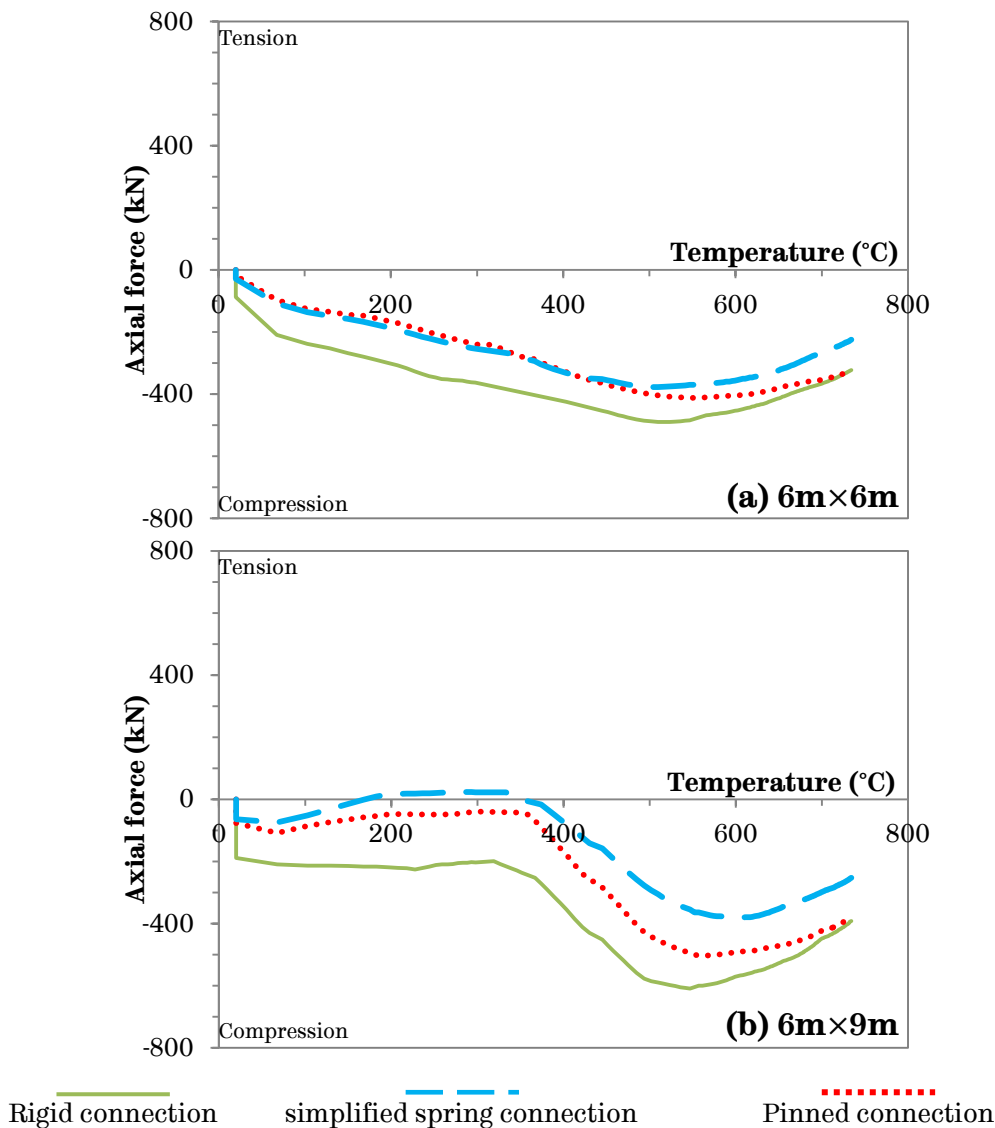
Figure 5-18 Axial forces acting on the secondary beam-to-column connections
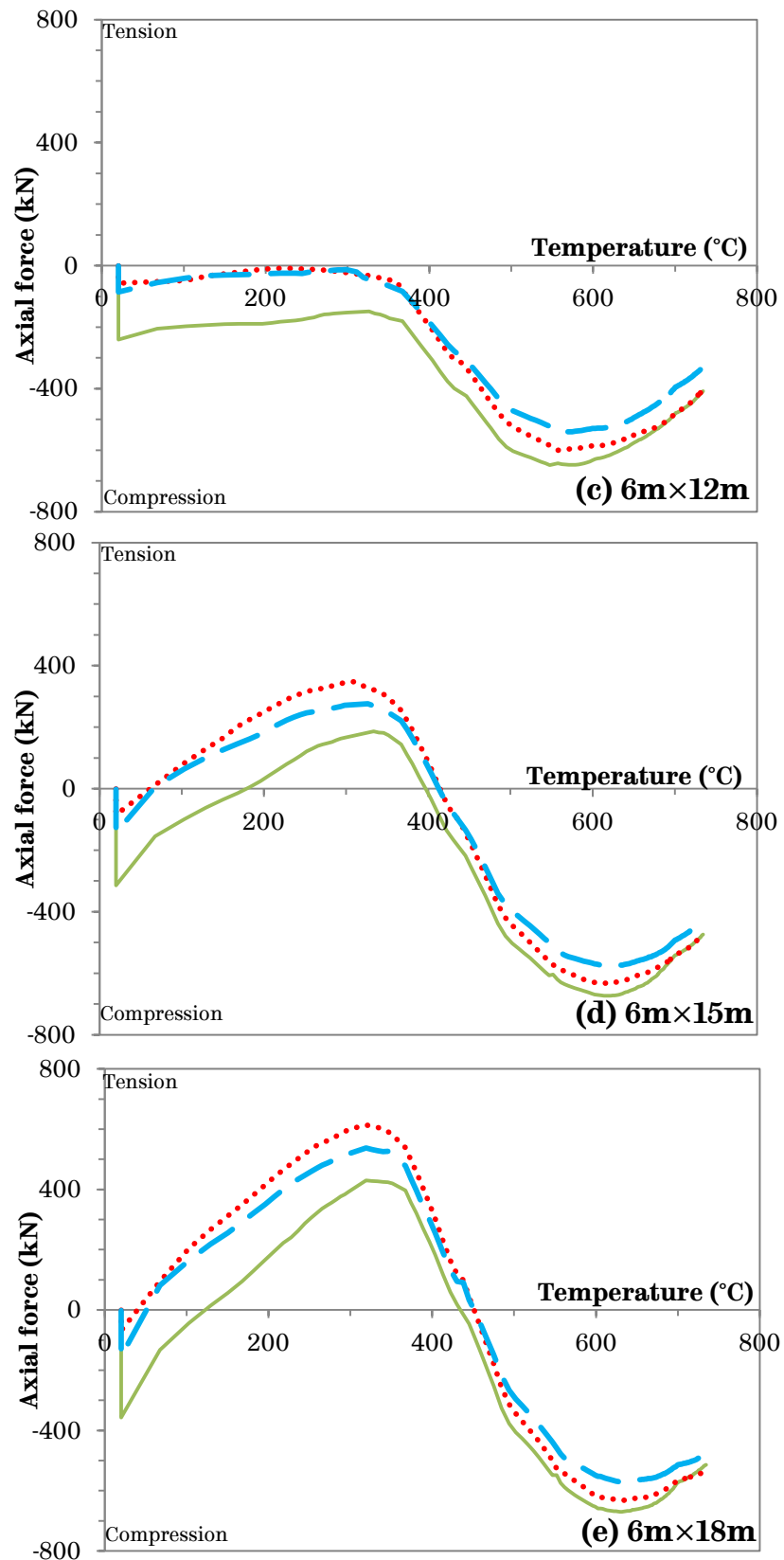
Figure 5-18 (cont'd) Axial forces acting on the secondary beam-to-column connections

			Simplified spring connection case		
Frame size	Rigid connection case (kN)	Pinned connection case (kN)	Axial force (kN)	Percentage of the rigid case (%)	Percentage of the pinned case (%)
6m×6m	490	413	378	77	92
6m×9m	609	504	380	62	75
6m×12m	648	600	542	84	90
6m×15m	673	633	577	86	91
6m×18m	670	632	571	85	90

Table 5-5 Maximum axial force at the connections comparisons

5.3.4 Influences of the beam load ratio on 3D composite frames

The 6m×12m 3D composite frame model from the last section is employed to investigate the influences of the load ratio, R, on the ductility demand of the connections. Four load ratios, starting from 0.2 to 0.8 in the intervals of 0.2, are used. The load for each load ratio case is calculated based on the secondary beam section selected for this frame size (UB457×152×82). Figure 5-19 presents the axial force developed with elevated temperature for each load ratio with the three connection types: rigid, pinned and simplified spring model.

It can be seen that, with increasing load ratio the relationships among models with different connections stays unchanged as discussed in the last section: the models with rigid connections stay the highest, while the models with axial ductile simplified spring connections have the lowest axial forces. However, the actual values vary and are presented in Table 5-6. The percentage values of the simplified spring connection case to the both the rigid and the pinned cases varied very slightly despite of the load ratio changed from 0.2 to 0.8.

(a) R = 0.2

(b) R = 0.4

(c) R = 0.6

(d) R = 0.8

——— Rigid connection　　– – – simplified spring connection　　......... Pinned connection
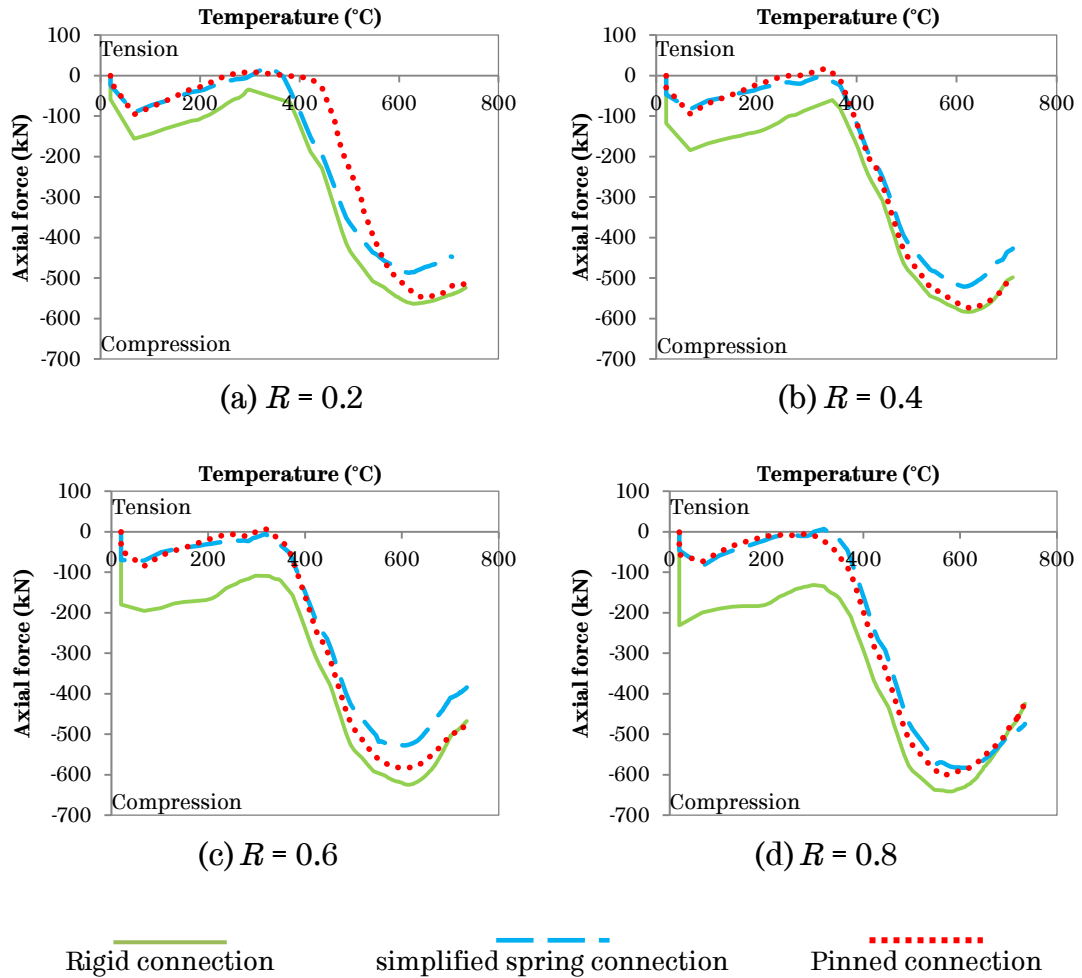
Figure 5-19 Axial forces acting on the secondary beam-to-column connections with various connection assumptions and load ratios, R

Table 5-6 Maximum axial force at the connections comparisons for various load ratios

Load ratio, R	Rigid connection case (kN)	Pinned connection case (kN)	Simplified spring connection case		
			Axial force (kN)	Percentage of the rigid case (%)	Percentage of the pinned case (%)
0.2	556	547	487	87.6	89.0
0.4	583	574	521	89.4	90.8
0.6	625	583	527	84.3	90.4
0.8	641	601	583	91.0	97.0

Compared with the change in load ratio, the differences in the percentage values are relatively small. Figure 5-20 illustrates the comparisons of the axial forces acting on the connections from models

with simplified spring connections with different load ratios. Increasing load ratio brings higher maximum compressive force at a lower temperature. Therefore higher axial ductility is required for beams with heavier loadings. The modelling results suggest that load ratios have an impact on the ductility demand of the connections and that higher load ratios require greater axial ductility of the connection. However, load ratios do not have a great influence on the percentage values of the axial force acting on the connections when using the simplified spring connection model or the rigid/pinned connections.
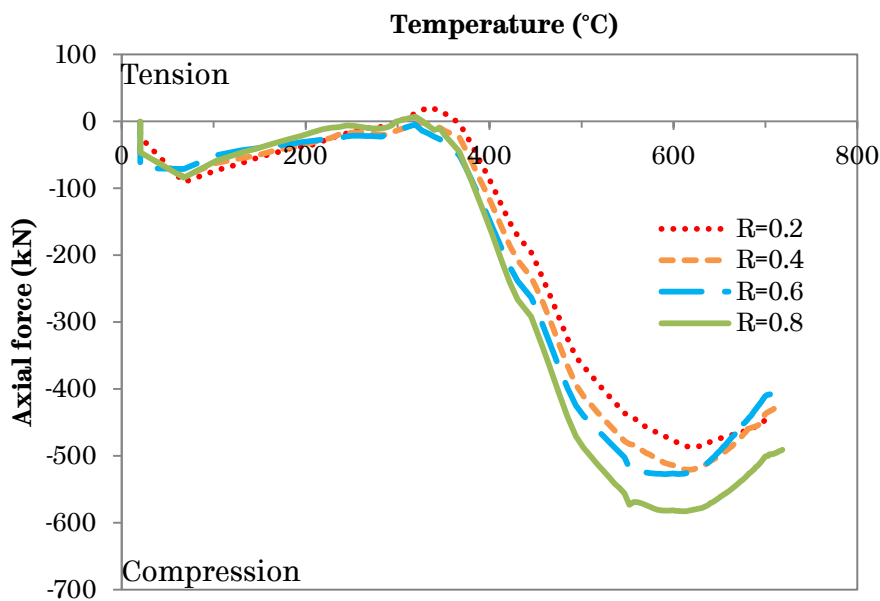
Figure 5-20 Axial forces acting on the secondary beam-to-column simplified spring connections with various load ratios, R

5.4   Chapter conclusions

In this chapter, the influences of the connection ductility on both 2D steel frames and 3D composite frames have been investigated. By including the axial and rotational ductile simplified spring connection

proposed in Chapter 4 in both 2D steel and 3D composite frame simulations, it is shown that the simulation results from the traditionally assumed rigid or pinned connections are not the most accurate representation of the frame response under fire conditions. The rigid and pinned connection assumptions lead to either over- or under-estimation of the axial forces acting on the connections.

The effect of varying the load ratio has also been studied in a 3D composite frame. It is shown that changing load ratio does not have a major impact on the reductions of the axial force acting on the connections from the rigid/pinned connection assumptions to the simplified spring connection assumption.

This chapter highlights the importance of including a realistic connection model of axial and rotational ductility in frame modelling. More accurate representations of frame behaviour are essential during design stage, so that over- or under-estimation of the demand of the structures can be avoided.

Page Intentionally Left Blank

6

Conclusions and Recommendations for Further Work

Page Intentionally Left Blank

6.1   Conclusions

This research project has developed a simplified spring connection modelling approach for steel flush endplate beam-to-column connections, which can be used in 2D steel or 3D composite frame analysis under elevated temperature. The simplified spring connection model was developed based on the existing spring connection model proposed by Sun (2012) which considers connections as assemblies of three non-linear springs with assumed stiffnesses. Instead of assigning hypothetical non-linear spring characteristics based on the type of the connection, the proposed simplified spring connection model can incorporate realistic connection configurations by adopting *ABAQUS* as a pre-processor. Connections are dismantled into two or three T-stubs, depending on their geometrical configurations, and the force-displacement characteristic of each T-stub is generated in *ABAQUS* through detailed finite element modelling. The generated force-displacement curves are then input into *VULCAN*, with corresponding lever arms to form the spring connection model. The axial and rotational ductilities can be represented by the sum or the difference of the springs. The proposed simplified spring connection model has been implemented into *VULCAN* and has been validated against both the same spring connection model in *ABAQUS* and against isolated tests.

Currently, frame analysis with multiple connections is hard to conduct with the available connection modelling approach – detailed

component based method – due to the high demand of computation and time. Connections in frame analyses are usually assumed to be either rigid or pinned, ignoring the axial and/or rotational ductility the connections may possess. The proposed simplified connection model enables the inclusion of more realistic steel beam-to-column connection behaviour in frame analyses.

In this research project, the influences of connection ductilities on frame behaviour in fire were investigated through simulations on a series of 2D steel and 3D composite internal sub-frames with the secondary beam-to-column connections modelled as rigid, pinned or using the proposed simplified spring connection model. The spans of beam varied from 6m to 18m for the 2D steel frame models and 6m to 12m for the 3D composite frame models. The models were assigned realistic loading conditions and temperature distributions.

In the 2D steel frames, generally the restrained steel beam goes through three stages with increasing temperature: (1) retrained thermal expansion induces axial compressive forces acting on the connections and reaches a maximum value; (2) the axial compressive force then reduces due to material degradation under elevated temperature and (3) the axial forces acting on the connections become net tensile due to the beam loss of strength causing it to hang cable-like between the two connections. It was observed from the 2D steel frame analyses that, the axial forces acting on the connections were over-estimated when

assuming the connections to be rigid, and were under-estimated by assuming the connections to be pinned. It is shown that these two conventionally assumptions cannot represent the behaviour of the frames in fire accurately.

The change in axial force acting on the connections in the 3D composite frame is much more complex due to the involvement of the composite slab, the temperature differences in the members and the complicated restraint arising from the surrounding cold structural members. The axial force acting on the critical edge secondary beam-to-column connections generally goes through three stages in fire: (1) axial compressive force induced by the initial mechanical loading at ambient temperature is reduced because of the differential expansion rate of the un-protected internal and protected edge secondary beams, the intermediate secondary beam pushes the primary beam outwards; (2) the axial compressive force then increases dramatically since the un-protected intermediate secondary beam starts to lose its strength in fire, pulling the primary beam inwards; and (3) the axial compressive force is reduced again as the protected edge secondary beams begin to lose their strength significantly. It was found that by assuming the connections to be rigid or pinned, the vertical deflections at the centre of the slab and the mid-span of the edge secondary beams were not affected significantly. However, influences of the connection ductility were shown in the axial forces acting on the secondary beam-to-column

connections. Compared with the results from the model using the proposed simplified spring connection, by assuming these connections to be rigid, the axial forces acting on them are over-estimated; by assuming them to be pinned, the axial forces acting on them are similar up to the end of Stage 2, but smaller peak axial forces were observed.

The above results emphasize the importance of including connection axial and rotational ductility in frame analysis at elevated temperature so that more realistic frame response can be predicted for performance based fire engineering.

6.2   Recommendations for future research

6.2.1   Inclusion of other connection types, configurations and orientations

In common practice, there are various types of steel beam-to-column connections that are in use, including flush, partial depth and extended endplates, fin plates, web cleats and reverse channels. This research project has focused on frame models involving flush endplate connections only, and simplified spring models for other types of connections can be created following a similar approach in future work.

In the current research version of *VULCAN* software only one connection configuration can be used in each simulation because only one set of spring stiffnesses is allowed for input. Ideally users should be

able to model frames which contain multiple connections that may have different configurations (e.g. various connection types, beam sizes, endplate thicknesses, bolt sizes, column sizes and material properties), which requires more than one set of spring stiffnesses to be input into *VULCAN* using the proposed simplified spring connection model.

Similarly, the orientation of the connections modelled can only be on the same plane, because the component based connection model embedded in *VULCAN* is two-dimensional at the moment, and the proposed simplified spring connection model is built based on the existing component based connection model.

In real frames, there are often primary and secondary beam-to-column connections and intermediate secondary beam-to-beam connections. This means that to be able to include all connections in global frame analyses, the above three limitations need be overcome. For example, consider a frame model whose primary beams are connected to the column web and fin-plate connections are adopted for the ease of installation, and the secondary beams are connected to the column flanges by flush endplate connections. In order to include these beam-to-column connections the following updates are required: (a) a simplified spring connection model needs to be developed for fin-plate connections following the proposed simplified spring connection model approach in this research project; (b) *VULCAN* requires updating so that it recognises at least two sets of spring stiffnesses for the two

simplified spring connection models; and (c) *VULCAN* must deal with connections that are in perpendicular planes. The first development can be done under the same principle introduced in this thesis, but the latter two developments require extensive work to the programme code of the research version of *VULCAN*.

It also worth mentioning that the connections selected in this project were all designed according to Joints in Steel Construction: Moment-resisting Joints to Eurocode 3 (the Green Book) (UK Connections Group, 2013). Due to the recommendations on the physical dimensions of the structural elements (such as the endplate thicknesses, the bolt sizes and section sizes) in the Green Book, the deformability and ductility of the connections were limited. Further investigations on simple connections rather than moment connections are suggested to gain a fuller picture of the effect of axial ductility on the behaviour of both 2D and 3D frames in fire.

6.2.2   Procedure optimisation

The proposed simplified spring connection approach requires pre-processing by using finite element software *ABAQUS* to generate spring force-displacement characteristics from detailed T-stub models. This initial procedure requires a considerable amount of computation and time, significantly prolonging the frame simulation when the proposed simplified spring connection model is adopted. The detailed T-stub models in *ABAQUS* are created based on the geometrical configurations

and the material properties of the T-stubs, together with the contact elements between each two T-stub components (beam flange and web, endplate, column flange and bolt assemblies). This pre-processing time can be shortened if the relationship of the tensile and compressive characteristics of similar T-stub assemblies can be quantified. Instead of running separate models in *ABAQUS*, one of the similar T-stubs is simulated to generate its force-displacement curve and the other T-stub's force-displacement curve can be deduced by applying a quantified factor. To generate this factor, considerable amount of simulations are required with extensive validation.

Page Intentionally Left Blank

References

ABAQUS, 2012. *Users Manual Ver.6.12-2.* Providence, RI: Dassault Systemes Simulia Corp..

Abolmaali, A., Matthys, J. H., Farooqi, M. & Choi, Y., 2005. Development of moment–rotation model equations for flush end-plate connections. *Journal of Constructional Steel Research,* Volume 61, pp. 1595-1612.

Al-Jabri, K. S., 1999. *The behaviour of steel and composite beam-to-column connections in fire.* PhD Thesis ed. s.l.:The University of Sheffield.

Al-Jabri, K. S., Seibi, A. & Karrech, A., 2006. Modelling of unstiffened flush endplate bolted connections in fire. *Journal of Constructional Steel Research,* Volume 62, pp. 151-159.

Astaneh, A., 1989. Demand and supply of ductility in steel shear connections. *Journal of Construction Steel Research,* Volume 14, pp. 1-19.

Augusto, H., Simoes da Silva, L., Rebelo, C. & Castro, J. M., 2016. Characterization of web panel components in double-extended bolted end-plate steel joints. *Journal of Constructional Steel Research,* Volume 116, pp. 271-293.

Bailey, C. G., 1995. *Simulation of the structural behaviour of steel-framed buildings.* PhD Thesis ed. s.l.:University of Sheffield.

Block, F. M., 2006. *Development of a component-based finite element for steel beam-to-column connections at elevated temperatures.* PhD thesis ed. s.l.:The University of Sheffield.

Block, F. M., Burgess, I. W., Davison, J. B. & Plank, R. J., 2004. *A component approach to modelling steelwork connections in fire: behaviour of column webs*

in compression. Nashville,Tenessee, Proceedings of ASCE Structures Congress 2004.

Block, F. M., Burgess, I. W., Davison, J. B. & Plank, R. J., 2007. The development of a component-based connection element for end-plate connections in fire. *Fire Safety Journal,* Volume 42, pp. 498-506.

BSI, 1981. *BS 3643-1:1981 Specification for ISO Metric Screw Threads - Part 1: Principles and Basic Data.* 1981 ed. London: British Standards Institution.

BSI, 1987. *BS 476-20:1987 Fire tests on building materials and structures. Method for determination of the fire resistance of elements of construction (general principles).* London: British Standards Institution.

BSI, 2007. *Specification for ISO Metric Screw Threads - Part 1: Principles and Basic Data.* 2007 ed. London: British Standards Institution.

BSI, 2013. *BS EN ISO 898-1, Mechanical properties of fasteners made of carbon steel and.* s.l.:BSI.

BSI, 2013. *BS EN ISO 898-1:2013, Mechanical properties of fasteners made of carbon steel and.* London: British Standards Institution.

Bull, L., 2014. *Microstructural Characterisation of Structural Bolt Assemblies in Fire,* Sheffield: The University of Sheffield.

Burgess, I. W., 2002. Fire resistance of framed buildings.. Volume 37(5), pp. 390-399.

Burgess, I. W., 2008. *Design procedures for steel and composite joints in fire.* Malta, COST C26-WG1, Urban and Construction under Catastrophic Events.

Burgess, I. W. & Davison, J. B., 2012. Briefing : Role of connections in preventing steel frame collapse in fire. *Engineering and Computational Mechanics,* Volume 165, pp. 219-221.

Burgess, I. W., Davison, J. B., Dong, G. & Huang, S. S., 2012. The role of connections in the response of steel frames to fire. *Structural Engineering International,* Volume 22(4), pp. 449-461.

Callister, W. & Rethwisch, D., 2007. *Materials science and engineering: an introduction.* 7 ed. New York: Wiley.

CEN, 2002. *BS EN 1991-1-2, Eurocode 1: General Actions - Part 1-2: Actions on Structures Exposed to Fire.* London: British Standards Institution.

CEN, 2005a. *Eurocode 3: Design of steel structures - Part 1-1: General rules, EN 1993-1-1.* Brussels: European Committee for Standardisation.

CEN, 2005b. *BS EN 1993-1-2:2005 Design of Steel Structures: Part 1.2: Structral Fire, EN 1993-1-2.* London: British Standards Institution.

CEN, 2005b. *EN 1993-1-2 Design of Steel Structures:Part 1-2 Structral Fire.* Brussels: European Committee for Standardisation.

CEN, 2005b. *Eurocode 3. Design of Steel Structures:Part 1-2 Structral Fire, EN 1993-1-2.* Brussels: European Committee for Standardisation.

CEN, 2005c. *BS EN 1993-1-8: 2005 Eurocode 3: Design of steel structures - Part 1-8: Design of joints.* London: British Standards Institute.

CEN, 2005d. *BS EN 1994-1-1:2004 Design of composite steel and concrete structures—Part 1.1: General rules and rules for buildings.* London: BritishStandards Institution.

CEN, 2005e. *BS EN 1994-1-2:2004 — Design of composite steel and concrete structres Part 1-2 Part 1-2: General rules — Structural fire design.* London: British Standards Institute.

Dai, X. H., Wang, Y. C. & Bailey, C. G., 2010. Numerical modelling of structural fire behaviour of restrained steel beam-column assemblies using typical joint types. *Engineering Structures,* Volume 32, pp. 2337-2351.

Daryan, A. S. & Yahyai, M., 2009. Behaviour of bolted top-seat angle connections in fire. *Journal of Constructional Steel Research,* Volume 65, pp. 531-541.

Dieter, G., Kuhn, H. & Semiatin, S. e., 2003. *Handbook of workability and process design.* s.l.:ASM International.

Dong, G., Burgess, I. W. & Davison, J. B., 2011. *Component-Based Element for Endplate Connections in Fire.* Prague, Proceedings of Application of Structural Fire Enginnering, pp. 195-200.

Dong, G., Burgess, I. W. & Davison, J. B., 2012. *Application of a General Component-Based Connection Element in Structural Fire Analysis.* Qingdao, Proceedings of 11th Int. Conference on Steel, Space and Composite Structures.

Dong, G., Burgess, I. W., Davison, J. B. & Sun, R.-R., 2015. Development of a General Component-Based Connection Element for Structural Fire Engineering Analysis. *Journal of Structural Fire Engineering,* Volume 6(4), pp. 247-253.

El-Rimawi, J. A., Burgess, I. W. & Plank, R. J., 1997. The influence of connection stiffness on the behaviour of steel beams in fire. *Journal of Constructional Steel Research,* Volume 43, pp. 1-15.

FEMA, 2002a. *World Trade Centre Building Performance Study.* USA: Federal Emergency Management Agency.

FEMA, 2002b. *World Trade Centre Building Performance Study: Data Collection, Preliminary Observations, and Recommendations.* USA: Federal Emergency Management Agency.

Gann, R., 2008. *Final Report on the Collapse of World Trade Center Building 7, Federal Building and Fire Safety Investigation of the World Trade Center Disaster (NIST NCSTAR 1A).* New York: NISTIR.

Gentili, F., Costa, R. & Simoes da Silva, L., 2014. *Development of a simplified model for joints in steel structures.* Aveiro, Proceedings of 9° Congresso Nacional de Mecânica Experimental.

Haremza, C. et al., 2016. Composite joints under MN at elevated temperatures. *Journal of Constructional Steel Research,* Volume 124, pp. 173-186.

Huang, Z., 2011. A connection element for modelling end-plate connections in fire. *Journal of Constructional Steel Research,* Volume 67(5), pp. 841-853.

Huang, Z., Burgess, I. W. & Plank, R. J., 1999a. Three-dimensional modelling of two full-scale fire tests on a composite building. *Proceedings of the Institution of Civil Engineers-Structures and Buildings,* Volume 134(3), pp. 243-255.

Huang, Z., Burgess, I. W. & Plank, R. J., 1999b. Nonlinear analysis of reinforced concrete slabs subjected to fire. *ACI Structural Journal,* Volume 96(1), pp. 127-135.

Huang, Z., Burgess, I. W. & Plank, R. J., 1999. Nonlinear Analysis of Reinforced Concrete Slabs Subjected to Fire. *ACI Structures Journal,* Volume 96(1), pp. 127-135.

Huang, Z., Burgess, I. W. & Plank, R. J., 2004. Fire resistance of composite floors subject to compartment fires. *Journal of Constructional Steel Research,* Volume 60.2, pp. 339-360.

Huang, Z., Burgess, I. W. & Plank, R. J., 2009. Three-Dimensional Analysis of Reinforced Concrete Beam-Column Structures in Fire. *Journal of Strutural Engineering,* Volume 135(10), pp. 1201-1212.

Hu, Y., 2009b. *Robustness of Flexible Endplate Connections under Fire Conditions.* PhD Thesis ed. s.l.:The University of Sheffield.

Hu, Y., Davison, J. B. & Burgess, I. W., 2007. *Comparative study of the behaviour of BS 4190 and BS EN ISO 4014 bolts in fire.* s.l., s.n.

Hu, Y., Davison, J. B., Burgess, I. W. & Plank, R. J., 2008. Experimental study on flexible end plate connections in fire. *Proceedings of 5th European Conference on Steel Structures,* pp. 1007-1012.

Hu, Y., Davison, J. B., Burgess, I. W. & Plank, R. J., 2009a. Component Modelling of Flexible End-plate Connections in Fire. *International Journal of Steel Structures,* Volume 9, pp. 29-38.

ISO, 1999. *Fire-resistance tests - Elements of building construction. General requirements. ISO 834-1: 1999.* Geneva: International Standards Organisation.

ISO, 1999. *ISO 834-1: 1999 Fire-resistance tests - Elements of building construction. General requirements..* Geneva: International Standards Organisation.

Kirby, B. R., 1995. The Behaviour of High-strength Grade 8.8 Bolts in Fire. *Journal of Construction Steel Research,* 33(1), pp. 3-38.

Lawson, R. M., 1990. Behaviour of steel beam-to-column connections in fire. *The Structural Engineer,* Volume 68(14), pp. 263-271.

Lawson, R. M., 1990. Behaviour of steel beam-to-column connections in fire. *The Structural Engineer,* Volume 68(14), pp. 263-271.

Lawson, R. M. & Newman, G. M., 1996. *tructural Fire Design to EC3 and EC4,.* Ascot: Steel Construction Institute.

Leston-Jones, L. C., 1997a. *The influence of semi-rigid connections on the performance of steel framed structures in fire.* PhD thesis ed. s.l.:The University of Sheffield.

Leston-Jones, L. C., Lennon, T., Plank, R. J. & Burgess, I. W., 1997b. Elevated temperature moment-rotation tests on steelwork connections. *Proceedings of the Institute of Civil Engineers - Structures and Buildings,* Volume 122, pp. 410-419.

Lin, S., 2014. *Development of robust connection models for steel and composite structures in fire.* PhD Thesis ed. s.l.:Brunel University.

Lin, T. D., Zwiers, R. I., Shirley, S. T. & Burg, R. G., 1989. Fire test of concrete slab reinforced with epoxy-coated bars. *ACI Structural Journal,* Volume 86(2), pp. 156-162.

Liu, T. C., 1996. Finite element modelling of behaviours of steel beams and connecitons in fire. *Journal of Constructional Steel Research,* Volume 36(3), pp. 181-199.

Liu, T. C., 1999. Moment-rotation-temperature characteristics of steel/composite connections. *Journal of Strutural Engineering,* Volume 125(10), pp. 1188-1197.

Liu, T. C., Fahad, M. K. & Davies, J. M., 2002. Experimental investigation of behaviour of axially restrained steel beams in fire. *Journal of Constructional Steel Research,* Volume 58, pp. 1211-1230.

Najjar, S. R. & Burgess, I. W., 1996. A nonlinear analysis for three-dimensional steel frame in fire conditions. *Engineering Structures,* Volume 18(1), pp. 77-89.

Newman, G. M., Robinson, J. T. & Bailey, C. G., 2006. *Fire safety design: a new approach to multi-storey steel framed building.* London: The Steel Construction Institute.

Purkiss, J. A., 2007. *Fire safety engineering design of structures.* 2nd ed. Oxford & Burlington: Butterworth-Heinemann.

Qian, Z. H., Tan, K. H. & Burgess, I. W., 2008. Behaviour of steel beam-to-column joints at elevated temperature: Experimental investigation. *Journal of Structual Engineering,* Volume 134(5), pp. 713-726.

Quan, G., Huang, S.-S. & Burgess, I. W., 2016. Component-Based Model of Buckling Panels of Steel Beams at Elevated Temperatures. *Journal of Constructional Steel Research,* Volume 118, pp. 91-104.

Ramberg, W. & Osgood, W. R., 1943. *Description of stress – strain curves by three parameters.* Technical Report 902 ed. s.l.:National Advisory Committee for Aeronautics.

Ramli-Sulong, N. H., Elghazouli, A. Y., Izzuddin, B. A. & Ajit, N., 2010. Modelling of beam-to-column connections at elevated temperature using the component method. *Steel and Composite Structures,* Volume 10(1), pp. 23-43.

Renner, A., 2005. *The effect of strain-rate on the elevated-temperature behaviour of structural steel,* UK: The University of Sheffield.

Saab, H. A., 1990. *Non-linear finite element analysis of steel frames in fire conditions.* PhD Thesis ed. s.l.:The Univercity of Sheffield.

Sarraj, M., 2007b. *The behaviour of steel fin plate connections in fire.* PhD Thesis ed. s.l.:University of Sheffield.

Sarraj, M., Burgess , I. W., Davison, J. B. & Plank, R. J., 2007a. Finite element modelling of steel fin plate connections in fire.. *Fire Safety Journal,* Volume 42, pp. 408-415.

Selamet, S. & Garlock, M. E., 2014. Fire resistance of steel shear connections. *Fire Safety Journal,* Volume 68, pp. 52-60.

Shi, Y. L., Chan, S. L. & Wong, Y. L., 1996. Modelling for moment-rotation characteristics for end-plate connections. *Journal of Structural Engineering,* Volume 122(11), pp. 1300-1306.

Shyam-Sunder, S., 2005. *Federal Building and Fire Safety Investigation of the World Trade Center Disaster: Final Report of the National Construction Safety Team on the Collapses of the World Trade Center Tower (NIST NCSTAR 1).* New York: NISTIR.

Simões da Silva, L., De Lima, L. & Da S. Vellasco, P. a. D. A. S., 2004. Behaviour of flush endplate beam-to-column joints under bendng and axial force. *Steel and Composite Structures*, 2 4, pp. 77-94.

Simoes da Silva, L. & Santiago, A., 2005. Behaviour of steel joints under fire loading. *Steel and Composite Structures,* Volume 5(6), pp. 485-513.

Simoes da Silva, L., Santiago, A. & Real, P. V., 2001. A component model for the behaviour of steel joints at elevated temperatures. *Journal of Constructional,* Volume 57, pp. 1169-1195.

Spyrou, S., 2002. *Development of a component-based model of steel beam-to-column joints at elevated temperatures.* PhD thesis ed. s.l.:The University of Sheffield.

Sun, R.-R., 2012. *Numerical Modelling for Progressive Collapse of Steel Framed Structures in Fire.* PhD Thesis ed. s.l.:The University of Sheffield.

Sun, R., Burgess, I., Huang, Z. & Dong, G., 2015. Progressive failure modelling and ductility demand of steel beam-to-column connections in fire. *Engineering Structures,* Volume 89, pp. 66-78.

Sun, R.-R., Burgess, I. W., Huang, Z.-H. & Dong, G., 2015. Progressive failure modelling and ductility demand of steel beam-to-column connections in fire. *Engineering Structures,* Volume 89, pp. 66-78.

Swinden Technology Centre, 1999. *The Behaviour of Multi-Storey Steel-Framed Buildings in Fire: A European Joint Research Programme.* Rotherham, UK: British Steel plc.

Taib, M., 2012. *The performance of steel framed structures with fin-plate connections in fire.* PhD Thesis ed. s.l.:The University of Sheffield.

Tian, Y., 2014. *The Tensile Membrane Action of Non-Orthogonal Composite Slabs at Elevated Temperatures.* PhD thesis ed. s.l.:The University of Sheffield.

Tschemmernegg, F. & Humer, C., 1988. The Design of Structural-Steel Frames under Consideration of the Nonlinear Behavior of Joints. *Journal of Constructional Steel Research,* Volume 11(2), pp. 73-103.

UK Connections Group, 1995. *Joints in Steel Construction - Moment Connections.* 1st ed. London: BCSA & SCI.

UK Connections Group, 2013. *Joints in steel construction: Moment-Resisting Joints to Eurocode 3.* s.l.:BCSA & SCI.

UK Connections Group, 2013. *Joints in steel construction: Moment-Resisting Joints to Eurocode 3.* s.l.:BCSA & SCI.

UK Connections Group, 2014. *Joints in steel construction: Moment-Resisting Joints to Eurocode 3.* 2nd ed. London: BCSA & SCI.

UK Connections Group, 2015. *Joints in steel construction: Moment-Resisting Joints to Eurocode 3.* 2nd ed. London: BCSA & SCI.

Wang, W. Y., Li, G. Q. & Dong, Y. L., 2007. Experimental study and spring-component modelling of extended end-plate joints in fire. *Journal of Constructional Research,* Volume 63, pp. 1127-1137.

Yu, H., Burgess, I. W., Davison, J. B. & Plank, R. J., 2007. *Experimental Investigation of the Robustness of Fin Plate Connections in Fire.* Singapore, Proceeding of ICASS, pp. 722-727.

Yu, H.-X., Burgess, I. W., Davison, J. B. & Plank, R. J., 2008a. *Experimental Investigation of the Behaviour of Flush End-plate Connections in Fire.* Singapore, Proc. of Structures in Fire Conference, pp. 150-157.

Yu, H.-X., Burgess, I. W., Davison, J. B. & Plank, R. J., 2009a. Experimental Investigation of the Behaviour of Fin Plate Connections in Fire. *Journal of Constructional Steel Research,* Issue 65, pp. 723-736.

Yu, H.-X., Burgess, I. W., Davison, J. B. & Plank, R. J., 2009b. Tying Capacity of Web Cleat Connections in Fire. Part 1: Test and Finite Element Simulation. *Engineering Structures,* 31(3), pp. 651-663.

Yu, H. X., Burgess, I. W., Davison, J. B. & Plank, R. J., 2009a. Experimental investigation of the behaviour of fin plate connections in fire. *Journal of Constructional Steel Research,* Volume 65, pp. 723-736.

Yu, H. X., Burgess, I. W., Davison, J. B. & Plank, R. J., 2009b. Tying capacity of web cleat connections in fire, Part 1: Test and finite element simulation. *Engineering Structures,* Volume 31, pp. 651-663.

Yu, H. X., Burgess, I. W., Davison, J. B. & Plank, R. J., 2009c. Tying capacity of web cleat connections in fire, Part 2: Development of component-based model. *Engineering Structures,* Volume 31, pp. 697-708.

Yu, H. X., Burgess, I. W., Davison, J. B. & Plank, R. J., 2011. Experimental and numerical investigations of the behaviour of flush end plate connections at elevated temperatures. *Journal of Structural Engineering,* Volume 137(1), pp. 80-87.

Appendix

Joint Axial & Rotational Stiffness Calculation Using Component Based Method for M20 Grade 8.8 Bolt

AP1 Joint geometry and mechanical properties

Model configurations
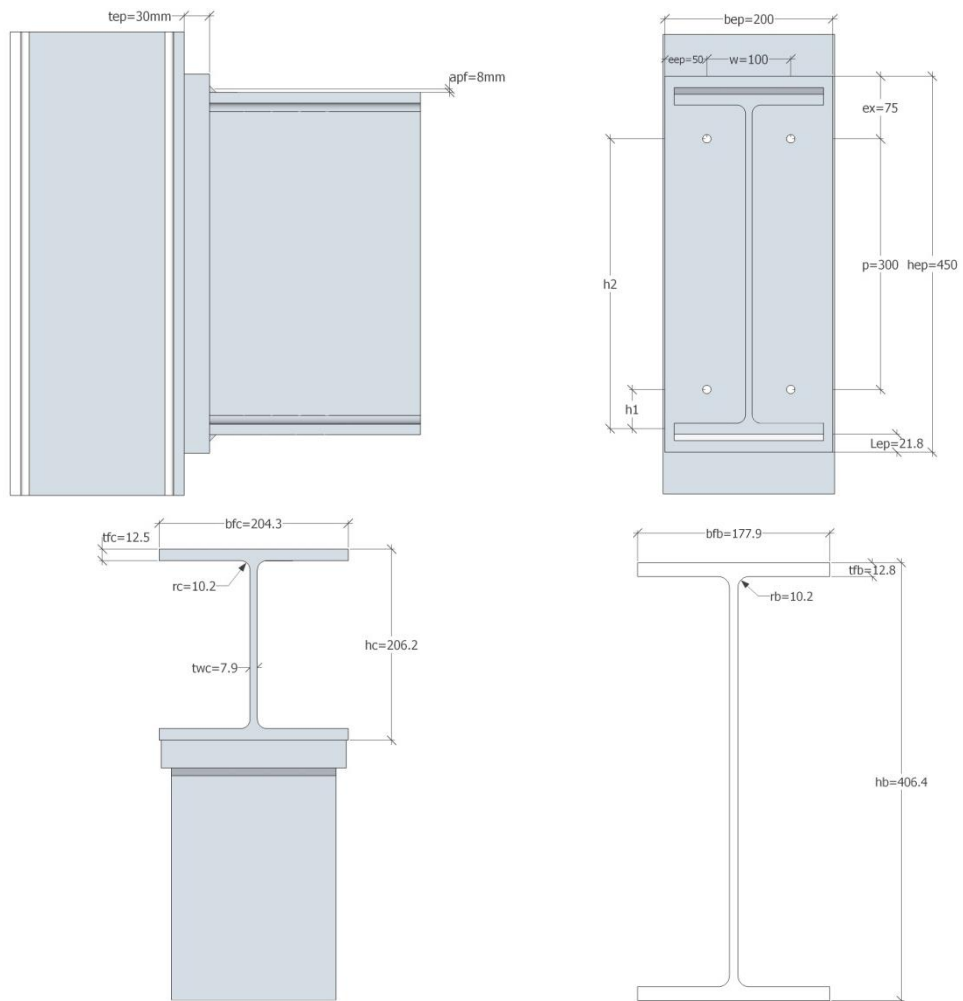
Figure AP-1 Geometry properties of joint model with UB406×178×60 and UC203×203×52

Young's Modulus of joint components for calculation

Column flange: $E_{cfb} = 1000000 N/mm^2$

Column web: $E_{cwt} = 1000000 N/mm^2$

Endplate: $E_{ep} = 1000000 N/mm^2$

Bolt: $E_b = 210000 N/mm^2$

Bolt row lever arms

- First bolt row lever arm

$$h_1 = p + \left(\frac{h_b}{2} - \frac{p}{2} - \frac{t_{fb}}{2}\right) = \frac{1}{2}\left(p + h_b - t_{fb}\right) = \frac{1}{2}(300 + 406.4 - 12.8) = 346.8mm$$

- Second bolt row lever arm

$$h_2 = \frac{h_b}{2} - \frac{p}{2} - \frac{t_{fb}}{2} = \frac{1}{2}(406.4 - 300 - 12.8) = 46.8mm$$

AP2   Translational stiffness of the first bolt row

Column flange in bending

- Distance between the bolt axis and the plastic hinge

$$m_c = \frac{w}{2} - \frac{t_{wc}}{2} - 0.8r_c = \frac{1}{2}(100 - 7.9) - 0.8 \times 10.2 = 37.89mm$$

- Effective width

$$b_{eff,cfb,1} = d_h + 2m_c = 30 + 2 \times 37.89 = 105.78mm$$

$$b_{eff,cfb,2} = \frac{d_h}{2} + m_c + \frac{p}{2} = \frac{30}{2} + 37.89 + \frac{300}{2} = 202.89mm$$

$$b_{eff,cfb} = min\{b_{eff,cfb,1}, b_{eff,cfb,2}\} = 105.78mm$$

- Axial stiffness

$$K_{cfb} = E_{cfb}\frac{0.5 \cdot b_{eff,cfb} \cdot t_{fc}{}^3}{m_c{}^3} = 1000000 \times \frac{0.5 \times 105.78 \times 12.5^3}{37.89^3} = 1899021N/mm$$

Column web in tension

- Clear depth of column web

$$d_{wc} = h_c - 2\left(t_{fc} + r_c\right) = 206.2 - 2(12.5 + 10.2) = 160.80mm$$

- Axial stiffness

$$K_{cwt} = E_{cwt}\frac{b_{eff,cwt} \cdot t_{wc}}{d_{wc}} = 1000000 \times \frac{105.78 \times 7.9}{160.80} = 5196903N/mm$$

Endplate in bending

- Distance between the bolt axis and the plastic hinge located in correspondence to the beam web

$$m_{ep} = \frac{w}{2} - \frac{t_{wb}}{2} - 0.8a_{pw}\sqrt{2} = \frac{1}{2}(100 - 7.9) - 0.8 \times 8 \times \sqrt{2} = 37.00mm$$

- Effective width of the first cantilever

$$b_{eff1,ep1} = d_h + 2m_{ep} = 30 + 2 \times 37 = 104mm$$

$$b_{eff1,ep2} = \frac{d_h}{2} + m_{ep} + \frac{p}{2} = \frac{30}{2} + 37 + \frac{300}{2} = 202mm$$

$$b_{eff1,ep} = min\{b_{eff1,ep1}, b_{eff1,ep2}\} = 104mm$$

- Distance between the bolt axis and the plastic hinge located in correspondence to the beam web

$$m_2 = e_x - L_{ep} - t_{fb} - 0.8a_{pw}\sqrt{2} = 75 - 21.8 - 12.8 - 0.8 \times 8 \times \sqrt{2} = 31.35mm$$

- Effective width of the second cantilever

$$b_{eff2,ep1} = d_h + 2m_2 = 30 + 2 \times 31.35 = 92.70mm$$

$$b_{eff2,ep2} = \frac{d_h}{2} + m_2 + e_{ep} = \frac{30}{2} + 31.35 + 50 = 96.35mm$$

$$b_{eff2,ep} = min\{b_{eff2,ep1}, b_{eff2,ep2}\} = 92.70mm$$

- Axial stiffness

$$K_{ep} = E_{ep} \cdot 0.5 \cdot t_{ep}{}^3 \left(\frac{b_{eff1,ep}}{m_{ep}{}^3} + \frac{b_{eff2,ep}}{m_2{}^3}\right) = 1000000 \times 0.5 \times 30^3 \times \left(\frac{104}{37^3} + \frac{92.7}{31.35^3}\right)$$

$$= 68338919N/mm$$

Bolts in tension

- Material thickness

$$L_b = \frac{1}{2}(12.5 + 16) + 2 \times 3 + 30 + 12.5 = 62.75mm$$

- Axial stiffness

$$K_b = E_b \frac{1.6A_S}{L_b} = 210000 \times 1.6 \times \frac{245}{62.75} = 1311873N/mm$$

Equivalent stiffness of the first bolt row

$$K_1^* = \frac{1}{\frac{1}{K_{cfb}} + \frac{1}{K_{cwt}} + \frac{1}{K_{ep}} + \frac{1}{K_b}} = \frac{1}{\frac{1}{1899021} + \frac{1}{5196903} + \frac{1}{68338919} + \frac{1}{1311873}}$$

$$= 668489N/mm$$

AP3   Translational stiffness of the second bolt row

Column flange in bending

- Effective width

$$b_{eff,cfb,1} = d_h + 2m_c = 30 + 2 \times 37.89 = 105.78mm$$

$$b_{eff,cfb,2} = \frac{d_h}{2} + m_c + \frac{p}{2} = \frac{30}{2} + 37.89 + \frac{300}{2} = 202.89mm$$

$$b_{eff,cfb} = min\{b_{eff,cfb,1}, b_{eff,cfb,2}\} = 105.78mm$$

- Axial stiffness

$$K_{cfb} = E_{cfb}\frac{0.5 \cdot b_{eff,cfb} \cdot t_{fc}{}^3}{m_c{}^3} = 1000000 \times \frac{0.5 \times 105.78 \times 12.5^3}{37.89^3} = 1899021N/mm$$

Column web in tension

- Axial stiffness

$$K_{cwt} = E_{cwt} \frac{b_{eff,cwt} \cdot t_{wc}}{d_{wc}} = 1000000 \times \frac{105.78 \times 7.9}{160.80} = 5196903 N/mm$$

Endplate in bending

- Distance between the bolt axis and the plastic hinge located in correspondence to the beam web

$$m_{ep} = \frac{w}{2} - \frac{t_{wb}}{2} - 0.8a_{pw}\sqrt{2} = \frac{1}{2}(100 - 7.9) - 0.8 \times 8 \times \sqrt{2} = 37.00 mm$$

- Effective width of the first cantilever

$$b_{eff,ep1} = d_h + 2m_{ep} = 30 + 2 \times 37 = 104 mm$$

$$b_{eff,ep2} = \frac{d_h}{2} + m_{ep} + \frac{p}{2} = \frac{30}{2} + 37 + \frac{300}{2} = 202 mm$$

$$b_{eff,ep} = min\{b_{eff,ep1}, b_{eff,ep2}\} = 104 mm$$

- Axial stiffness

$$K_{ep} = E_{ep} \cdot \frac{0.5b_{eff,ep} \cdot t_{ep}^3}{m_{ep}^3} = 1000000 \times \frac{0.5 \times 104 \times 30^3}{37^3} = 27719660 N/mm$$

Bolts in tension

- Material thickness

$$L_b = \frac{1}{2}(12.5 + 16) + 2 \times 3 + 30 + 12.5 = 62.75 mm$$

- Axial stiffness

$$K_b = E_b \frac{1.6A_S}{L_b} = 210000 \times 1.6 \times \frac{245}{62.75} = 1311873 N/mm$$

Equivalent stiffness of the first bolt row

$$K_2^* = \frac{1}{\frac{1}{K_{cfb}} + \frac{1}{K_{cwt}} + \frac{1}{K_{ep}} + \frac{1}{K_b}} = \frac{1}{\frac{1}{1899021} + \frac{1}{5196903} + \frac{1}{27719660} + \frac{1}{1311873}}$$

$$= 659042 N/mm$$

AP4   Equivalent overall translational stiffness

- Lever arm

$$h_t = \frac{K_1^* h_1^2 + K_2^* h_2^2}{K_1^* h_1 + K_2^* h_2} = \frac{668489 \times 346.8^2 + 659042 \times 46.8^2}{668489 \times 346.8 + 659042 \times 46.8} = 311.57 mm$$

- *Equivalent overall translational stiffness*

$$\boldsymbol{K_t} = \frac{K_1^* h_1 + K_2^* h_2}{h_t} = \frac{668489 \times 346.8 + 659042 \times 46.8}{311.57} = 843058 N/mm$$

$$\approx \boldsymbol{8.43 \times 10^5 N/mm}$$

AP5   Overall rotational stiffness

Column web in shear

- Shear area

$$A_{vc} = t_{wc}(h_c - 2t_{fc}) + t_{fc}(t_{wc} + 2r_c) + (2r_c)^2 - \pi r_c^2$$
$$= 7.9(206.2 - 2 \times 12.5) + 12.5(7.9 + 2 \times 10.2) + (2 \times 10.2)^2 - \pi$$
$$\times 10.2^2 = 1874.70 mm^2$$

- Coefficient β

  Assume $\beta = 1$ to be on the safe side

- Axial stiffness

$$K_{cws} = 0.38 \frac{E_{cws} A_{vc}}{\beta h_t} = 0.38 \frac{1000000 \times 1874.70}{1 \times 311.57} = 2286414 N/mm$$

Column web in compression

- Effective width

$$b'_{eff,cwc} = t_{fb} + 2\sqrt{2}a_{pf} + 5k = t_{fb} + 2\sqrt{2}a_{pf} + 5(t_{fc} + r_c)$$
$$= 12.8 + 2\sqrt{2} \times 8 + 5(12.5 + 10.2) = 148.93 mm$$

- Axial stiffness

$$K_{cwc} = E_{cwc} \frac{b'_{eff,cwc} t_{wc}}{d_{wc}} = 1000000 \frac{148.93 \times 7.9}{160.8} = 7316708 N/mm$$

Overall rotational stiffness

$$\boldsymbol{K_\varphi} = \frac{h_t^2}{\dfrac{1}{K_{cws}} + \dfrac{1}{K_{cwc}} + \dfrac{1}{K_t}} = \frac{338.92^2}{\dfrac{1}{2286414} + \dfrac{1}{7316708} + \dfrac{1}{7316708}}$$
$$= 55152020247 N \cdot mm/rad \approx \boldsymbol{5.52 \times 10^{10} N \cdot mm/rad}$$